Supplementary Information

Cross-coupled phenyl- and alkynyl-based phenanthrolines and their effect on the photophysical and electrochemical properties of heteroleptic Cu(I) photosensitizers

Florian Doettinger,[a,b] Yingya Yang,[b] Marie-Ann Schmid,[b] Wolfgang Frey,[a] Michael Karnahl,[*,a] and Stefanie Tschierlei[*,b]

[a] Institute of Organic Chemistry, University of Stuttgart, Pfaffenwaldring 55, 70569 Stuttgart, Germany.
E-mail: michael.karnahl@oc.uni-stuttgart.de

[b] Department Energy Conversion, Institute of Physical and Theoretical Chemistry, Technische Universität Braunschweig, Gaußstr. 17, 38106 Braunschweig, Germany.
E-mail: s.tschierlei@tu-bs.de

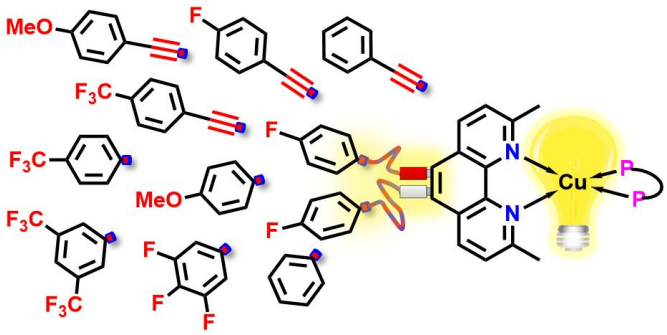

Electronic Supplementary Information - Table of Contents

1 Experimental Details

NMR spectroscopy. Nuclear magnetic resonance (NMR) measurements were performed using spectrometers of the *Bruker Avance* series (300 MHz, 400 MHz, 500 MHz, or 700 MHz) at 293 K. The solvent used for each measurement is indicated at the corresponding NMR data. The chemical shifts δ are denoted in ppm relative to the residual solvent signal of the deuterated solvent.[1] NMR multiplicities are denoted as: *s* (singlet), *d* (doublet), *t* (triplet), *q* (quartet), *m* (multiplet), *b* (broad). Coupling constants *J* are given in Hz. Measurements at 500 MHz and 700 MHz were conducted by an institutional service of the University of Stuttgart.

Mass spectrometry. Mass spectrometric (MS) measurements were carried out by the analytical service of the Institute of Organic Chemistry at the University of Stuttgart. Data were acquired from either a *Bruker MicroTOFQ* (ESI) or *Finnigan MAT 95* (EI) instrument. MS values are denoted in *m*/*z*.

Infrared spectroscopy. Infrared (IR) spectra were collected from the solid state samples by the analytical service of the Institute of Organic Chemistry at the University of Stuttgart using a Bruker Vector 22 FT-IR spectrometer and an ATR module (Golden Gate). The location of the IR signals is given in wavenumbers.

X-ray diffraction. Single-crystal X-ray diffraction analysis was carried out at 135 K on a Bruker Kappa APEXII Duo diffractometer using graphite-monochromated Mo-K_α (λ = 0.71073 Å) or Cu-K_α (λ = 1.54178 Å) radiation by using Omega-Phi scan technique.[2] The structures were solved by direct methods using SHELXL97 software. Mercury 4.2.0 was utilized for structural analysis. Structural representations of ORTEP molecular graphics were performed by XP software.[3] The structural data were deposited at the Cambridge Crystallographic Data Centre with the respective deposition numbers (CCDC): 2059397 (**C1**), 2059398 (**C$_P$4**), 2059399 (**C$_P$6**), 2059400 (**C$_P$7**) and 2059401 (**C$_A$4**). These data can be accessed free of charge at the joint Cambridge Crystallographic Data Centre and Fachinformationszentrum Karlsruhe Access Structures service via the web at www.ccdc.cam.ac.uk/structures/ or by emailing data_request@ccdc.cam.ac.uk or by contacting The Cambridge Crystallographic Data Centre, 12 Union Road, Cambridge CB2 1EZ, UK.

Cyclic voltammetry was carried out in acetonitrile using 0.1 M Bu_4NPF_6 as the supporting electrolyte. Measurements were performed on an Autolab potentiostat PGSTAT204 from Metrohm using a three-electrode configuration with a working electrode: glassy carbon disc with 3 mm diameter stick; counter electrode: platinum wire and reference electrode: Ag/Ag^+ electrode (0.01 M $AgNO_3$ in acetonitrile). All data was referenced against the ferrocene/ferricenium (Fc/Fc^+) couple, which was added to the solution after each measurement. The scan rate was 100 mV/s unless otherwise stated.

Steady-state UV/vis absorption spectra were measured with a JASCO V-670 spectrophotometer. The complexes were dissolved in acetonitrile of spectroscopic grade and the spectra were recorded applying a standard 10 mm fluorescence quartz glass cuvette.

Steady-state emission spectra were recorded with a JASCO FP-8500 spectrofluorometer. All samples were measured in acetonitrile solution under inert conditions (unless stated otherwise) using a sealed 10 mm

---

1 Gottlieb, H. E.; Kotlyar, V.; Nudelmann, A., NMR Chemical Shifts of Common Laboratory Solvents as Trace Impurities *J. Org. Chem.* **1997**, 62, 7512-7515

2 Bruker, APEX2 and SAINT. Bruker AXs Inc., Madison, Wisconsin, USA, **2008**.

3 G. M. Sheldrick, *Acta Crystallogr. C*, **2015**, 71, 3-8.

fluorescence quartz glass cuvette and applying an optical density of approximately 0.1 at excitation wavelength.

Time-resolved emission spectroscopy. Emission lifetimes were determined using a Q-switched pulsed Nd:YAG laser. The excitation pulses were centered at 355 nm with a pulse duration of approx. 6 ns with a beam power of approximately 1.1 mJ per pulse at the sample. A photo multiplier tube inside a LP980 spectrometer from Edinburgh Instruments was applied as detector. All emission lifetimes were recorded either under oxygen free conditions in dry acetonitrile or under atmospheric conditions in standard spectroscopic grade acetonitrile in 10 mm fluorescence quartz glass cuvettes. The respective solutions had an optical density of approximately 0.1 at excitation wavelength. Measurements were taken at room temperature and at the respective emission maximum of the sample.

DFT calculations. Calculations at the density functional theory (DFT) level were performed using the ORCA program package (Version 4.1.2).[4] For geometry optimizations of the electronic ground state, the BP86 exchange-correlation functional was used.[5] As basis sets the triple zeta valance plus polarization functions (def2-TZVP) were used.[6] Solvation effects were accounted for by the conductor-like polarizable continuum model, CPCM, with an appropriate dielectric constant and refractive index of acetonitrile.[7] All stationary points on the potential energy surface of the S_0 state were verified by calculations of the energy second derivatives with respect to nuclear coordinates. Visualizations of the molecular orbitals were made with IboView v20150427.[8]

[4] a) F. Neese, *WIREs Comput. Mol. Sci.*, **2017**, 8. b) F. Neese, *Interdiscip. Rev. Comput. Mol. Sci.*, **2012**, 2, 73.

[5] a) K. Eichkorn, O. Treutler, H. Öhm, M. Häser and R. Ahlrichs, *Chem. Phys. Lett.*, **1995**, 242, 652-660. b) F. Weigend, *Phys. Chem. Chem. Phys.*, **2006**, 8, 1057-1065.

[6] F. Weigend, R. Ahlrichs, *Phys. Chem. Chem. Phys.,* **2005**, 7, 3297-3305.

[7] V. Barone, M. Cossi, *J. Phys. Chem. A*, **1998**, 102, 1995.

[8] G. Knizia, *J. Chem. Theory Comput.*, **2013**, 9, 4834-4883.

2 Synthetic Details

All chemicals were purchased from commercial suppliers (*e.g*. Sigma-Aldrich, VWR, Acros Organics or ABCR) and used as received, if not stated otherwise. Substrates, precursors, ligands, and complexes were synthesized according to the procedures described herein.
Solvents were purified and dried according to standard procedures or taken from a MBraun solvent purification system (MB-SPS-800).[9] Dry dichloromethane (DCM) and dry tetrahydrofurane (THF) used for synthesis or complexation were purified by distillation over appropriate drying agents under nitrogen atmosphere. Degassed water was prepared by intensive bubbling through with nitrogen inside a Schlenk tube for several hours. Degassing other solvents than water was performed by the freeze-pump-thaw technique.[10]

Reactions with air- and/or moisture-sensitive substrates, reagents, catalysts, or complexes were carried out in dried glassware and under nitrogen atmosphere. Glassware was vacuum dried while heated with a heat gun at 500 °C for several minutes and flushed with nitrogen three times. Column chromatography was performed using silica or aluminum oxide (neutral or basic) as stationary phase. Overpressure was applied by hand utilizing a pump ball. Selecting an appropriate column size was expedient in several cases. Hence, the length and diameter of the column chosen for separation are noted where decisive.

2.1 Synthesis of the precatalyst XPhos-Pd-G2

The synthesis of the XPhos-Pd-G2 precatalyst was performed according to a literature known procedure.[11]

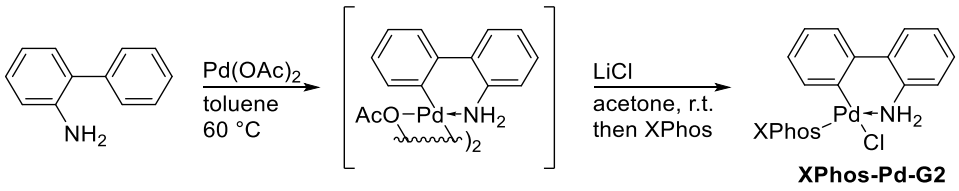

XPhos-Pd-G2

A mixture of $Pd(OAc)_2$ (0.518 g, 2.3 mmol, 1.0 eq.) and 2-aminobiphenyl (0.429 g, 2.5 mmol, 1.1 eq.) in toluene (anhydrous, 13.5 mL) was stirred at 60 °C under inert atmosphere for 60 min. During this time the red colour fades and a grey precipitate forms. After the reaction was allowed to cool to room temperature, toluene was removed *via* syringe. The remaining solid was washed with toluene (anhydrous, 3 x 3.0 mL) and suspended in acetone (anhydrous, distilled from $CaCl_2$, degassed, 13.5 mL). After addition of lithium chloride (0.293 g, 7.0 mmol, 3.0 eq.), the resulting slurry was stirred at room temperature under argon for 1 hour followed by the formation of a red-brown suspension.

XPhos ligand (0.990 g, 2.1 mmol, 0.9 eq.) was added portion wise over 5 min. The mixture was stirred at room temperature for 2.5 hours. Removal of about 90 % of the solvent under vacuum gave a pale yellow slurry which was treated with methyl tert-butyl ether (MTBE) (4.0 mL) and pentane (10.0 mL). The mixture

[9] L. A. Wilfred and L. L. C. Christina, Purification of Laboratory Chemicals (Sixth Edition), Butterworth-Heinemann, Oxford, **2009**.

[10] D. F. Shiver and M. A. Drezdzon, The Manipulation of Air-Sensitive Compounds (Second Edition), John Wiley & Sons. Inc, **1986**.

[11] Kinzel, Zhang and Buchwald, *J. Am. Chem. Soc*., **2010**, 132, 14073–14075

was stored at 0 °C for one hour and the solid was collected *via* filtration, washed with water (3 x 2.0 mL), and dried under vacuum to obtain the product as grey solid.

Yield: 1.72 g (98 %)

$C_{45}H_{59}ClNPPd$ (M = 786.80 g/mol). **^{1}H NMR** ($CDCl_3$, 400 MHz): complex spectrum (see Figure S1.1). **^{31}P NMR** ($CDCl_3$, 400 MHz): δ = 66.59, 64.21 (two rotamers [5]).

2.2 Synthesis of 5,6-Dibromo-2,9-Dimethyl-1,10-Phenanthroline L1

The synthesis of **L1** was performed by altering a literature known procedure.[12] It was found that excluding air from the beginning and sealing the apparatus with a back-pressure valve was indispensable to achieve a reliable reaction. Applying a constant flow of nitrogen decreases the concentration of SO_3 inside the apparatus and ultimately brings the reaction to a halt. Using highly concentrated oleum (ω_{SO3} = 65 %) leads to tri- and tetrabrominated products instead.

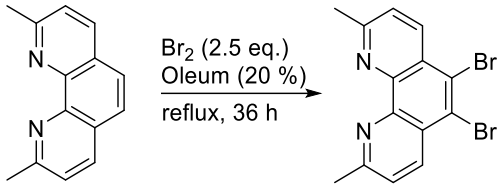

dmp **L1**

Into a nitrogen flushed apparatus, cold oleum (ω_{SO3} = 20 %, 25 mL) was added to 2,9-dimethyl-1,10-phenanthroline (dmp, 2.00 g, 9.60 mmol, 1 eq.) (remarks: the apparatus was sealed with a vitreous back-pressure valve to exclude moisture and keep SO_3 inside the apparatus). After the dmp had completely dissolved, an excess of bromine (1.23 mL, 24.01 mmol, 2.5 eq.) was added to the solution. This mixture was heated at 75 °C for 36 hours and then poured onto ice. The mixture was cooled with an ice bath and carefully neutralized with 6 M KOH solution. (The precipitate forms quickly, turns orange upon increasing pH and colours blood red at pH 3-6. The precipitate at pH 7 is yellowish white or slightly orange.) Several portions of chloroform were used to dissolve the precipitate straight from the neutralized mixture. The organic phase was washed with water once and filtered to obtain a clear yellow solution, which was dried with Mg_2SO_4. The solvent was evaporated and the resulting solid dried at 40 °C *in vacuo* to afford the pale yellow product in high yield (2.82 g, 7.69 mmol, 80 %). It should be noted, that the product is hygroscopic. The reproducibility has been tested in three independent multi-gram approaches, where **L1** was received in yields of 80 %, 76 %, and 79 %, respectively (see below).

dmp	Oleum	Bromine	Yield
2.00 g, 9.60 mmol, 1.0 eq.	25 mL	1.23 mL, 24.01 mmol, 2.5 eq.	2.82 g, 7.69 mmol, **80 %**
2.00 g, 9.60 mmol, 1.0 eq.	25 mL	1.23 mL, 24.01 mmol, 2.5 eq.	2.68 g, 7.32 mmol, **76 %**
4.00 g, 19.21 mmol, 1.0 eq.	50 mL	2.46 mL, 48.02 mmol, 2.5 eq.	5.55 g, 15.16 mmol, **79 %**

$C_{14}H_{10}Br_2N_2$ (M = 366.06 g/mol). **^{1}H NMR** ($CDCl_3$, 400 MHz): δ = 8.56 (*d*, *J* = 9.08 Hz, 2H, Ar-*H*), 7.49 (*d*, *J* = 7.8 Hz, 2H, Ar-*H*), 2.88 (*s*, 6H, C*H*$_3$). **^{13}C NMR** ($CDCl_3$, 500 MHz): δ = 159.50, 143.80, 136.39, 125.86, 123.94, 123.02, 24.59. **HRMS** (ESI+) *m/z*: calcd. for $[M+H]^+$: 364.9283, 366.9264, and 368.9244; found: 364.9286, 366.9273, and 368.9246. **Mp.**: 166 °C (*lit*. 163 °C – 166 °C).

[12] Afsar *et al.*, Chem. Commun., **2013**, 49, 8534–8536

2.3 Synthesis of the Ligands L_P2-L_P7 and L_A2-L_A5

2.3.1 Syntheses of the Ligands L_P2-L_P7

General Synthetic Procedure

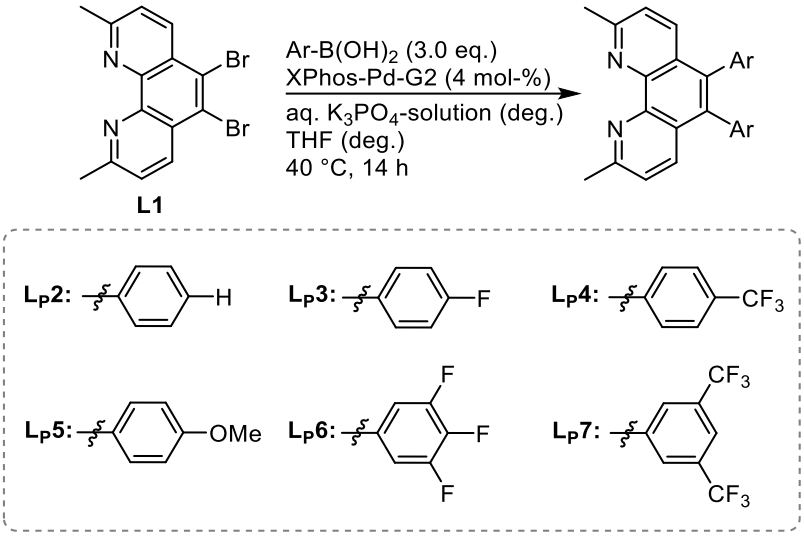

In a general synthetic procedure (GSP) a 100 mL round bottomed flask was equipped with a magnetic stir bar and charged with the precatalyst XPhos-Pd-G2 (0.04 eq.), 5,6-dibromo-2,9-dimethyl-1,10-phenanthroline **L1** ($dmpBr_2$) (1.0 eq.), and the corresponding boronic acid (3.0 eq.). The vessel was sealed with a septum, then evacuated and backfilled with nitrogen (this process was repeated three times). Degassed THF was added via syringe and the mixture was stirred for several minutes. Afterwards, degassed aqueous 0.5 M K_3PO_4 solution was added and the reaction was stirred at 40 °C for 14 hours.
THF was evaporated directly from the reaction mixture, which resulted in a precipitation of the product. The remaining basic aqueous phase was extracted with DCM three times. The combined organic layer was washed with saturated Na_2CO_3 solution, water, and brine. The solvent was dried with Mg_2SO_4 and finally evaporated to yield the corresponding crude product as solid. In most reactions, subsequent recrystallization was necessary (*vide infra*).

Synthesis of L_P2

The reaction was conducted after the GSP in Section **2.3.1** using PBA = phenylboronic acid. After workup, the crude product was recrystallized from chloroform.

L1	PBA	Cat.	THF	K_3PO_4 solution	Yield
300.0 mg (0.82 mmol)	299.8 mg (2.46 mmol)	25.2 mg (0.033 mmol)	12 mL	14 mL	192.3 mg (65 %)

$C_{26}H_{20}N_2$ (M = 360.46 g/mol): **^{1}H NMR** ($CDCl_3$, 400 MHz): δ = 7.75 (*d*, *J* = 8.5 Hz, 2H, Ar-*H*), 7.31 (*d, J* = 8.5 Hz, 2H, Ar-*H*), 7.18 (*m*, 6H, Ar-*H*), 7.09 (*m*, 4H, Ar-*H*), 2.89 (*s*, 6H, C*H*$_3$). **^{13}C NMR** ($CDCl_3$, 500 MHz): 158.96, 144.81, 138.11, 135.93, 135.44, 131.03, 127.77, 126.91, 126.71, 123.38, 25.84. **HRMS** (ESI+) *m/z*: calcd. for $[M+H]^+$: 361.1699; found: 361.1699.

Synthesis of L_P3

The reaction was conducted after the GSP in Section **2.3.1** using 4F-PBA = 4-fluorophenylboronic acid. The product was recrystallized from a hot mixture of chloroform and *n*-hexane (1:1).

L1	4F-PBA	Cat.	THF	K_3PO_4 solution	Yield
325.0 mg (0.89 mmol)	372.7 mg (2.67 mmol)	27.3 mg (0.036 mmol)	15 mL	17 mL	292.6 mg (90.1 %)

$C_{26}H_{18}F_2N_2$ (M = 396.44 g/mol): **^{1}H NMR** ($CDCl_3$, 400 MHz): δ = 7.75 (*d*, *J* = 8.4 Hz, 2H, Ar-*H*); 7.36 (*d*, *J* = 8.4 Hz, 2H, Ar-*H*), 7.04 (*m*, 4H, Ar-*H*), 6.93 (*t*, *J* = 8.7 Hz, 4H, Ar-*H*), 2.94 (s, 6H, C*H*$_3$). **^{13}C NMR** ($CDCl_3$, 500 MHz): δ = 163.05, 160.60, 159.32, 144.68, 135.33, 133.74, 132.59, 126.65, 123.69, 115.09, 25.60. **^{19}F NMR** ($CDCl_3$, 400 MHz): -114.6. **HRMS** (EI) *m/z*: calcd. for $[M]^+$: 396.1438; found: 396.1441.

Synthesis of L_P4

The reaction was conducted after the GSP in Section **2.3.1** using 4CF_3-PBA = 4-(trifluoromethyl)-phenylboronic acid. After workup, the crude product was recrystallized from a hot mixture of ethanol and water.

L1	4CF_3-PBA	Cat.	THF	K_3PO_4 solution	Yield
300 mg (0.82 mmol)	467.0 mg (2.50 mmol)	25.2 mg (0.033 mmol)	10 mL	20 mL	285.2 mg (70.1 %)

$C_{28}H_{18}F_6N_2$ (M = 496.46 g/mol): **^{1}H NMR** ($CDCl_3$, 400 MHz): δ = 7.65 (*d*, *J* = 8.4 Hz, 2H, Ar-*H*), 7.50 (*d*, *J* = 8.2 Hz, 4H, Ar-*H*), 7.36 (*d, J* = 8.4 Hz, 2H, Ar-*H*), 7.23 (*d*, *J* = 8.2 Hz, 4H, Ar-*H*), 2.91 (*s*, 6H, C*H*$_3$). **^{13}C NMR** ($CDCl_3$, 500 MHz): 159.84, 141.43, 135.11, 134.73, 131.28, 129.81, 129.55, 126.05, 125.11, 123.90, 122.88, 25.82. **^{19}F NMR** ($CDCl_3$, 400 MHz): -62.49. **HRMS** (ESI+) *m/z*: calcd. for $[M+H]^+$: 497.1447; found: 497.1449.

Synthesis of L_P5

The reaction was conducted after the GSP in Section **2.3.1** using 4OMe-PBA = 4-methoxyphenylboronic acid. After workup, the crude product was dissolved in hot toluene and filtered through a plug of celite.

L1	4OMe-PBA	Cat.	THF	K_3PO_4 solution	Yield
370.0 mg (1.01 mmol)	460.8 mg (3.03 mmol)	31.1 mg (0.040 mmol)	19 mL	23 mL	398 mg (94 %)

$C_{28}H_{24}N_2O_2$ (M = 420.51 g/mol): **^{1}H NMR** ($CDCl_3$, 400 MHz): δ = 7.78 (*d*, *J* = 8.5 Hz, 2H, Ar-*H*), 7.30 (*d, J* = 8.5 Hz, 2H, Ar-*H*), 6.99 (*d*, *J* = 8.4 Hz, 4H, Ar-*H*), 6.75 (*d*, *J* = 8.4 Hz, 4H, Ar-*H*), 3.74 (*s*, 6H, OC*H*$_3$), 2.88 (*s*, 6H, C*H*$_3$). **^{13}C NMR** ($CDCl_3$, 500 MHz): 157.73, 157.29, 143.76, 134.82, 134.45, 131.06, 129.47, 126.07, 122.27, 112.27, 54.13, 24.76.

Synthesis of L_P6

The reaction was conducted after the GSP in Section **2.3.1** using 3,4,5F_3-PBA = 3,4,5-Trifluorophenylboronic acid). After workup, the crude product was recrystallized from toluene and the solid washed with *n*-hexane.

L1	3,4,5F_3-PBA	Cat.	THF	K_3PO_4 solution	Yield
200.0 mg (0.55 mmol)	288.3 mg (1.64 mmol)	16.8 mg (0.022mmol)	9 mL	10 mL	162.0 mg (63.3 %)

$C_{26}H_{14}F_6N_2$ (M = 468.40 g/mol):): **^{1}H NMR** ($CDCl_3$, 400 MHz): δ = 7.65 (*d*, *J* = 8.4 Hz, 2H, Ar-*H*), 7.50 (*d*, *J* = 8.2 Hz, 4H, Ar-*H*), 7.36 (*d, J* = 8.4 Hz, 2H, Ar-*H*), 7.23 (*d*, *J* = 8.2 Hz, 4H, Ar-*H*), 2.91 (*s*, 6H, CH_3). **^{19}F NMR** ($CDCl_3$, 400 MHz): -133.13, -160.19. **HRMS** (ESI+) *m/z*: calcd. for $[M+H]^+$: 469.1134; found: 469.1146.

Synthesis of L_P7

The reaction was conducted after the GSP in Section **2.3.1** using 3,5$(CF_3)_2$-PBA = 3,5-bis(trifluoromethyl) phenylboronic acid. After workup, the crude product was recrystallized from an EtOH/water mixture.

L1	3,5$(CF_3)_2$-PBA	Cat.	THF	K_3PO_4 solution	Yield
180.0 mg (0.49 mmol)	380.5 mg (1.48 mmol)	15.1 mg (0.022 mmol)	9 mL	10 mL	311.0 mg (64.0 %)

$C_{30}H_{16}F_{12}N_2$ (M = 632.45 g/mol): **^{1}H NMR** ($CDCl_3$, 400 MHz): δ = 7.73 (*s*, 2H, Ar-*H*), 7.69 (*d*, *J* = 8.5 Hz, 2H, Ar-*H*), 7.55 (*s,* 4H, Ar-*H*), 7.46 (*d*, *J* = 8.5 Hz, 2H, Ar-*H*), 2.96 (*s*, 6H, CH_3). **^{19}F NMR** ($CDCl_3$, 400 MHz): -63.22.

2.3.2 Syntheses of the Ligands L_A2-L_A5

Sonogashira cross-coupling reactions for the preparation of the ligands **L_A2-L_A5** were performed on the homoleptic substrate complex [Cu(**L1**)$_2$]PF_6 using a "chemistry-on-the-complex" method. Therefore, the synthesis of [Cu(**L1**)$_2$]PF_6 is also described in this section.

The cross-coupling towards the different alkynyl-based ligands **L_A2-L_A5** was conducted following slightly differing synthetic procedures (see below). Afterwards, the desired ligands **L_A2-L_A5**s were liberated from the homoleptic target complex by decomplexation using KCN. As the crude products were contaminated to different extends the respective work-up procedures were customized for each ligand.

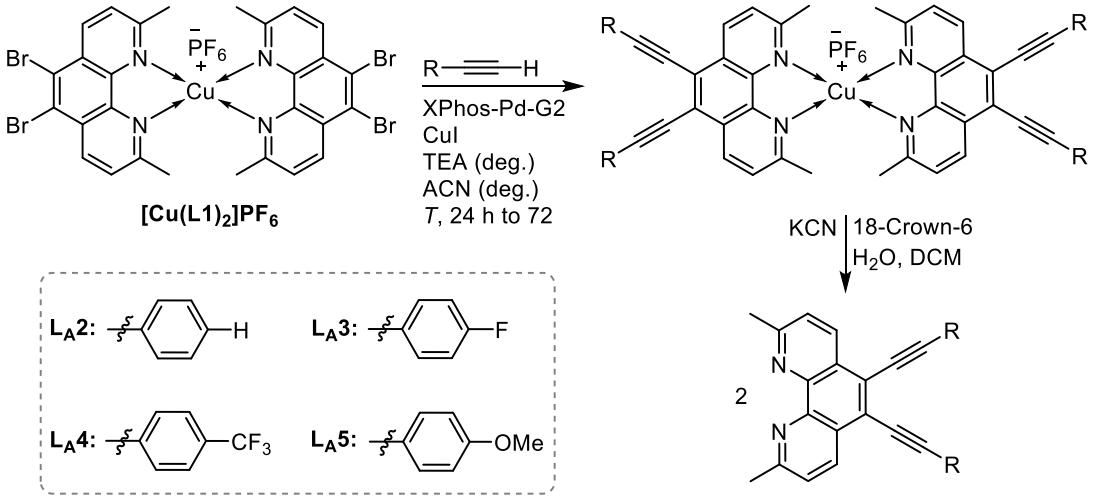

Synthesis of the Substrate Complex [Cu(L1)$_2$]PF_6

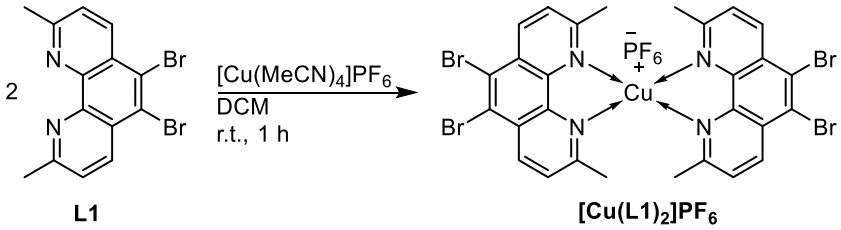

Into a dried Schlenk-tube equipped with a stir bar, tetrakis(acetonitrile)-copper(I) hexafluorophosphate ([Cu(MeCN)$_4$]PF_6, 857 mg, 2.30 mmol, 1.0 eq.) and 5,6-dibromo-2,9-dimethyl-1,10-phenanthroline (1684 mg, 4.60 mmol, 2.0 eq.) were added. The vessel was set under vacuum and refilled with nitrogen three times. Dry DCM (200 mL) was added and the dark red solution stirred for 1 hour. The complex was precipitated with *n*-hexane and the solid washed with *n*-hexane once. The complex was obtained as dark red crystalline solid in excellent yield (2078 mg, 96 %).

$C_{28}H_{20}Br_4CuF_6N_4P$ (M = 940.62 g/mol). **^{1}H NMR** (CD_3CN, 400 MHz): δ = 8.95 (*d*, *J* = 8.5 Hz, 4H, Ar-*H*); 7.94 (*d*, *J* = 8.5 Hz, 4H, Ar-*H*), 2.41 (s, 12H, C*H*$_3$). **^{19}F NMR** (CD_3CN, 400 MHz): -72.09 (*s*, 3H, P*F*$_6$), -73.91 (*s*, 3H, P*F*$_6$).

Synthesis of L_A2

Into a dried 250 mL Schlenk flask [Cu(**L1**)$_2$]PF_6 (400.0 mg, 0.43 mmol, 1.0 eq.), CuI (40.5 mg, 0.21 mmol, 0.5 eq.), and XPhos-Pd-G2 (32.7 mg, 0.043 mmol, 10 mol- %) were added and the flask was then flushed with nitrogen three times. Dry and degassed acetonitrile (30 mL) and phenyl acetylene (260.6 mg, 2.55 mmol, 6.0 eq.) were added. After stirring for several minutes, dry and degassed triethylamine (30 mL) was added, the flask securely sealed, and the reaction was left to stir at 50 °C for 43 hours.

Acetonitrile and triethylamine were evaporated and the remaining solid mixture dissolved in DCM. An appropriate amount of silica was added and the solvent evaporated to dry-load a short column for flash column chromatography (L ≈ 20 cm, Ø ≈ 6 cm). Impurities were washed away with pure DCM and the red target complex was eluted with DCM:MeOH = 25:1.

After evaporation of the solvents, the solid was dissolved in DCM and catalytic amounts of 18-crown-6 were added. Diluted aqueous Na_2CO_3 solution and excess KCN were added and the mixture was stirred vigorously for one hour to subsequently destroy the target complex and liberate the desired ligand **L_A2**. The phases were separated, the organic phase washed with water, brine, and dried with Mg_2SO_4. After evaporation of the solvent, the solid was dissolved in acetone and precipitated by adding water. Collecting and drying to solid yielded 188 mg (54 %) of **L_A2**.

$C_{30}H_{20}N_2$ (M = 408.50 g/mol). **^{1}H NMR** ($CDCl_3$, 400 MHz): δ = 8.65 (*d*, *J* = 8.3 Hz, 2H, Ar-*H*); 7.63 (*m*, 4H, Ar-*H*), 7.52 (*d*, *J* = 8.3 Hz, 2H, Ar-*H*), 7.34 (*m*, 6H, Ar-*H*), 2.90 (*s*, 6H, C*H*$_3$). **^{13}C NMR** ($CDCl_3$, 500 MHz): 160.38, 144.79, 135.20, 131.78, 128.98, 128.58, 126.23, 124.18, 123.00, 122.46, 99.83, 86.17, 25.93. **IR**: ν(C≡C) = 2197.39 cm^{-1}. **HRMS** (ESI) *m/z*: calcd. for [M+H]$^+$: 409.1699; found: 409.1699.

Synthesis of L_A3

Into a dried 250 mL Schlenk flask [Cu(**L1**)$_2$]PF_6 (577.4 mg, 0.61 mmol, 1.0 eq.), CuI (58.5 mg, 190.4 mmol, 0.5 eq.), and XPhos-Pd-G2 (47.2 mg, 0.061 mmol, 10 mol- %) were added and then the flask was flushed with nitrogen three times. Dry and degassed acetonitrile (35 mL) and 1-ethynyl-4-flurobenzene (442.5 mg, 3.68 mmol, 6.0 eq.) were added. After stirring for several minutes, dry and degassed triethylamine (35 mL) was added, the flask securely sealed, and the reaction was left to stir at 50 °C for 65 hours.

Acetonitrile and triethylamine were evaporated and the remaining solid mixture dissolved in DCM. An appropriate amount of silica was added and the solvent evaporated to dry-load a short column for flash column chromatography (L ≈ 20 cm, Ø ≈ 6 cm). Impurities were washed away with pure DCM and the red target complex was eluted with DCM:MeOH = 25:1.

After evaporation of the solvents, the solid was dissolved in DCM and catalytic amounts of 18-crown-6 were added. Diluted aqueous Na_2CO_3 solution and excess KCN were added and the mixture was stirred vigorously for one hour to subsequently destroy the target complex and liberate the desired ligand **L_A3**.

Subsequently, column chromatography on neutral aluminum oxide (L ≈ 45 cm, Ø ≈ 3.5 cm, gradient DCM/MeOH: 0 % → 4 %) was performed and the isolated product recrystallized from toluene to finally yield 168 mg (31 %) of **L_A3**.

$C_{30}H_{18}F_2N_2$ (M = 444.48 g/mol). **^{1}H NMR** ($CDCl_3$, 400 MHz): δ = 8.85 (*d*, *J* = 8.5 Hz, 2H, Ar-*H*); 7.57 (*m*, 4H, Ar-*H*), 7.49 (*d*, *J* = 8.5 Hz, 2H, Ar-*H*), 6.88 (*t*, *J* = 8.7 Hz, 4H, Ar-*H*), 2.89 (*s*, 6H, C*H*$_3$). **^{13}C NMR** ($CDCl_3$, 500 MHz): 162.81, 160.49, 144.81, 135.08, 133.70, 126.11, 124.19, 122.30, 119.06, 115.99, 98.61, 85.85, 25.91. **^{19}F NMR** ($CDCl_3$, 400 MHz): -109.29. **IR**: ν(C≡C) = 2198.43 cm^{-1}. **HRMS** (EI) *m/z*: calcd. for [M]$^+$: 444.1438; found: 444.1440.

Synthesis of L_A4

Into a dried 250 mL Schlenk flask was added [Cu(**L1**)$_2$]PF_6 (500.0 mg, 0.53 mmol, 1.0 eq.), CuI (50.6 mg, 0.27 mmol, 0.5 eq.) and XPhos-Pd-G2 (40.9 mg, 0.053 mmol, 10 mol- %) were added and then the flask was flushed with nitrogen three times. Dry and degassed acetonitrile (35 mL) and 4-ethynyl-α,α,α-trifuorotoluene (542.6 mg, 3.19 mmol, 6.0 eq.) were added. After stirring for several minutes, dry and degassed triethylamine (35 mL) was added, the flask securely sealed, and the reaction was left to stir at 50 °C for 48 hours.

Acetonitrile and triethylamine were evaporated and the remaining solid mixture dissolved in DCM. An appropriate amount of silica was added and the solvent evaporated to dry-load a short column for flash column chromatography (*L* ≈ 20 cm, Ø ≈ 6 cm). Impurities were washed away with pure DCM and the red target complex was eluted with DCM:MeOH = 25:1.

After evaporation of the solvents, the solid was dissolved in DCM and catalytic amounts of 18-crown-6 were added. Diluted aqueous Na_2CO_3 solution and excess KCN were added and the mixture was stirred vigorously for one hour to subsequently destroy the target complex and liberate the desired ligand **L_A4**. Subsequently, column chromatography on neutral aluminum oxide (*L* ≈ 45 cm, Ø ≈ 3.5 cm, gradient DCM/MeOH: 0 % → 4 %) was performed and the isolated product dried *in vacuo* to obtain 285 mg (49 %).

$C_{32}H_{18}F_6N_2$ (M = 544.50 g/mol). **^{1}H NMR** ($CDCl_3$, 400 MHz): δ = 8.57 (*d*, *J* = 8.4 Hz, 2H, Ar-*H*); 7.69 (*d*, *J* = 8.3 Hz, 4H, Ar-*H*), 7.60 (*d*, *J* = 8.3 Hz, 4H, Ar-*H*), 7.52 (*d*, *J* = 8.4 Hz, 2H, Ar-*H*), 2.91 (*s*, 6H, CH_3). **^{13}C NMR** ($CDCl_3$, 500 MHz): 160.9455, 144.95, 135.02, 131.90, 130.80, 126.53, 125.96, 125.63, 125.16, 124.37, 122.38, 98.20, 88.12, 25.93. **^{19}F NMR** ($CDCl_3$, 400 MHz): -62.72. **IR**: *v*(C≡C) = 2206.39 cm^{-1}. **HRMS** (EI) *m/z*: calcd. for [M]$^+$: 544.1369; found: 544.1376.

Synthesis of L_A5

Into a dried 100 mL Schlenk flask [Cu(**L1**)$_2$]PF_6 (300 mg, 0.32 mmol, 1.0 eq.), CuI (6.7 mg, 0.035 mmol, 0.11 eq.), and XPhos-Pd-G2 (12.3 mg, 0.016 mmol, 5 mol- %) were added and then the flask was flushed with nitrogen three times. Dry and degassed acetonitrile (40 mL) and 4-ethynylanisole (254.2 mg, 1.92 mmol, 6.0 eq.) were added. After stirring for several minutes, dry and degassed triethylamine (7.5 mL) was added, the vessel tightly sealed, and the reaction was left to stir at room temperature for 24 hours.

The inhomogeneous mixture was cleared by filtering off precipitated impurities. The desired complex was precipitated by adding *n*-hexane to the cleared solution, washed with *n*-hexane and afterwards dissolved in DCM. An appropriate amount of silica was added and the solvent evaporated to dry-load a short column for flash column chromatography (*L* ≈ 20 cm, Ø ≈ 6 cm). Impurities were washed away with pure DCM and the red target complex was eluted with DCM:MeOH = 25:1.

The solid was dissolved in DCM (10 mL) and water (10 mL), KCN (50 mg, 0.8 mmol), and catalytic amounts of 18-crown-6 were added. The mixture was stirred vigorously for one hour. The phases were separated, the organic phase washed with water, brine, and dried with Mg_2SO_4. After evaporation of the solvent, the solid was recrystallized from EtOH to yield 101 mg (34 %) of pure **L_A5**.

$C_{32}H_{24}N_2O_2$ (M = 468.56 g/mol). **^{1}H NMR** ($CDCl_3$, 400 MHz): δ = 8.65 (*d*, *J* = 8.3 Hz, 2H, Ar-*H*); 7.57 (*d*, *J* = 8.7 Hz, 4H, Ar-*H*), 7.51 (*d*, *J* = 8.3 Hz, 2H, Ar-*H*), 6.88 (d, *J* = 8.7 Hz, 4H, Ar-*H*), 3.81 (*s*, 6H, OCH_3), 2.94 (*s*, 6H, CH_3). **IR**: *v*(C≡C) = 2190.19 cm^{-1}. **HRMS** (EI) *m/z*: calcd. for [M]$^+$: 468.1838; found: 468.1840.

2.4 Synthesis of the Complexes C1, C_P2-C_P7, and C_A2-C_A5

This section encompasses the complexation of the ligands **L1**, **L_P2-L_P7**, and **L_A2-L_A5** towards the respective heteroleptic Cu(I) complexes. The general synthetic procedure (GSP) is described hereafter, followed by details about chemical quantities used, yields obtained, and analytical data for each complex.

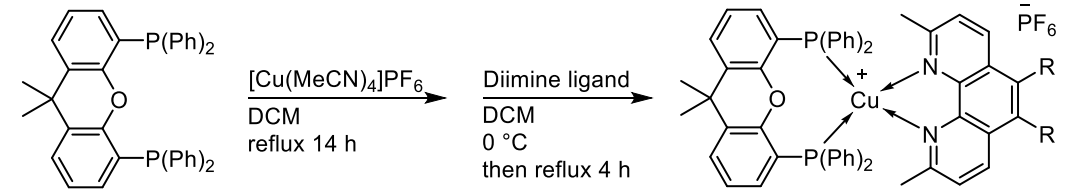

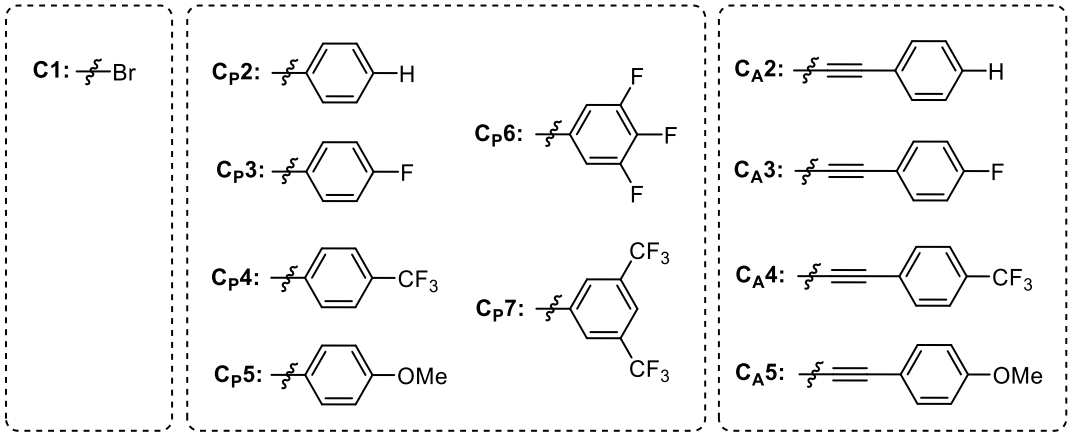

GSP: Into a dried Schlenk-tube equipped with a stir bar tetrakis(acetonitrile)-copper(I) hexafluorophosphate ([Cu(MeCN)$_4$]PF$_6$, 1.0 eq.) and xantphos (xant, 1.0 eq.) were added. The vessel was linked to a condenser and the whole apparatus was put under vacuum and refilled with nitrogen three times. Dry and degassed DCM was added and the solution refluxed overnight.
After cooling to 0 °C, a solution of the respective diimine ligand (1.0 eq.) in dry and degassed DCM was added dropwise carefully. Then, the solution was stirred for another 30 minutes and finally refluxed for four hours. The heteroleptic target complex was precipitated with *n*-hexane. The crystalline solid was collected and washed with *n*-hexane. The solid was re-dissolved in acetonitrile, the solution filtered until clear and finally dried *in vacuo*.

C1: [(xant)Cu(L1)]PF$_6$

[Cu(MeCN)$_4$]PF$_6$	Xantphos	Diimine	DCM	Yield
52.9 mg (0.115 mmol)	66.5 mg (0.115 mmol)	42.1 mg (0.115 mmol)	13 mL + 13 mL	122.3 mg (92 %)

$C_{53}H_{42}Br_2CuF_6N_2OP_3$ (M = 1153.20 g/mol). **^{1}H NMR** (CD_3CN, 500 MHz): δ = 8.74 (*d*, *J* = 8.8 Hz, 2H, Ar-*H*); 7.81 (*d*, *J* = 7.6 Hz, 2H, Ar-*H*), 7.67 (*d*, *J* = 8.8 Hz, 2H, Ar-*H*), 7.30 (*m*, 6H, Ar-*H*), 7.10 (*m*, 16H, Ar-*H*), 7.05 (*m*, 2H, Ar-*H*), 2.32 (*s*, 6H, C*H*$_3$), 1.76 (*s*, 6H, C*H*$_3$). **^{13}C NMR** (CD_3CN, 500 MHz): δ = 159.65, 154.37, 142.13, 138.01, 133.55, 132.55, 130.9, 129.95, 129.69, 128.31, 127.76, 127.31, 126.53, 125.08, 123.71, 120.88, 35.6, 27.68, 26.36. **^{31}P NMR** (CD_3CN, 400 MHz): -12.70 (*s*, Ar-*P*), -144.62 (*qi*, *J* = 708 Hz, *P*F$_6$). **HRMS** (ESI) *m/z*: calcd. for $[C_{53}H_{42}Br_2CuN_2OP_2]^+$: 1007.0415; found: 1007.0399.

C_P2: [(xant)Cu(L_P2)]PF_6

$[Cu(MeCN)_4]PF_6$	Xantphos	Diimine	DCM	Yield
46.6 mg (0.125 mmol)	72.3 mg (0.125 mmol)	45.1 mg (0.125 mmol)	13 mL + 13 mL	136.3 mg (95 %)

$C_{65}H_{52}CuF_6N_2OP_3$ (M = 1147.60 g/mol). **^{1}H NMR** (CD_3CN, 400 MHz): δ = 7.80 (*t*, *J* = 8.1 Hz, 4H, Ar-*H*); 7.46 (*d*, *J* = 8.6 Hz, 2H, Ar-*H*), 7.37 (*m*, 10H, Ar-*H*), 7.28 (*t*, *J* = 7.6 Hz, 2H, Ar-*H*), 7.22 (*m*, 4H, Ar-*H*), 7.15 (*m*, 16H, Ar-*H*), 7.08 (*m*, 2H, Ar-*H*), 2.32 (*s*, 6H, CH_3), 1.75 (*s*, 6H, CH_3). **^{13}C NMR** (CD_3CN, 500 MHz): 157.77, 154.32, 141.66, 136.50, 135.98, 135.72, 133.36, 132.43, 131.00, 130.24, 129.72, 129.50, 128.11, 127.56, 127.47, 127.22, 127.04, 124.85, 124.76, 121.02, 35.42, 27.44, 26.20. **^{31}P NMR** (CD_3CN, 400 MHz): -12.90 (*s*, Ar-*P*), -144.62 (*qi*, *J* = 701 Hz, *P*F_6). **HRMS** (ESI) *m/z*: calcd. for $[C_{65}H_{52}CuN_2OP_2]^+$: 1001.2845; found: 1001.2845.

C_P3: [(xant)Cu(L_P3)]PF_6

$[Cu(MeCN)_4]PF_6$	Xantphos	Diimine	DCM	Yield
46.6 mg (0.125 mmol)	72.3 mg (0.125 mmol)	49.6 mg (0.125 mmol)	13 mL + 13 mL	101.3 mg (67 %)

$C_{65}H_{50}CuF_8N_2OP_3$ (M = 1183.58 g/mol). **^{1}H NMR** (CD_3CN, 500 MHz): δ = 7.85 (*d*, *J* = 8.6 Hz, 2H, Ar-*H*); 7.80 (*d*, *J* = 7.5 Hz, 2H, Ar-*H*), 7.49 (*d*, *J* = 8.5 Hz, 2H, Ar-*H*), 7.38 (*m*, 4H, Ar-*H*), 7.29 (*t*, *J* = 7.7 Hz, 2H, Ar-*H*), 7.22 (*m*, 4H, Ar-*H*), 7.15 (*m*, 20H, Ar-*H*), 7.08 (*m*, 2H, Ar-*H*), 2.33 (*s*, 6H, CH_3), 1.76 (*s*, 6H, CH_3). **^{13}C NMR** (CD_3CN, 500 MHz): δ = 162.89, , 160.94, 158.45, 154.64, 142.1, 136.24, 135.48, 133.73, 132.78, 132.59, 131.35, 130.08, 129.84, 128.46, 127.84, 127.45, 125.23, 121.34, 114.94, 114.77, 35.88, 27.88, 26.59. **^{19}F NMR** (CD_3CN, 400 MHz): -72.00, -73.86, -155.81. **^{31}P NMR** (CD_3CN, 400 MHz): -12.90 (*s*, Ar-*P*), -144.63 (*qi*, *J* = 708 Hz, *P*F_6). **HRMS** (ESI) *m/z*: calcd. for $[C_{65}H_{50}CuF_2N_2OP_2]^+$: 1037.2657; found: 1037.2658.

C_P4: [(xant)Cu(L_P4)]PF_6

$[Cu(MeCN)_4]PF_6$	Xantphos	Diimine	DCM	Yield
46.6 mg (0.125 mmol)	72.3 mg (0.125 mmol)	62.1 mg (0.125 mmol)	13 mL + 13 mL	142.9 mg (89 %)

$C_{67}H_{50}CuF_{12}N_2OP_3$ (M = 1283.60 g/mol). **^{1}H NMR** (CD_3CN, 500 MHz): δ = 7.67 (*t*, *J* = 9.5 Hz, 4H, Ar-*H*); 7.58 (*d*, *J* = 8.2 Hz, 4H, Ar-*H*), 7.34 (*d*, *J* = 8.5 Hz, 2H, Ar-*H*), 7.28 (*m*, 8H, Ar-*H*), 7.17 (*t*, *J* = 7.5 Hz, 2H, Ar-*H*), 7.03 (*m*, 16H, Ar-*H*), 6.96 (*m*, 2H, Ar-*H*), 2.21 (*s*, 6H, CH_3), 1.64 (*s*, 6H, CH_3). **^{13}C NMR** (CD_3CN, 500 MHz): 158.83, 154.66, 142.15, 140.63, 136.12, 134.92, 133.74, 132.77, 131.38, 131.17, 130.08, 129.86, 129.20, 128.93, 128.47, 127.88, 126.88, 125.43, 125.22, 124.94, 121.34, 35.76, 27.81, 26.62. **^{19}F NMR** ($CDCl_3$, 400 MHz): -62.69, -72.78, -74.77. **^{31}P NMR** ($CDCl_3$, 400 MHz): -12.09 (*s*, Ar-*P*), -144.47 (*qi*, *J* = 711 Hz, *P*F_6). **HRMS** (ESI) *m/z*: calcd. for $[C_{67}H_{50}CuF_6N_2OP_2]^+$: 1137.2593; found: 1137.2591.

C_P5: [(xant)Cu(L_P5)]PF_6

[Cu(MeCN)$_4$]PF_6	Xantphos	Diimine	DCM	Yield
46.6 mg (0.125 mmol)	72.3 mg (0.125 mmol)	52.6 mg (0.125 mmol)	13 mL + 13 mL	111.1 mg (73 %)

$C_{67}H_{56}CuF_6N_2O_3P_3$ (M = 1207.65 g/mol). **^{1}H NMR** (CD_3CN, 400 MHz): δ = 7.86 (*d*, *J* = 8.5 Hz, 2H, Ar-*H*); 7.79 (*dd*, *J* = 7.9 Hz, *J* = 1.2 Hz, 2H, Ar-*H*), 7.46 (*d*, *J* = 8.5 Hz, 2H, Ar-*H*), 7.37 (*m*, 4H, Ar-*H*), 7.28 (*t*, *J* = 7.6 Hz, 2H, Ar-*H*), 7.13 (*m*, 20H, Ar-*H*), 7.06 (*m*, 20H, Ar-*H*), 6.92 (*d*, *J* = 8.5 Hz, 4H, Ar-*H*), 3.81 (*s*, 6H, OCH_3), 2.31 (*s*, 6H, CH_3), 1.76 (*s*, 6H, CH_3). **^{13}C NMR** (CD_3CN, 500 MHz): 158.54, 157.75, 154.49, 141.82, 136.20, 135.93, 133.54, 132.59, 131.61, 131.19, 129.88, 129.64, 128.88, 128.26, 127.77, 127.62, 125.01, 124.81, 121.21, 113.06, 54.61, 35.59, 27.59, 26.34. **^{31}P NMR** (CD_3CN, 400 MHz): -12.71 (*s*, Ar-*P*), -144.63 (*qi*, *J* = 701 Hz, *P*F_6). **HRMS** (ESI) *m/z*: calcd. for $[C_{67}H_{56}CuN_2O_3P_2]^+$: 1061.3057; found: 1061.3061.

C_P6: [(xant)Cu(L_P6)]PF_6

[Cu(MeCN)$_4$]PF_6	Xantphos	Diimine	DCM	Yield
49.2 mg (0.132 mmol)	76.4 mg (0.132 mmol)	61.8 mg (0.132 mmol)	13 mL + 13 mL	132.3 mg (82 %)

$C_{65}H_{46}CuF_{12}N_2OP_3$ (M = 1255.54 g/mol). **^{1}H NMR** ($CDCl_3$, 700 MHz): δ = 7.79 (*d*, *J* = 8.5 Hz, 2H, Ar-*H*); 7.65 (*d*, *J* = 7.9 Hz, 2H, Ar-*H*), 7.49 (*d*, *J* = 8.5 Hz, 2H, Ar-*H*), 7.29 (*t*, *J* = 7.0 Hz, 4H, Ar-*H*), 7.20 (*t*, *J* = 7.7 Hz, 2H, Ar-*H*), 7.07 (*m*, 16H, Ar-*H*), 6.97 (*m*, 2H, Ar-*H*), 6.80 (*t*, *J* = 6.3 Hz, 2H, Ar-*H*), 2.30 (*s*, 6H, CH_3), 1.74 (*s*, 6H, CH_3). **^{13}C NMR** (CD_3CN, 500 MHz): 158.99, 153.68, 136.01, 133.56, 133.04, 132.67, 131.11, 130.87, 129.93, 129.7, 128.56, 128.39, 127.72, 126.38, 125.48, 125.08, 125.05, 115.12, 114.97, 114.62, 35.66, 27.65, 26.45. **^{19}F NMR** ($CDCl_3$, 400 MHz): -72.00, -74.74, -132.11, -159.17. **^{31}P NMR** ($CDCl_3$, 400 MHz): -12.20 (*s*, Ar-*P*), -144.62 (*qi*, *J* = 712 Hz, *P*F_6). **HRMS** (ESI) *m/z*: calcd. for $[C_{65}H_{46}CuF_6N_2OP_2]^+$: 1109.2280; found: 1109.2284.

C_P7: [(xant)Cu(L_P7)]PF_6

[Cu(MeCN)$_4$]PF_6	Xantphos	Diimine	DCM	Yield
46.6 mg (0.125 mmol)	72.3 mg (0.125 mmol)	79.1 mg (0.125 mmol)	13 mL + 13 mL	132.7 mg (75 %)

$C_{69}H_{48}CuF_{18}N_2OP_3$ (M = 1419.59 g/mol). **^{1}H NMR** (CD_3CN, 500 MHz): δ = 8.01 (s, 2H, Ar-*H*); 7.94 (*d*, *J* = 8.6 Hz, 2H, Ar-*H*), 7.81 (*d*, *J* = 7.6 Hz, 2H, Ar-*H*), 7.76 (*m*, 4H, Ar-*H*), 7.57 (*d*, *J* = 8.6 Hz, 2H, Ar-*H*), 7.38 (*m*, 4H, Ar-*H*), 7.30 (*t*, *J* = 7.6 Hz, 2H, Ar-*H*), 7.16 (*q*, *J* = 3.6 Hz 16H, Ar-*H*), 7.03 (*m*, 2H, Ar-*H*), 2.36 (*s*, 6H, CH_3), 1.77 (*s*, 6H, CH_3). **^{13}C NMR** (CD_3CN, 500 MHz): 159.51, 154.54, 142.24, 138.32, 136.07, 134.12, 133.65, 132.67, 131.21, 131.04, 131.02, 129.96, 129.73, 128.4, 27.7, 126.11, 125.71, 125.11, 123.94, 121.78, 121.14, 35.78, 27.61. **^{19}F NMR** (CD_3CN, 400 MHz): -63.64, -72.03, -73.89. **^{31}P NMR** (CD_3CN, 400 MHz): -13.02 (*s*, Ar-*P*), -144.63 (*qi*, *J* = 701 Hz, *P*F_6). **HRMS** (ESI) *m/z*: calcd. for $[C_{69}H_{48}CuF_{12}N_2OP_2]^+$: 1273.2341; found: 1273.2337.

C_A2: [(xant)Cu(L_A2)]PF6

$[Cu(MeCN)_4]PF_6$	Xantphos	Diimine	DCM	Yield
59.6 mg (0.160 mmol)	95.6 mg (0.160 mmol)	65.4 mg (0.160 mmol)	13 mL + 13 mL	179.2 mg (94 %)

$C_{69}H_{52}CuF_6N_2OP_3$ (M = 1195.65 g/mol). **^{1}H NMR** (CD_3CN, 400 MHz): δ = 8.84 (*d, J* = 8.5 Hz, 2H, Ar-*H*); 7.98 (*m,* 6H, Ar-*H*), 7.65 (*d*, *J* = 8.5 Hz, 2H, Ar-*H*), 7.52 (*m*, 6H, Ar-*H*), 7.28 (*m*, 6H, Ar-*H*), 7.09 (*m*, 16H, Ar-*H*), 6.98 (*m*, 2H, Ar-*H*), 2.30 (*s*, 6H, C*H*$_3$), 1.74 (*s*, 6H, C*H*$_3$). **^{13}C NMR** (CD_3CN, 500 MHz): 159.76, 154.70, 142.17, 136.21, 133.79, 132.79, 131.69, 131.24, 130.11, 129.86, 129.70, 128.84, 128.51, 127.81, 126.92, 126.04, 125.26, 122.13, 121.87, 121.29, 100.81, 84.61, 35.81, 27.71, 26.57. **^{31}P NMR** (CD_3CN, 400 MHz): -12.99 (*s*, Ar-*P*), -144.62 (*qi*, *J* = 706 Hz, *P*F_6). **HRMS** (ESI) *m/z*: calcd. for $[C_{69}H_{52}CuN_2OP_2]^+$: 1049.2845; found: 1049.2810.

C_A3: [(xant)Cu(L_A3)]PF_6

$[Cu(MeCN)_4]PF_6$	Xantphos	Diimine	DCM	Yield
59.6 mg (0.160 mmol)	92.6 mg (0.160 mmol)	71.1 mg (0.160 mmol)	13 mL + 13 mL	168.5 mg (86 %)

$C_{69}H_{50}CuF_8N_2OP_3$ (M = 1231.63 g/mol). **^{1}H NMR** (CD_3CN, 400 MHz): δ = 8.85 (*d, J* = 8.5 Hz, 2H, Ar-*H*); 7.82 (*m*, 6H, Ar-*H*), 7.68 (*d*, *J* = 8.5 Hz, 2H, Ar-*H*), 7.30 (*m*, 10H, Ar-*H*), 7.11 (*m*, 16H, Ar-*H*), 7.38 (*m*, 2H, Ar-*H*), 2.32 (*s*, 6H, C*H*$_3$), 1.76 (*s*, 6H, C*H*$_3$). **^{13}C NMR** (CD_3CN, 500 MHz): 163.03, 159.59, 154.49, 141.94, 136.00, 133.86, 133.59, 132.59, 131.04, 129.90, 129.67, 128.32, 127.62, 126.64, 125.85, 125.07, 121.78, 121.13, 118.01, 115.89, 99.47, 84.15, 35.61, 27.49, 26.38. **^{19}F NMR** (CD_3CN, 400 MHz): -72.09, -73.93, -110.19. **^{31}P NMR** (CD_3CN, 400 MHz): -12.97 (*s*, Ar-*P*), -144.63 (*qi*, *J* = 701 Hz, *P*F_6). **HRMS** (ESI) *m/z*: calcd. for $[C_{69}H_{50}CuF_2N_2OP_2]^+$: 1085.2657; found: 1085.2614.

C_A4: [(xant)Cu(L_A4)]PF_6

$[Cu(MeCN)_4]PF_6$	Xantphos	Diimine	DCM	Yield
33.5 mg (0.090 mmol)	52.1 mg (0.090 mmol)	49.0 mg (0.090 mmol)	10 mL + 10 mL	108.3 mg (90 %)

$C_{71}H_{50}CuF_{12}N_2OP_3$ (M = 1331.64 g/mol). **^{1}H NMR** (CD_3CN, 500 MHz): δ = 8.85 (*d, J* = 8.2 Hz, 2H, Ar-*H*); 7.96 (*d, J* = 8.2 Hz, 4H, Ar-*H*), 7.85 (*d*, *J* = 8.2 Hz, 4H, Ar-*H*), 7.81 (*d, J* = 8.2 Hz, 2H, Ar-*H*), 7.69 (*d, J* = 8.2 Hz, 2H, Ar-*H*), 7.31 (*m*, 6H, Ar-*H*), 7.12 (*m*, 16H, Ar-*H*), 7.02 (*m*, 2H, Ar-*H*), 2.33 (*s*, 6H, C*H*$_3$), 1.77 (*s*, 6H, C*H*$_3$). **^{13}C NMR** (CD_3CN, 500 MHz): 160.15, 154.64, 142.24, 136.18, 133.75, 132.75, 132.28, 131.16, 130.18, 130.07, 129.85, 128.50, 127.83, 126.69, 126.16, 125.82, 125.68, 125.25, 122.84, 122.06, 121.18, 99.12, 86.46, 5.78, 27.69, 26.59. **^{19}F NMR** (CD_3CN, 400 MHz): -63.36, -71.95, -73.88. **^{31}P NMR** (CD_3CN, 400 MHz): -12.92 (*s*, Ar-*P*), -144.63 (*qi*, *J* = 704 Hz, *P*F_6). **HRMS** (ESI) *m/z*: calcd. for $[C_{71}H_{50}CuF_6N_2OP_2]^+$: 1185.2593; found: 1185.2593.

C_A5: [(xant)Cu(L_A5)]PF_6

[Cu(MeCN)$_4$]PF_6	Xantphos	Diimine	DCM	Yield
33.5 mg (0.090 mmol)	52.1 mg 0.090 mmol)	42.2 mg (0.090 mmol)	10 mL + 10 mL	82.9 mg (73 %)

$C_{71}H_{56}CuF_6N_2O_3P_3$ (M = 1255.70 g/mol). **^{1}H NMR** (CD_3CN, 500 MHz): δ = 8.82 (*d*, *J* = 8.4 Hz, 2H, Ar-*H*); 8.80 (*d*, *J* = 7.4 Hz, 2H, Ar-*H*), 7.37 (*d*, *J* = 8.8 Hz, 4H, Ar-*H*), 7.65 (*d*, *J* = 8.4 Hz, 2H, Ar-*H*), 7.31 (*m*, 6H, Ar-*H*), 7.11 (*m*, 16H, Ar-*H*), 7.07 (*d*, *J* = 8.2 Hz, 4H, Ar-*H*), 7.00 (*m*, 2H, Ar-*H*), 3.90 (*s*, 6H, OCH_3), 2.30 (*s*, 6H, CH_3), 1.76 (*s*, 6H, CH_3). **^{13}C NMR** (CD_3CN, 500 MHz): 160.56, 159.19, 154.51, 141.80, 135.97, 133.59, 133.16, 132.59, 131.05, 129.88, 129.66, 128.31, 127.59, 126.76, 125.70, 125.06, 121.67, 121.22, 114.27, 113.61, 100.88, 83.60, 54.93, 35.61, 27.47, 26.34. **^{31}P NMR** (CD_3CN, 400 MHz): -12.96 (*s*, Ar-*P*), -144.61 (*qi*, *J* = 706 Hz, PF_6). **IR**: ν(C≡C) = 2190.19 cm^{-1}. **HRMS** (ESI) *m/z*: calcd. for $[C_{71}H_{56}CuN_2O_3P_2]^+$: 1109.3057; found: 1109.3059.

3 NMR spectra of XPhos-Pd-G2 and the Complexes C1, L_P2-L_P7, and L_A2-L_A5

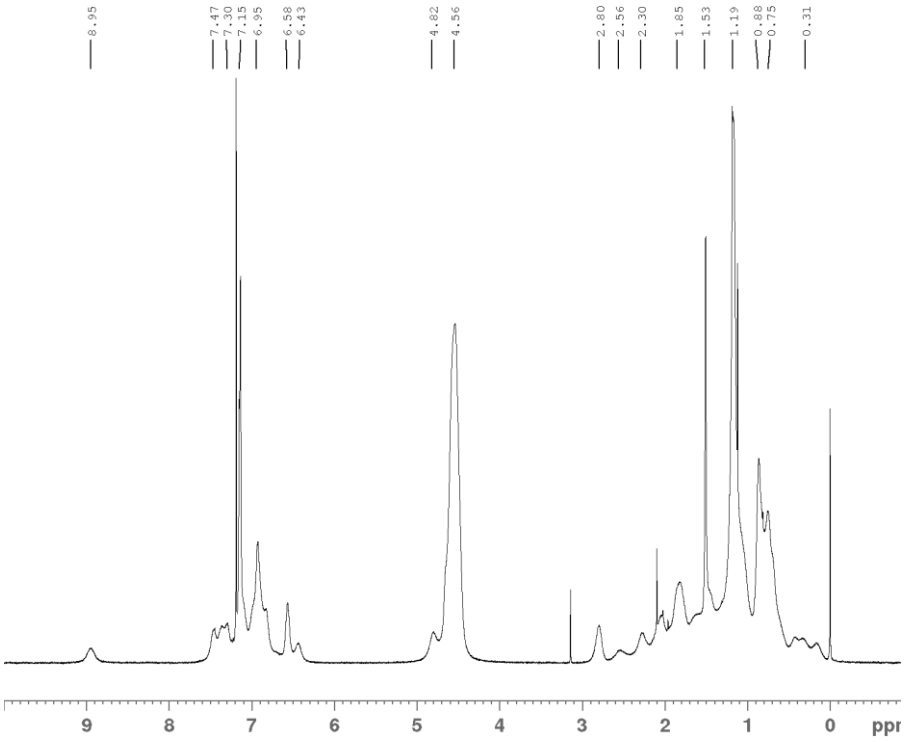

Figure S1.1: ^{1}H NMR spectrum of the precatalyst XPhos-Pd-G2 ($CDCl_3$, 400 MHz).

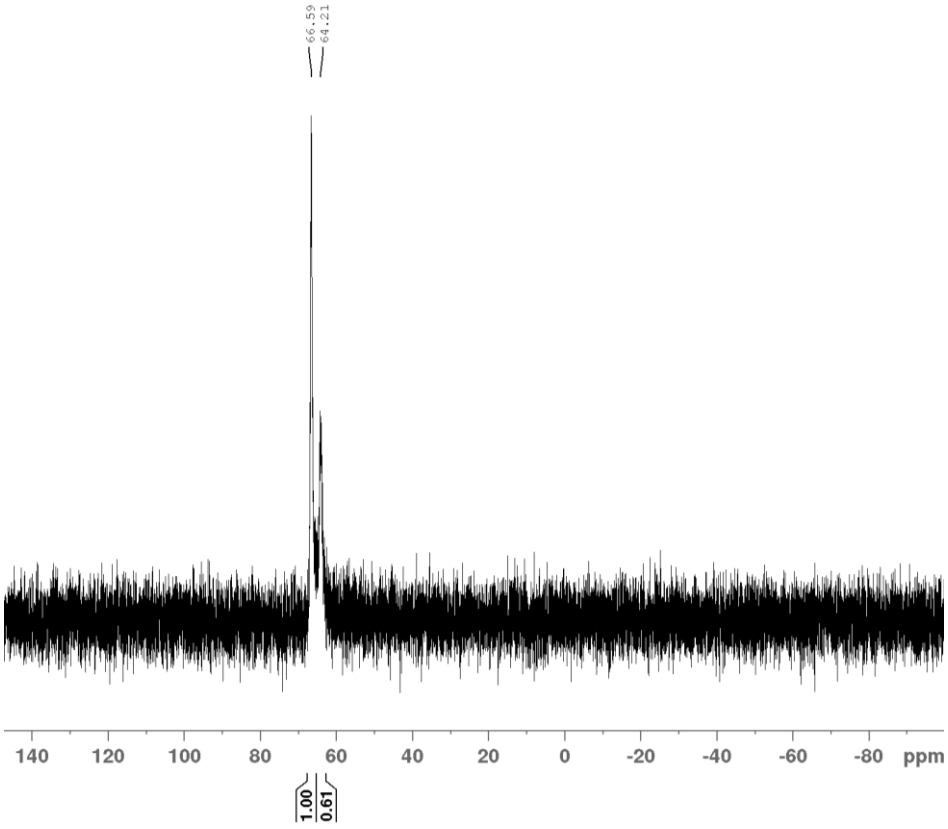

Figure S1.2: ^{31}P NMR spectrum of the precatalyst XPhos-Pd-G2 ($CDCl_3$, 400 MHz).

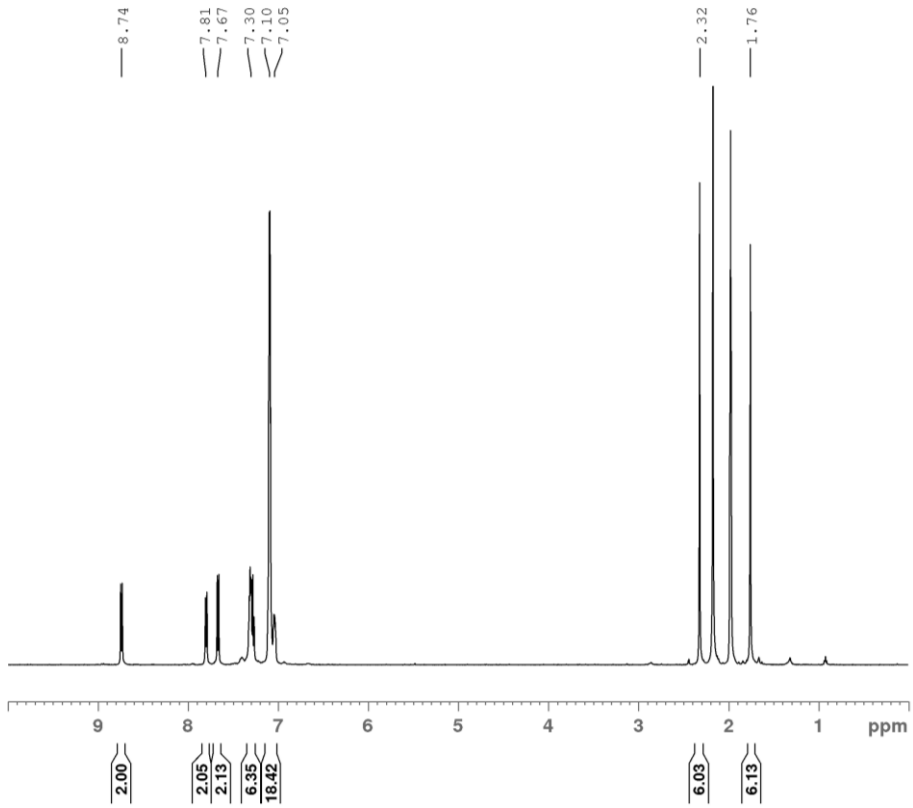

Figure S1.3: ^{1}H NMR spectrum of [(xant)Cu(**L1**)]PF_6 **C1** (CD_3CN, 500 MHz).

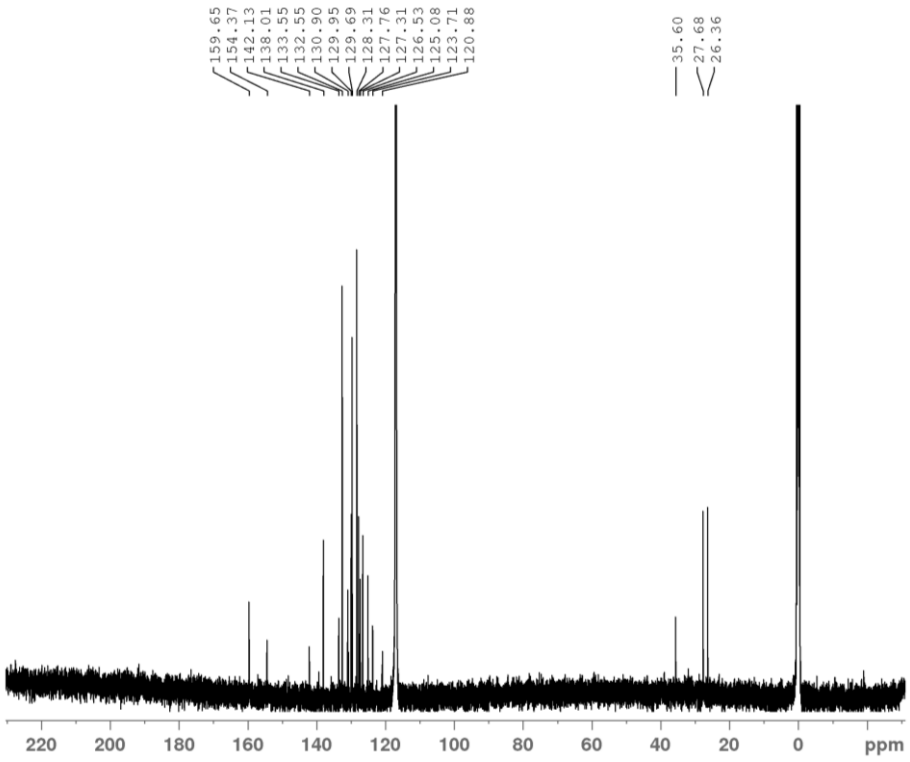

Figure S1.4: ^{13}C NMR spectrum of [(xant)Cu(**L1**)]PF_6 **C1** (CD_3CN, 500 MHz).

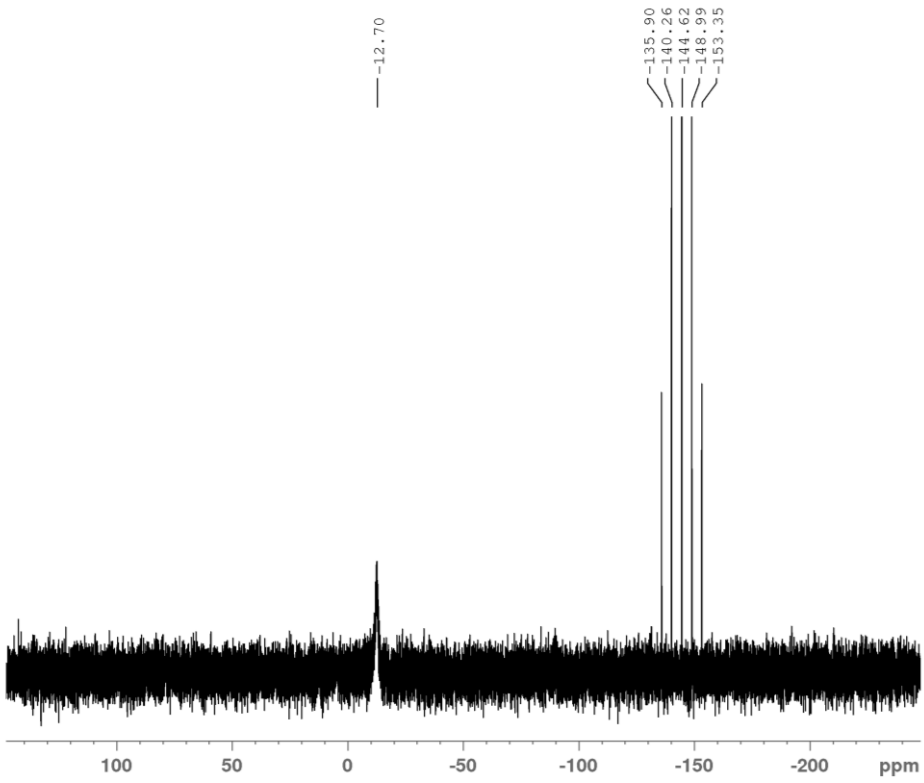

Figure S1.5: ^{31}P NMR spectrum of [(xant)Cu(**L1**)]PF_6 **C1** (CD_3CN, 400 MHz).

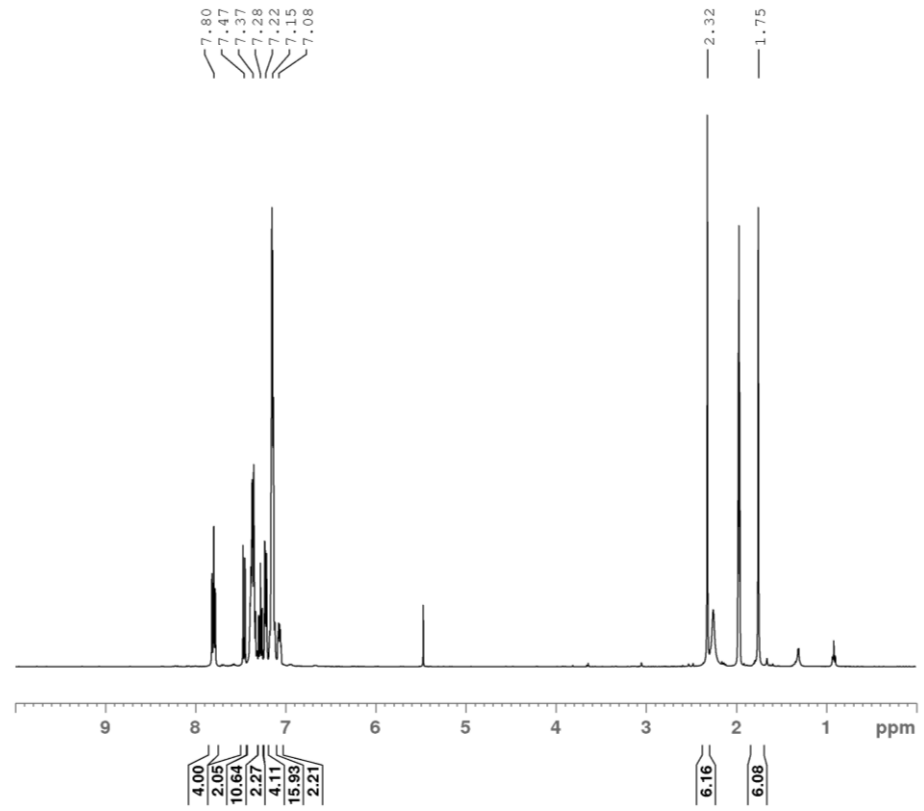

Figure S1.6: ^{1}H NMR spectrum of [(xant)Cu(**L$_P$2**)]PF_6 **C$_P$2** (CD_3CN, 400 MHz).

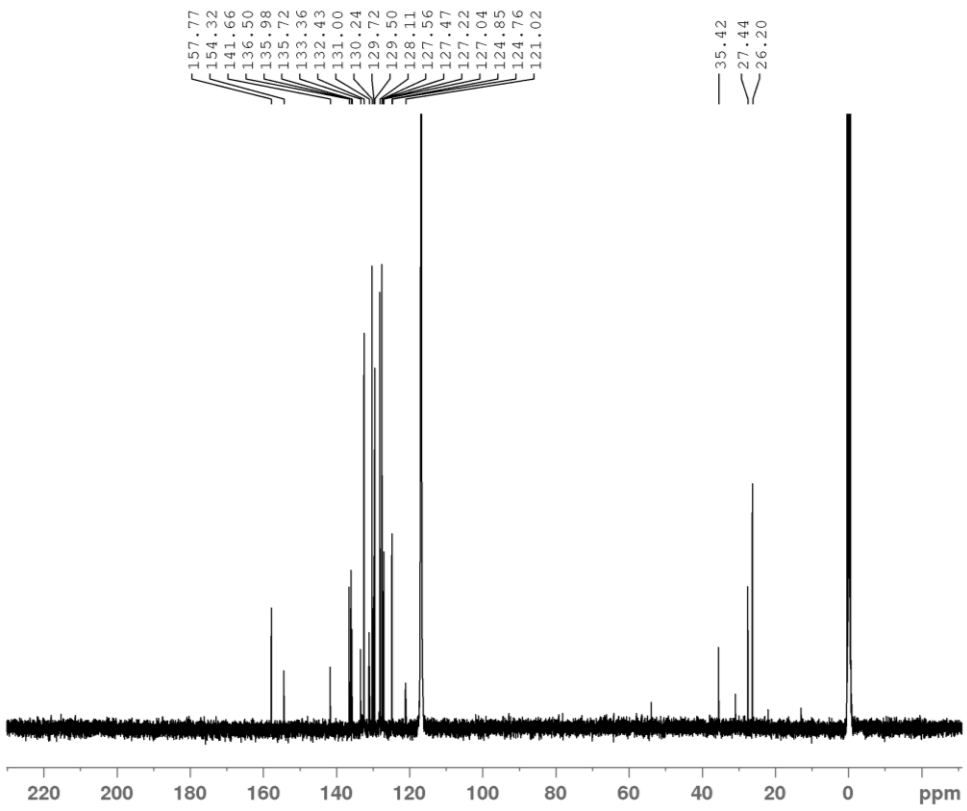

Figure S1.7: ^{13}C NMR spectrum of [(xant)Cu(**L$_P$2**)]PF_6 **C$_P$2** (CD_3CN, 500 MHz).

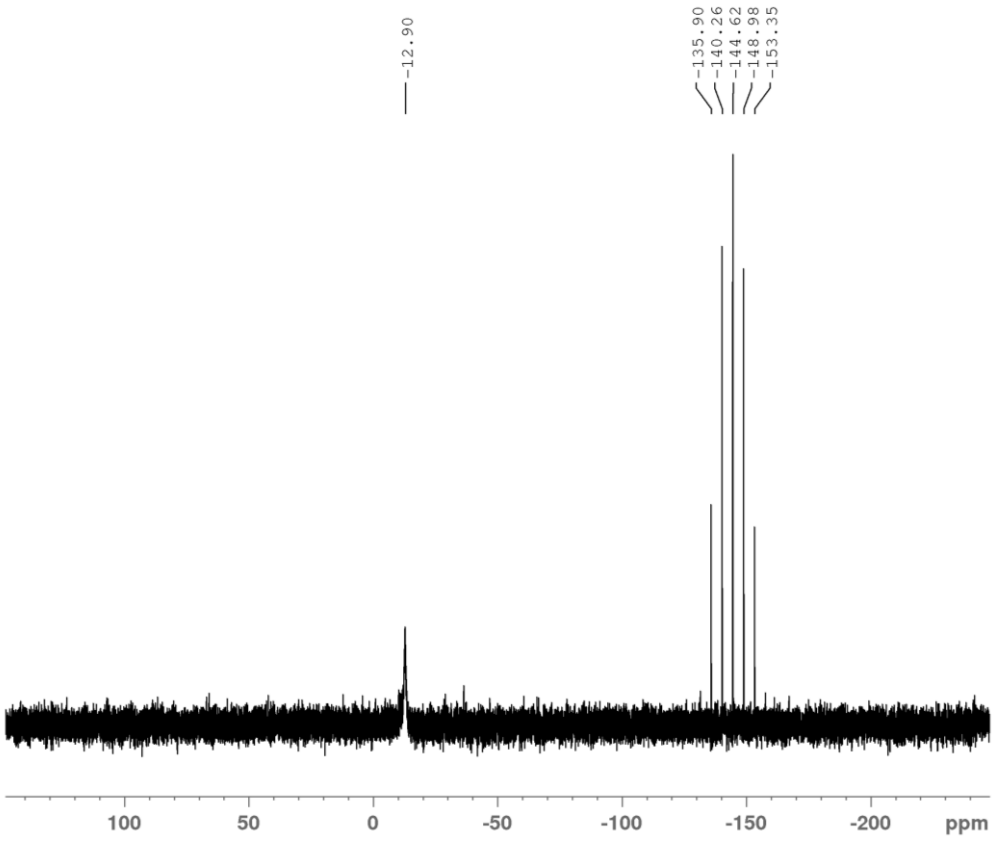

Figure S1.8: ^{31}P NMR spectrum of [(xant)Cu(**L$_P$2**)]PF_6 **C$_P$2** (CD_3CN, 400 MHz).

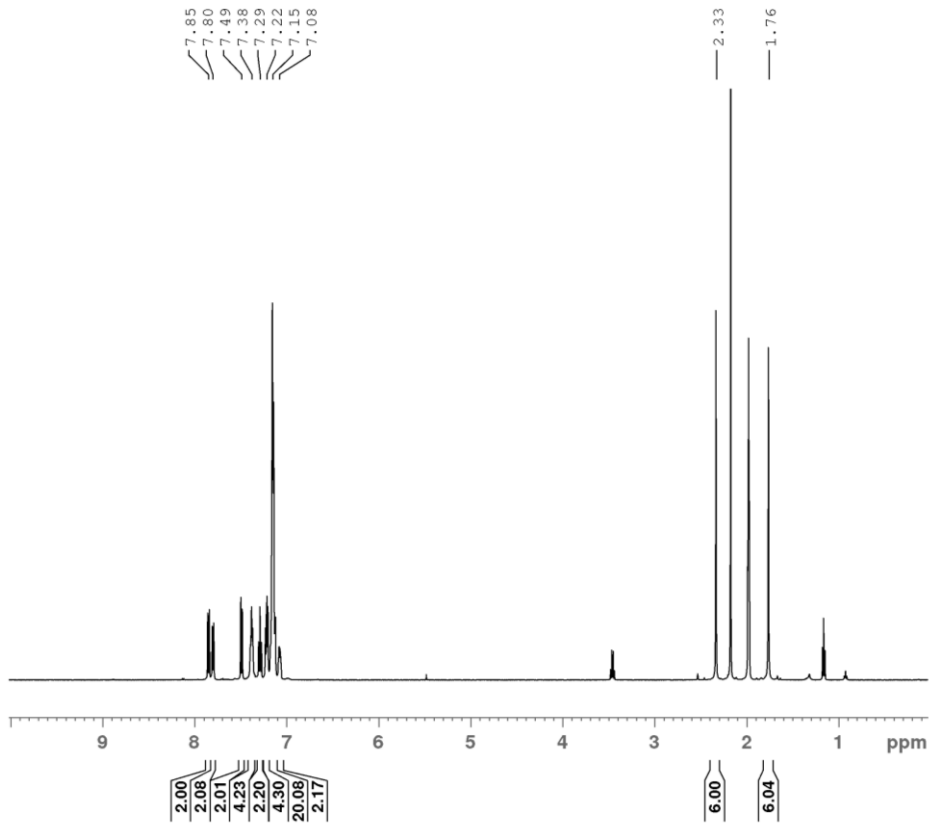

Figure S1.9: ^{1}H NMR spectrum of [(xant)Cu(**L$_P$3**)]PF_6 **C$_P$3** (CD_3CN, 500 MHz).

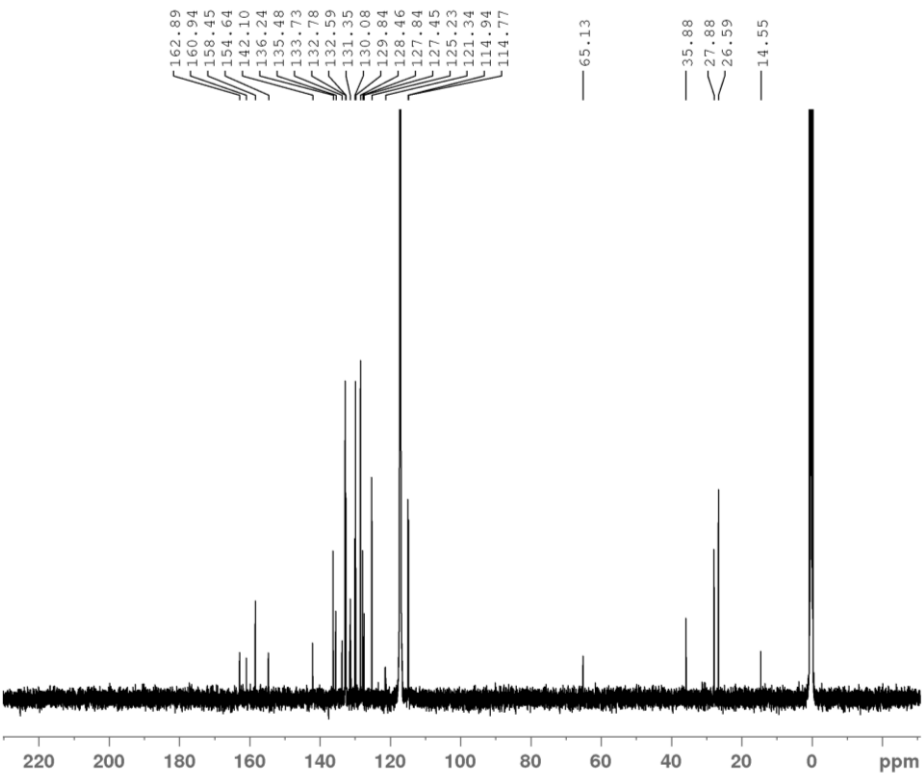

Figure S1.10: ^{13}C NMR spectrum of [(xant)Cu(**L$_P$3**)]PF_6 **C$_P$3** (CD_3CN, 500 MHz).

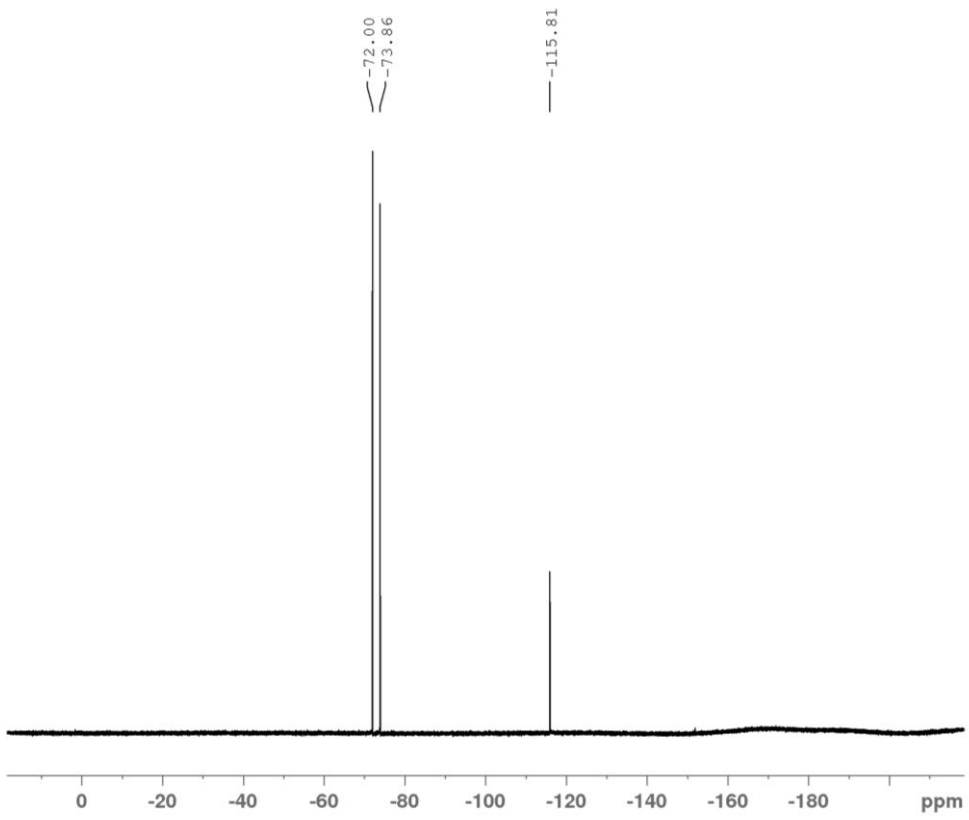

Figure S1.11: ^{19}F NMR spectrum of [(xant)Cu(**L$_P$3**)]PF_6 **C$_P$3** (CD_3CN, 400 MHz).

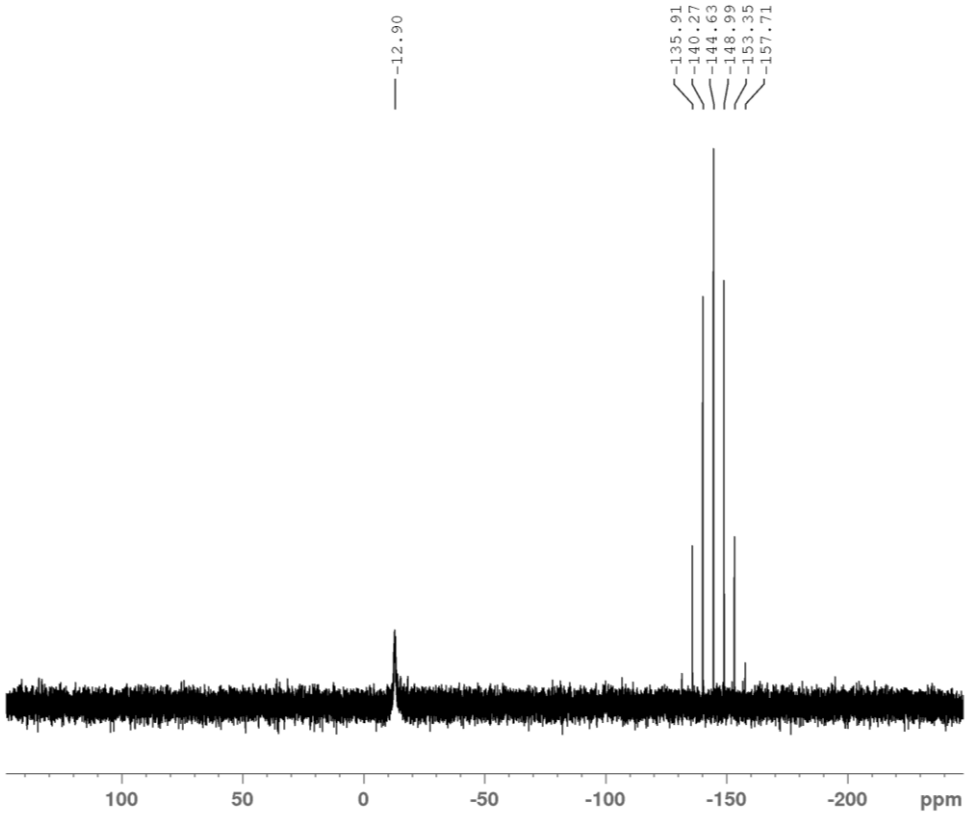

Figure S1.12: ^{31}P NMR spectrum of [(xant)Cu(**L$_P$3**)]PF_6 **C$_P$3** (CD_3CN, 400 MHz).

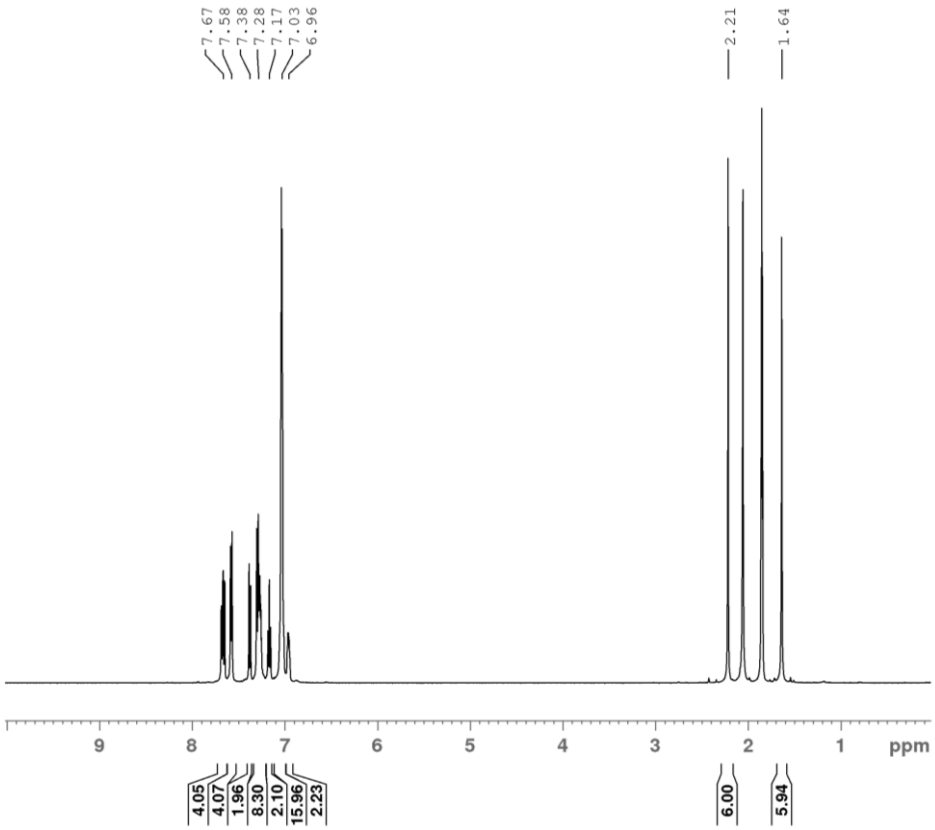

Figure S1.13: ^{1}H NMR spectrum of [(xant)Cu(**L$_P$4**)]PF$_6$ **C$_P$4** (CD_3CN, 500 MHz).

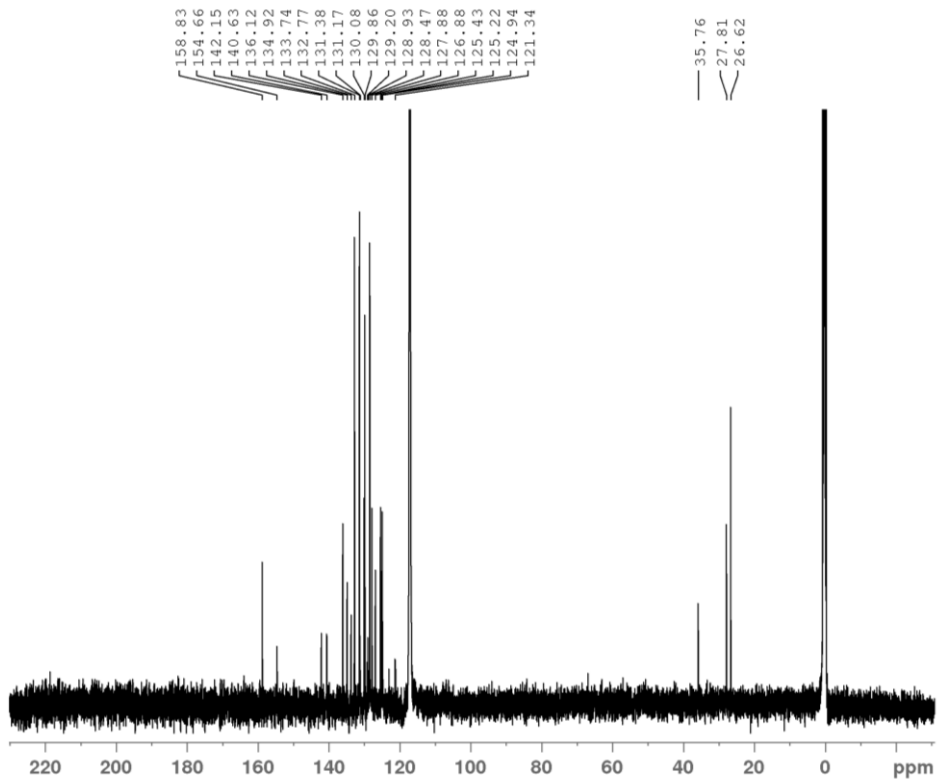

Figure S1.14: ^{13}C NMR spectrum of [(xant)Cu(**L$_P$4**)]PF$_6$ **C$_P$4** (CD_3CN, 500 MHz).

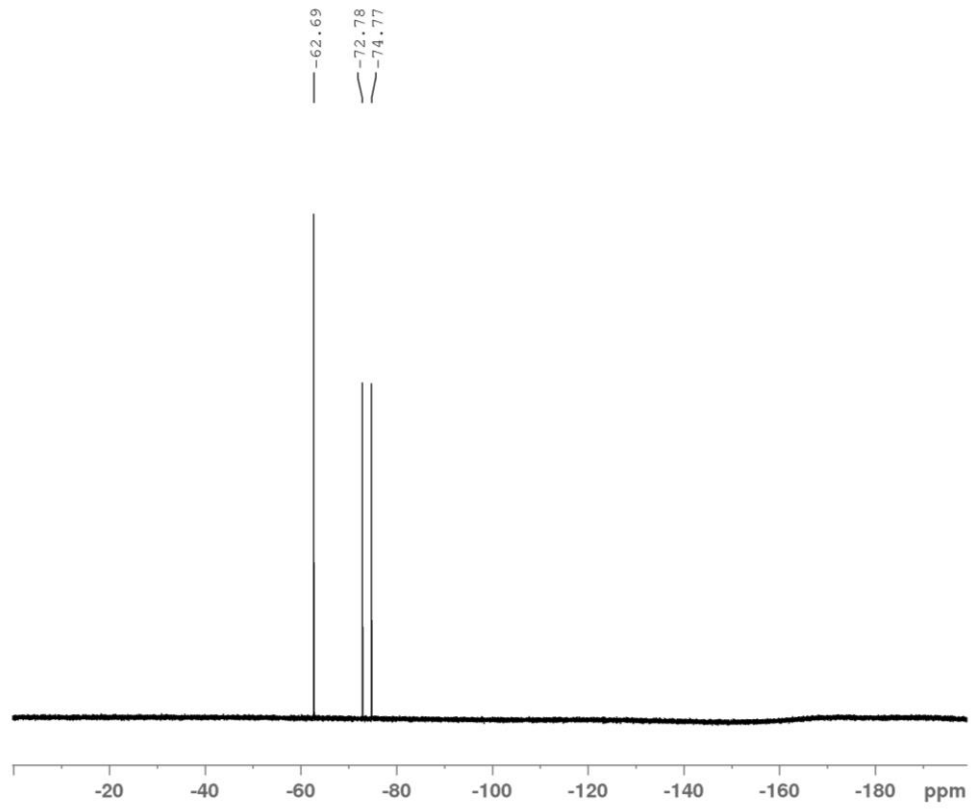

Figure S1.15: ^{19}F NMR spectrum of [(xant)Cu(**L$_P$4**)]PF_6 **C$_P$4** (CD_3CN, 400 MHz).

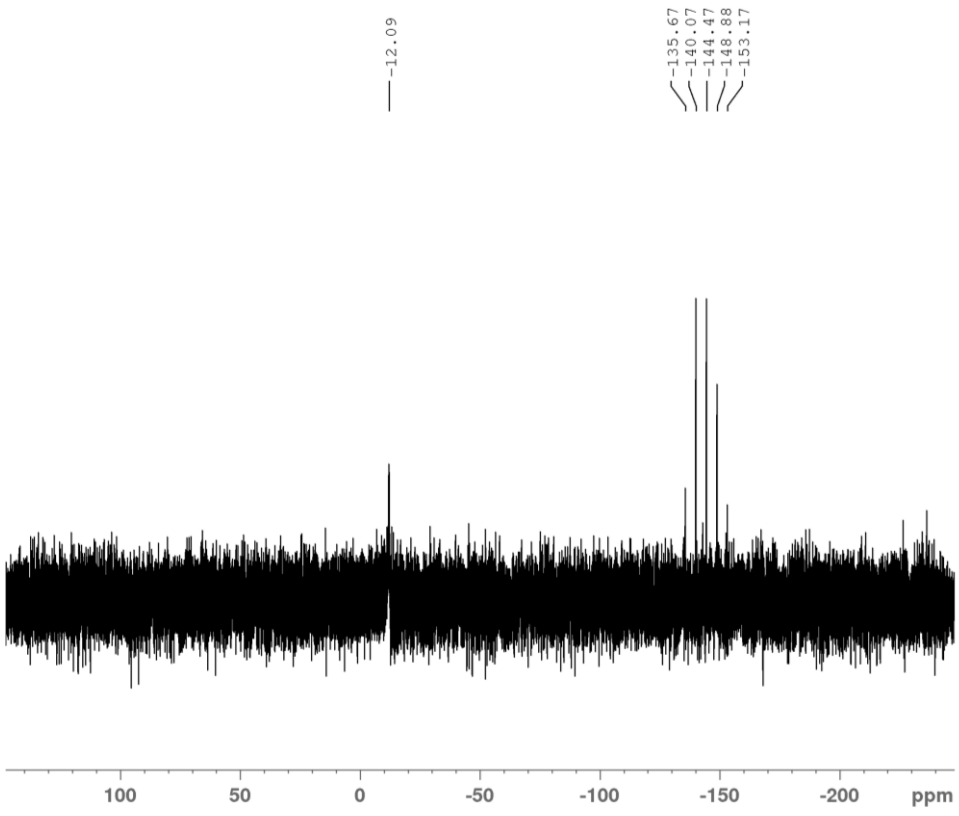

Figure S1.16: ^{31}P NMR spectrum of [(xant)Cu(**L$_P$4**)]PF_6 **C$_P$4** (CD_3CN, 400 MHz).

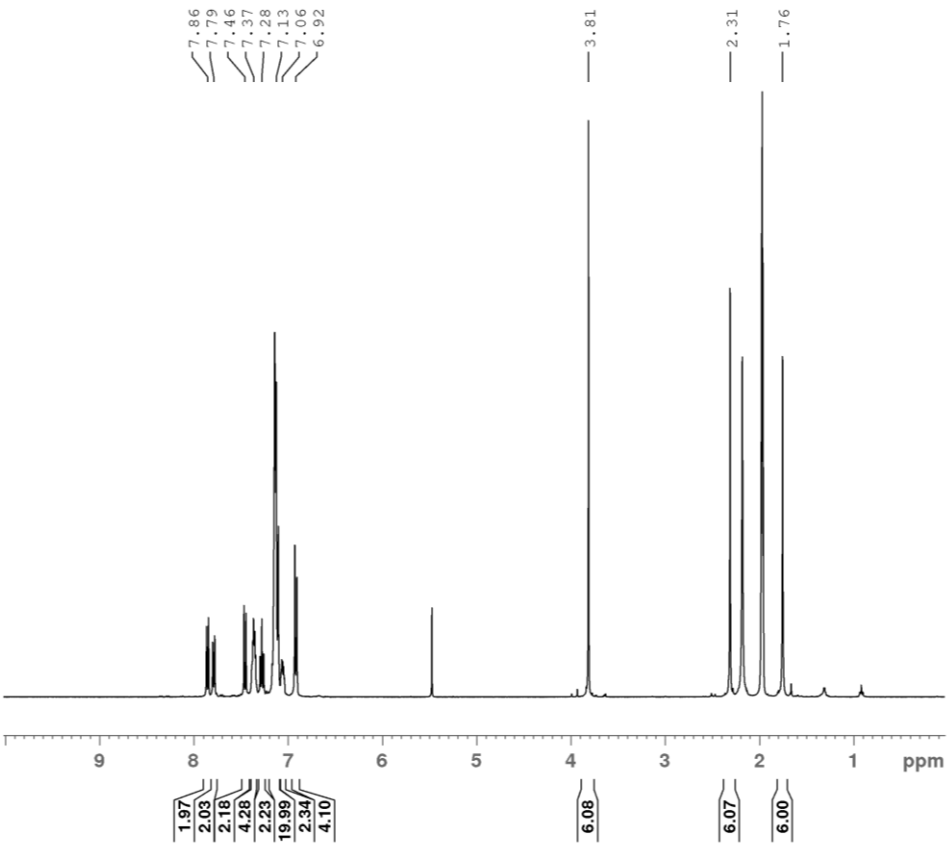

Figure S1.17: ^{1}H NMR spectrum of [(xant)Cu(**L$_P$5**)]PF_6 **C$_P$5** (CD_3CN, 400 MHz).

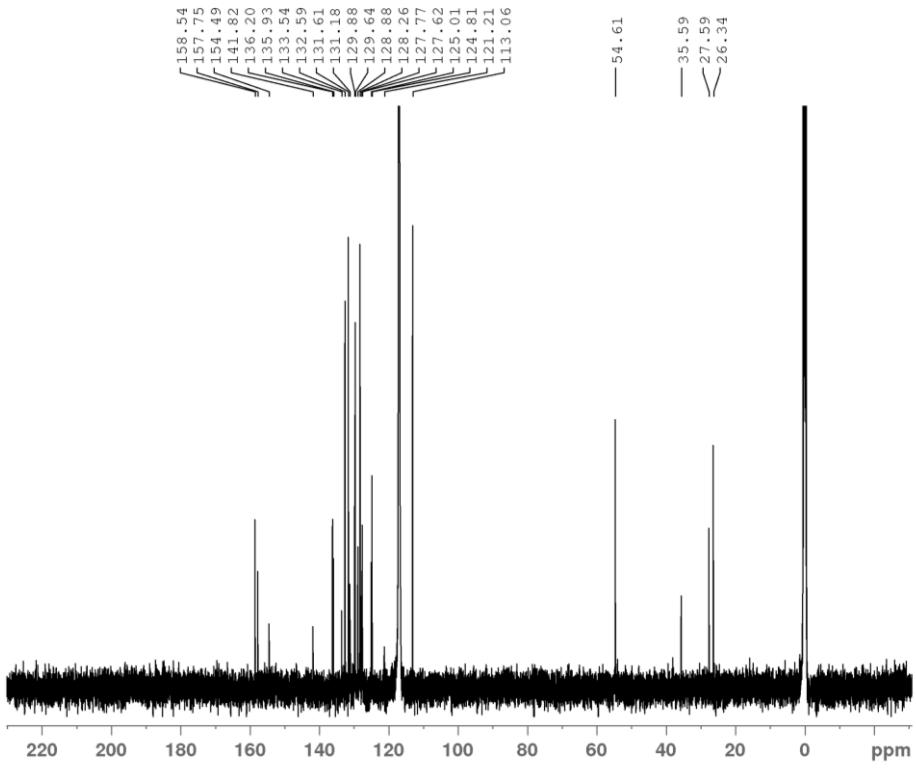

Figure S1.18: ^{13}C NMR spectrum of [(xant)Cu(**L$_P$5**)]PF_6 **C$_P$5** (CD_3CN, 500 MHz).

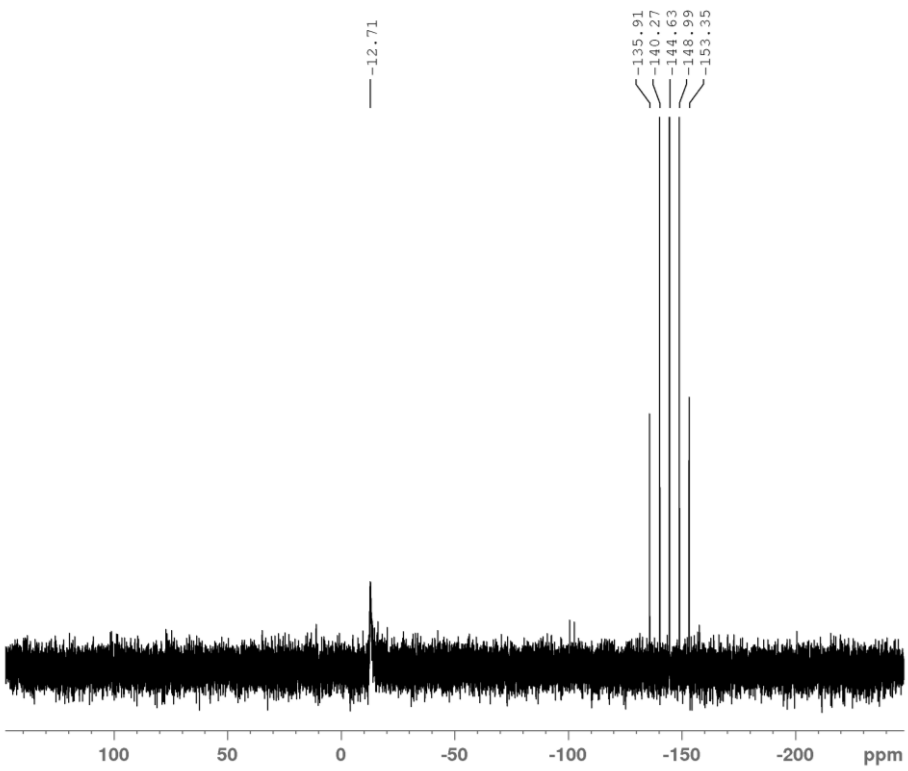

Figure S1.19: ^{31}P NMR spectrum of [(xant)Cu(**L$_P$5**)]PF_6 **C$_P$5** (CD_3CN, 400 MHz).

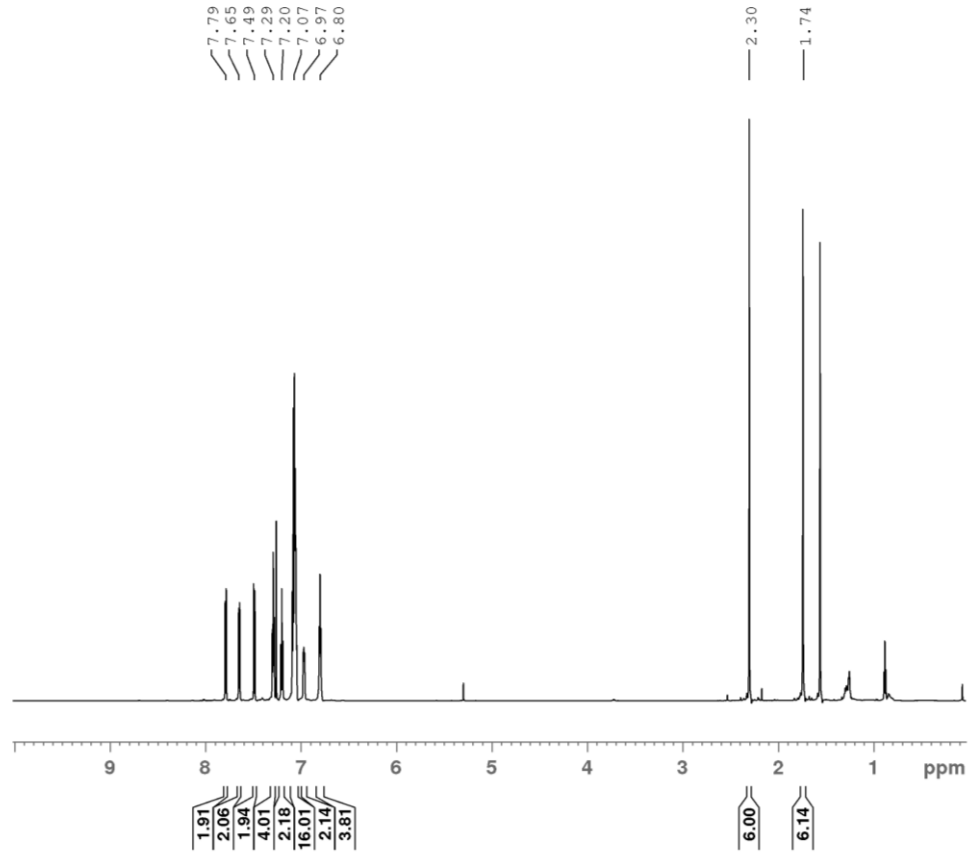

Figure S1.20: ^{1}H NMR spectrum of [(xant)Cu(**L$_P$6**)]PF_6 **C$_P$6** ($CDCl_3$, 700 MHz).

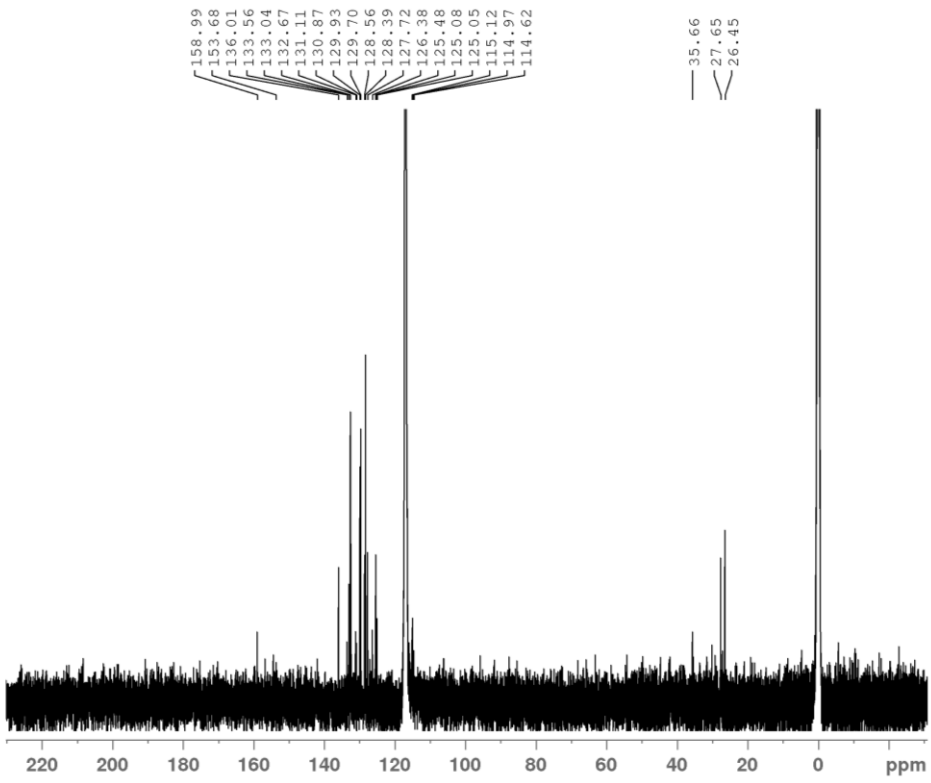

Figure S1.21: ^{13}C NMR spectrum of [(xant)Cu(**L$_P$6**)]PF_6 **C$_P$6** (CD_3CN, 500 MHz).

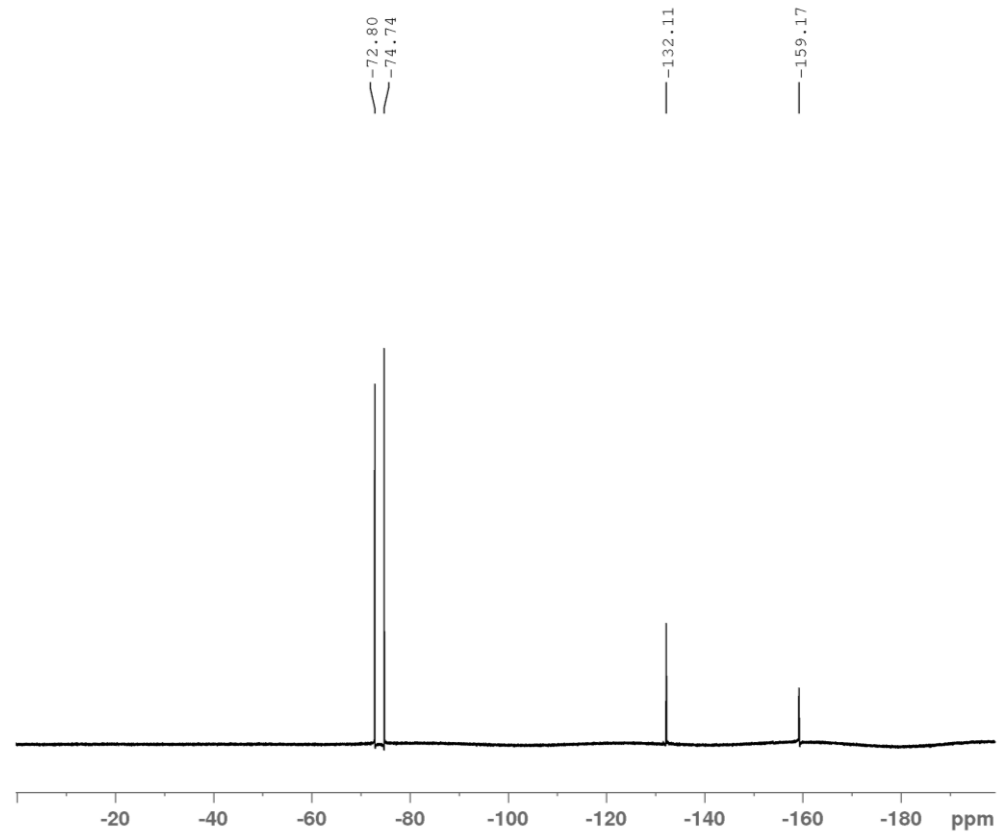

Figure S1.22: ^{19}F NMR spectrum of [(xant)Cu(**L$_P$6**)]PF_6 **C$_P$6** ($CDCl_3$, 400 MHz).

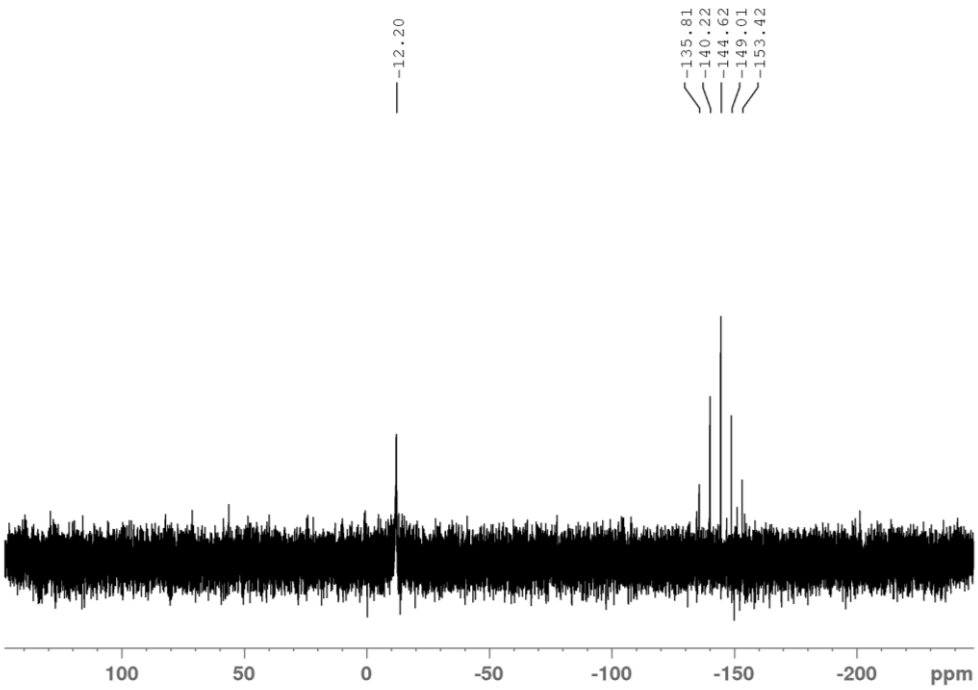

Figure S1.23: ^{31}P NMR spectrum of [(xant)Cu(**L$_P$6**)]PF_6 **C$_P$6** ($CDCl_3$, 400 MHz).

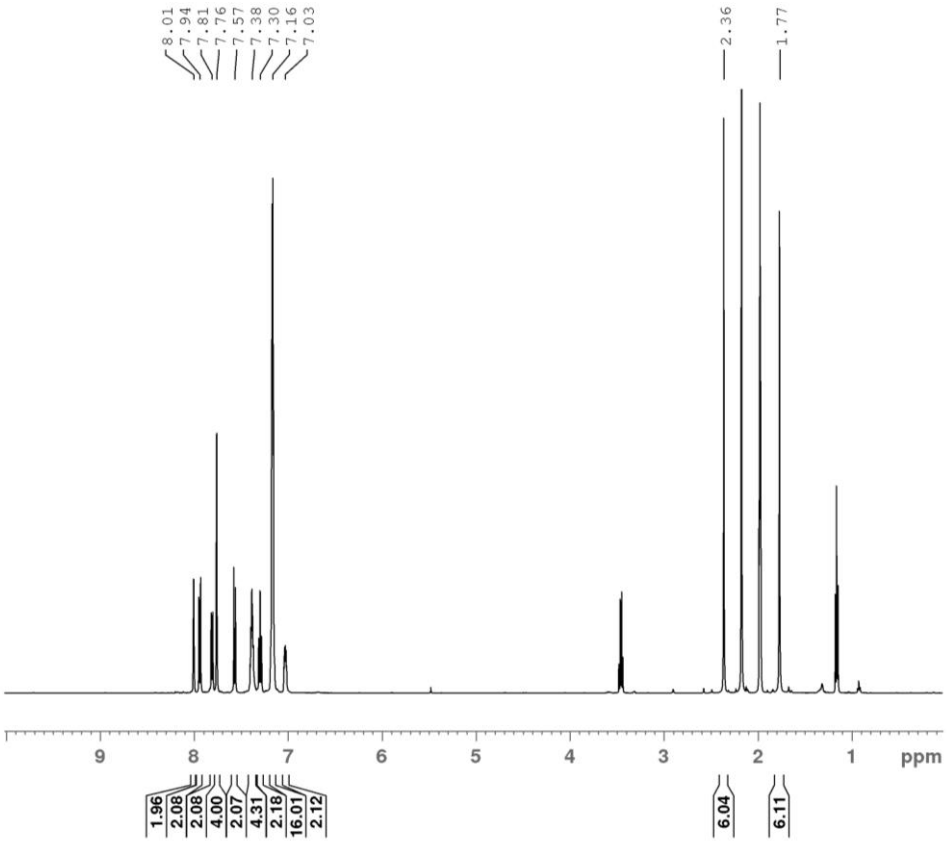

Figure S1.24: ^{1}H NMR spectrum of [(xant)Cu(**L$_P$7**)]PF_6 **C$_P$7** (CD_3CN, 500 MHz).

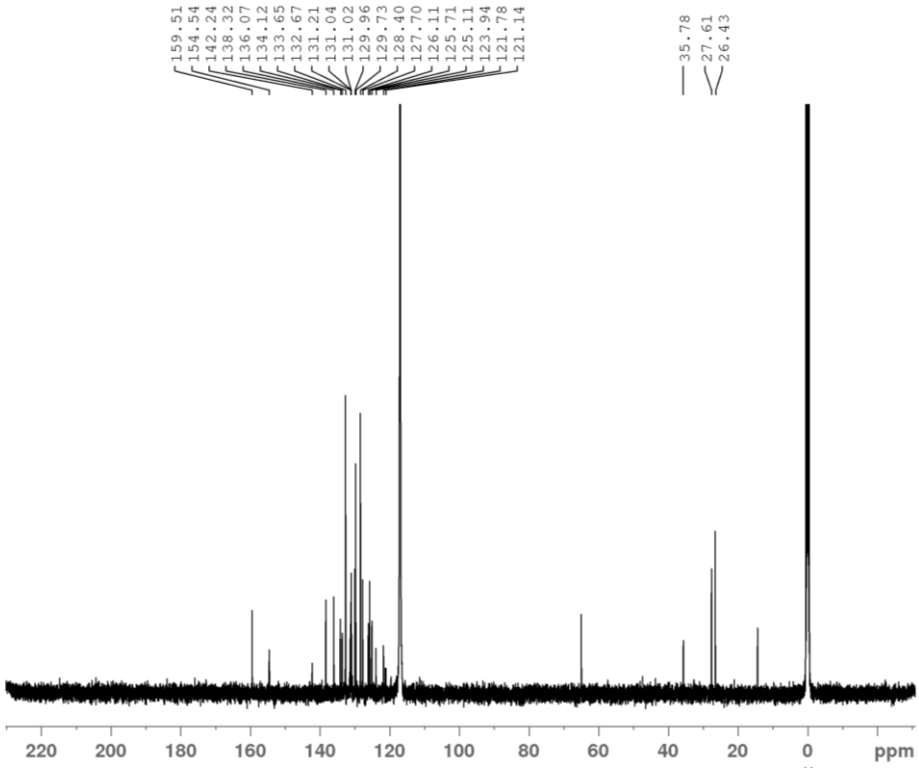

Figure S1.25: ^{13}C NMR spectrum of [(xant)Cu(**L$_P$7**)]PF_6 **C$_P$7** (CD_3CN, 500 MHz).

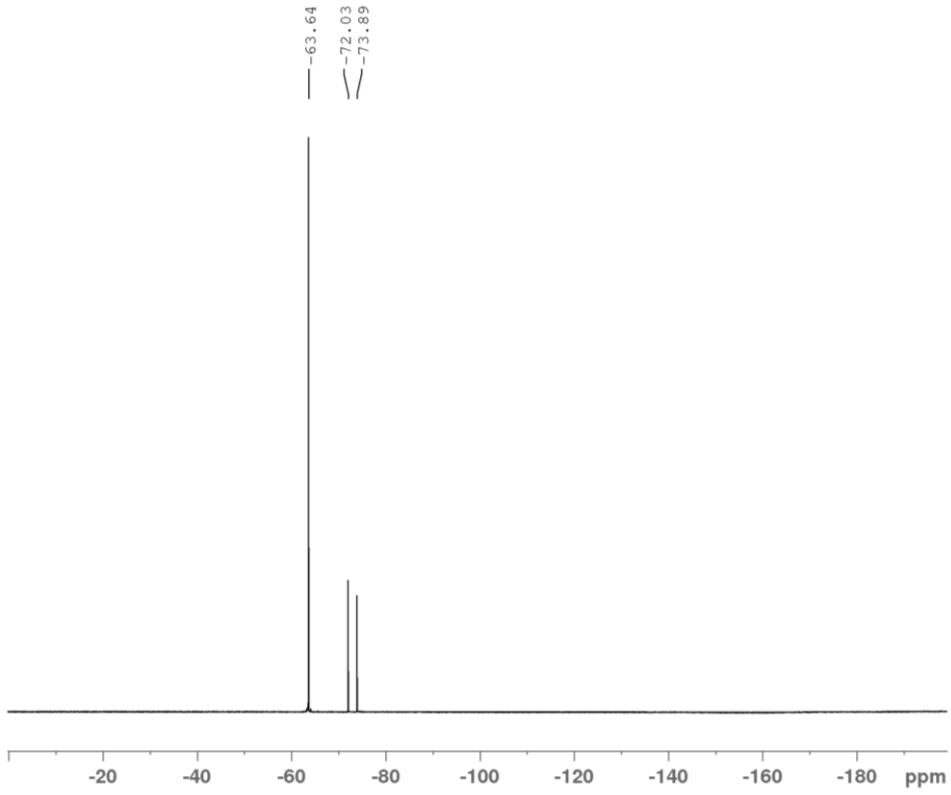

Figure S1.26: ^{19}F NMR spectrum of [(xant)Cu(**L$_P$7**)]PF_6 **C$_P$7** (CD_3CN, 400 MHz).

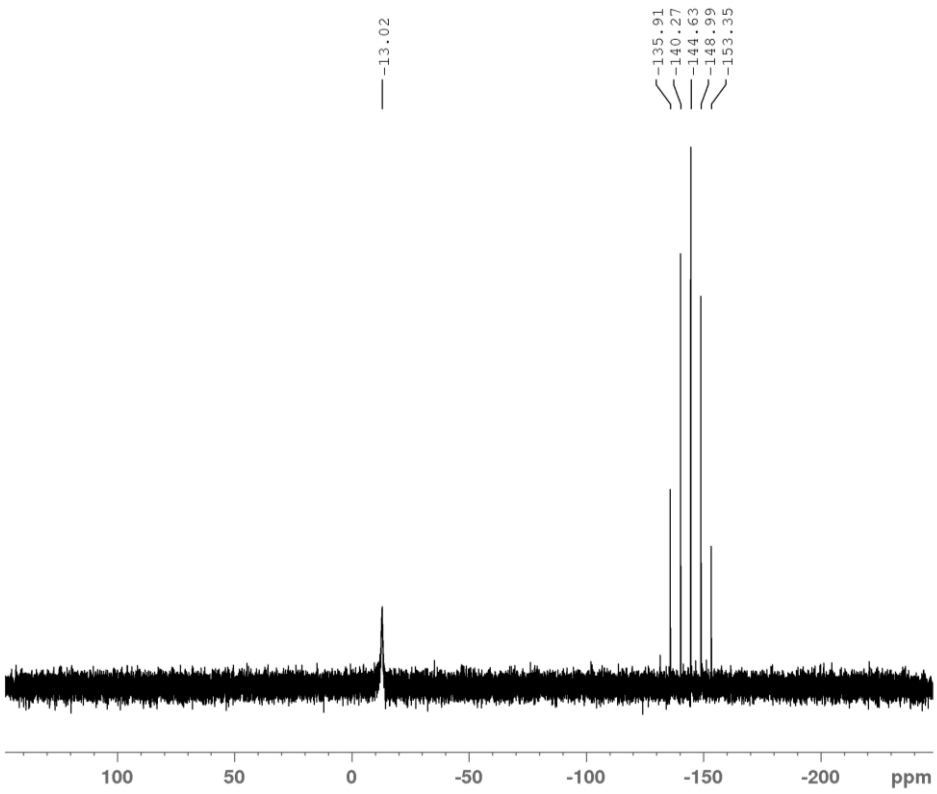

Figure S1.27: ^{31}P NMR spectrum of [(xant)Cu(**L$_P$7**)]PF_6 **C$_P$7** (CD_3CN, 400 MHz).

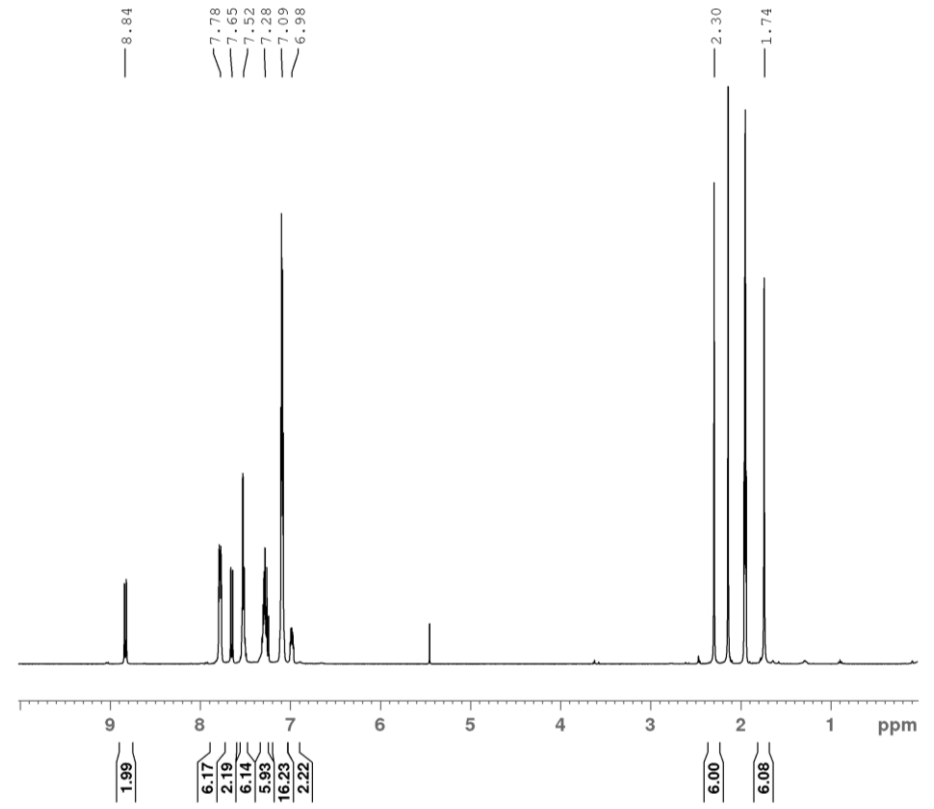

Figure S1.28: ^{1}H NMR spectrum of [(xant)Cu(**L$_A$2**)]PF_6 **C$_A$2** (CD_3CN, 400 MHz).

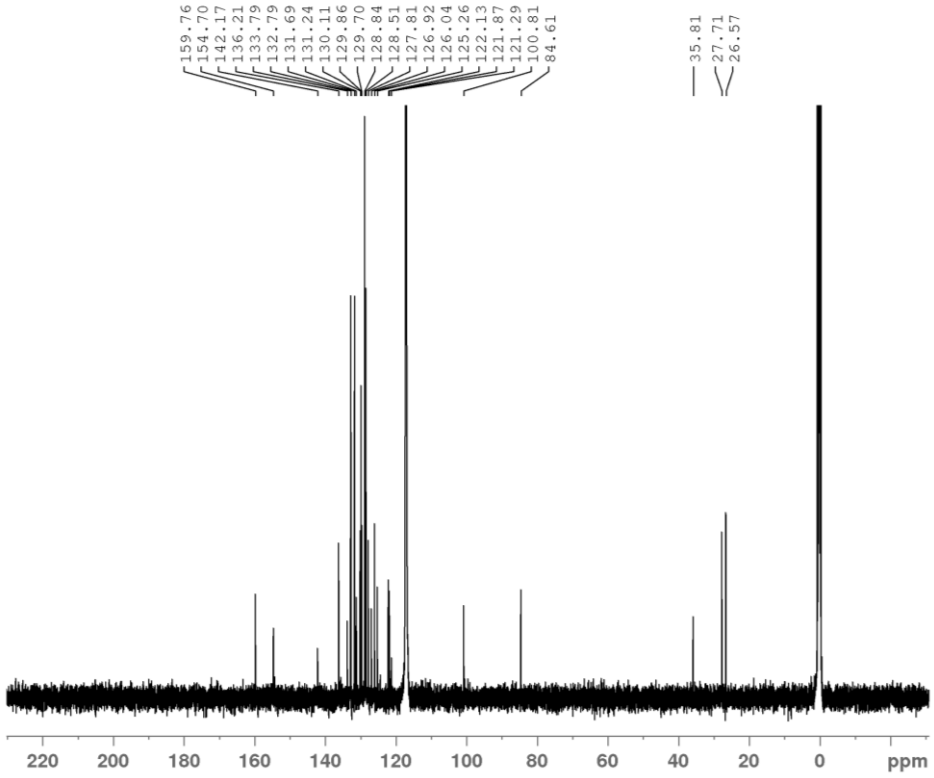

Figure S1.29: ^{13}C NMR spectrum of [(xant)Cu(**L$_A$2**)]PF_6 **C$_A$2** (CD_3CN, 500 MHz).

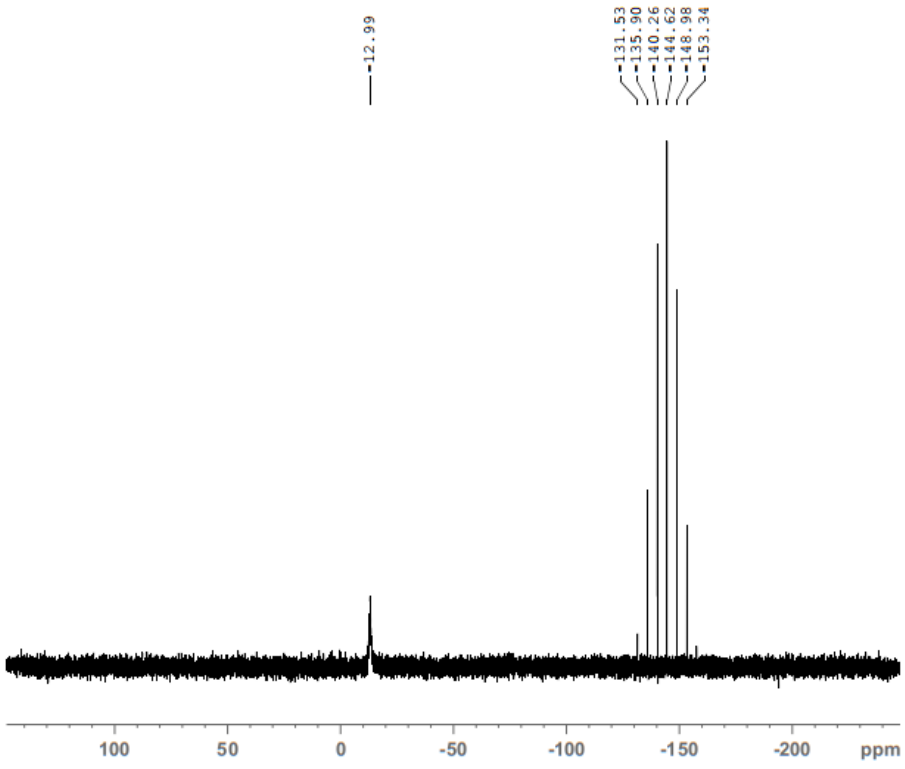

Figure S1.30: ^{31}P NMR spectrum of [(xant)Cu(**L$_A$2**)]PF_6 **C$_A$2** (CD_3CN, 400 MHz).

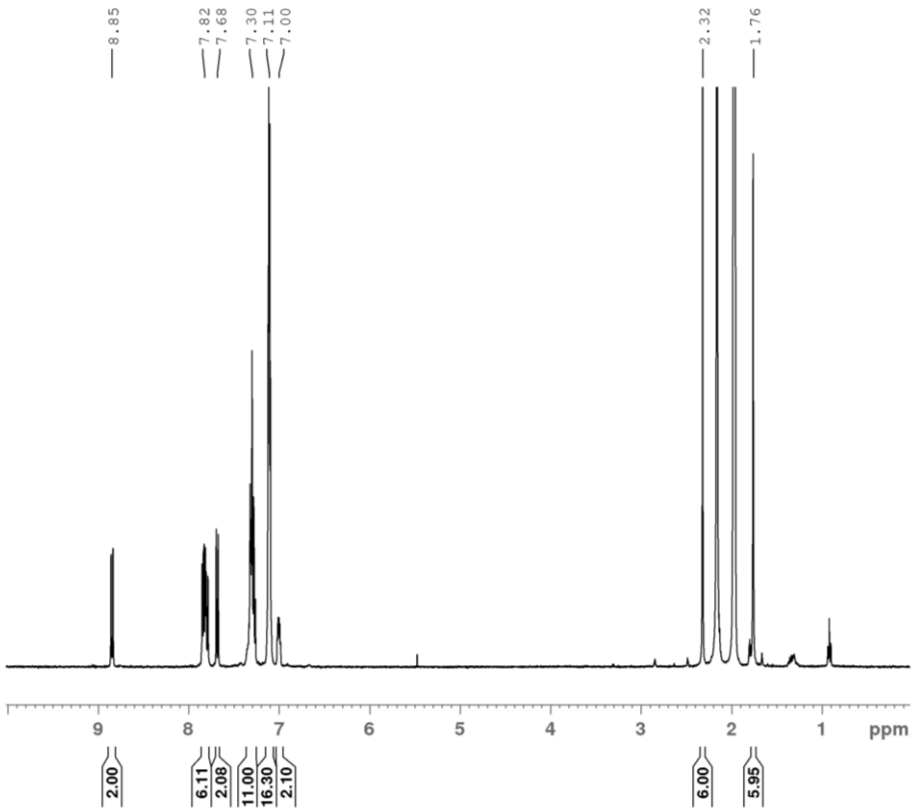

Figure S1.31: ^{1}H NMR spectrum of [(xant)Cu(**L$_A$3**)]PF_6 **C$_A$3** (CD_3CN, 400 MHz).

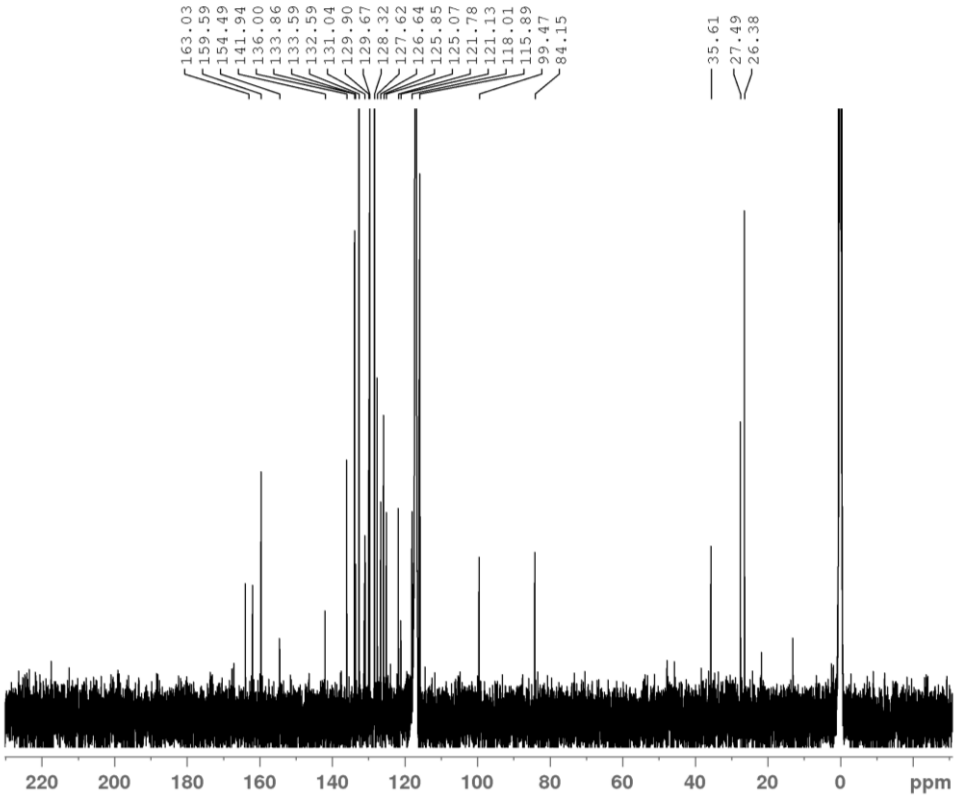

Figure S1.32: ^{13}C NMR spectrum of [(xant)Cu(**L$_A$3**)]PF_6 **C$_A$3** (CD_3CN, 500 MHz).

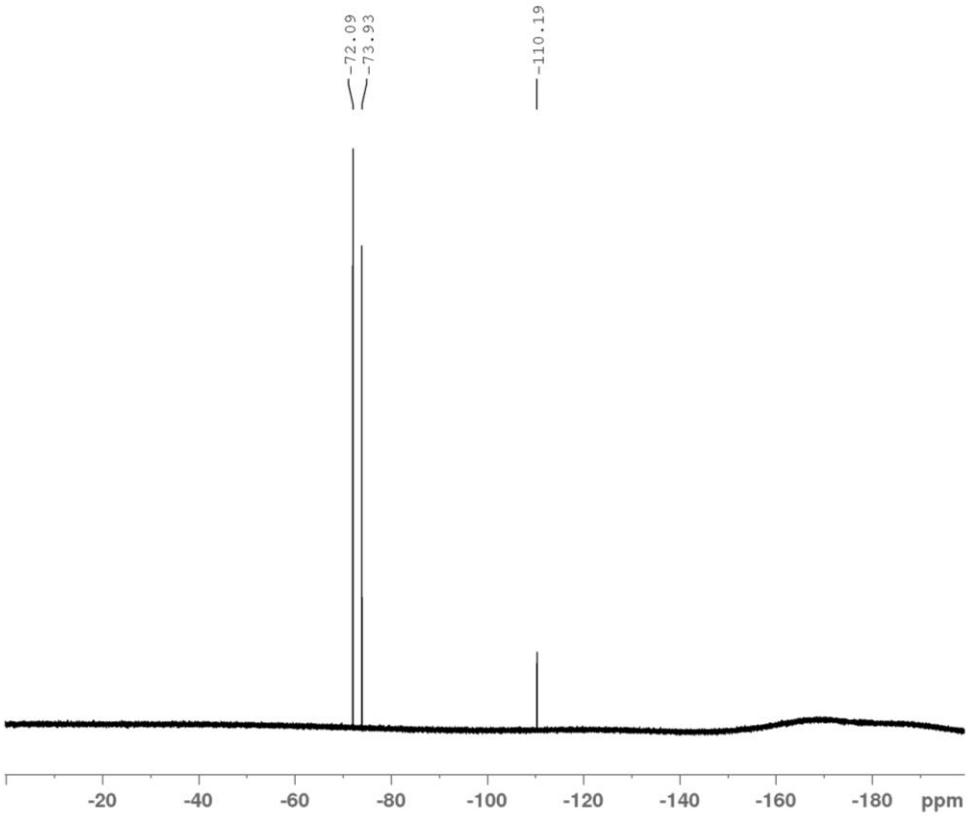

Figure S1.33: ^{19}F NMR spectrum of [(xant)Cu(**L_A3**)]PF_6 **C_A3** (CD_3CN, 400 MHz).

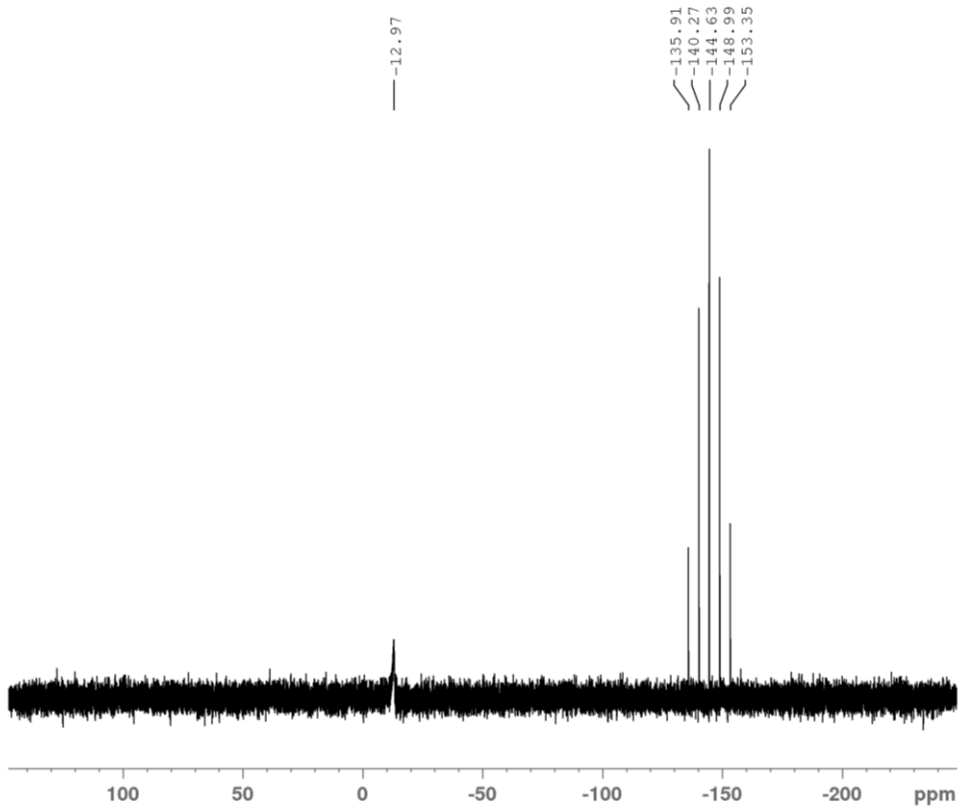

Figure S1.34: ^{31}P NMR spectrum of [(xant)Cu(**L_A3**)]PF_6 **C_A3** (CD_3CN, 400 MHz).

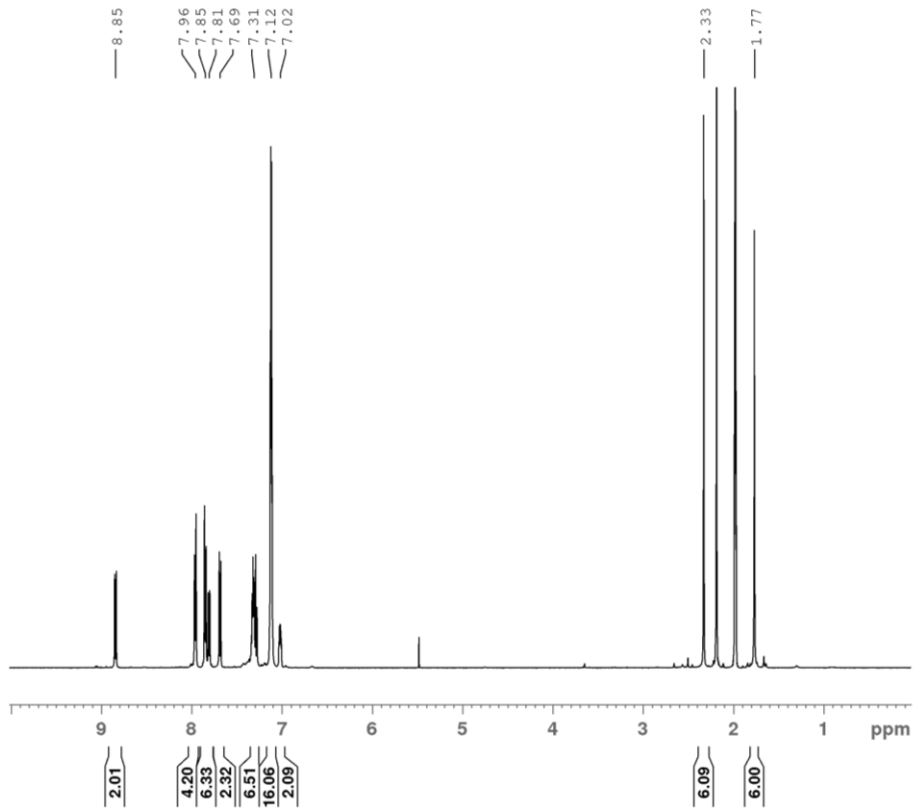

Figure S1.35: ^{1}H NMR spectrum of [(xant)Cu(**L$_A$4**)]PF_6 **C$_A$4** (CD_3CN, 500 MHz).

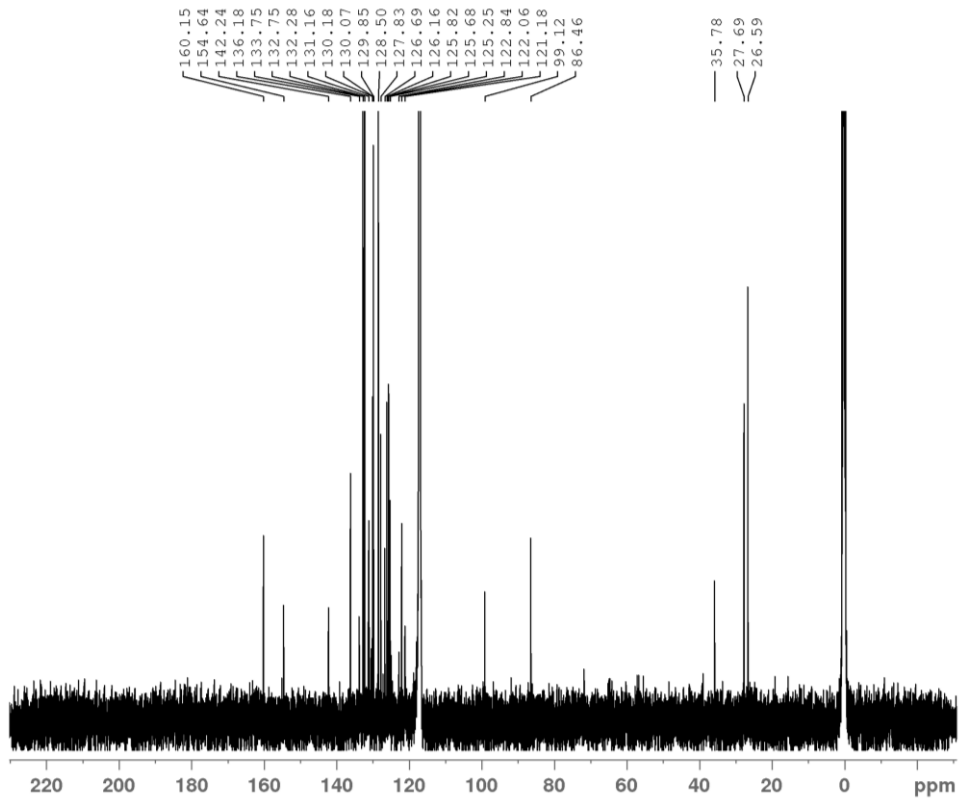

Figure S1.36: ^{13}C NMR spectrum of [(xant)Cu(**L$_A$4**)]PF_6 **C$_A$4** (CD_3CN, 500 MHz).

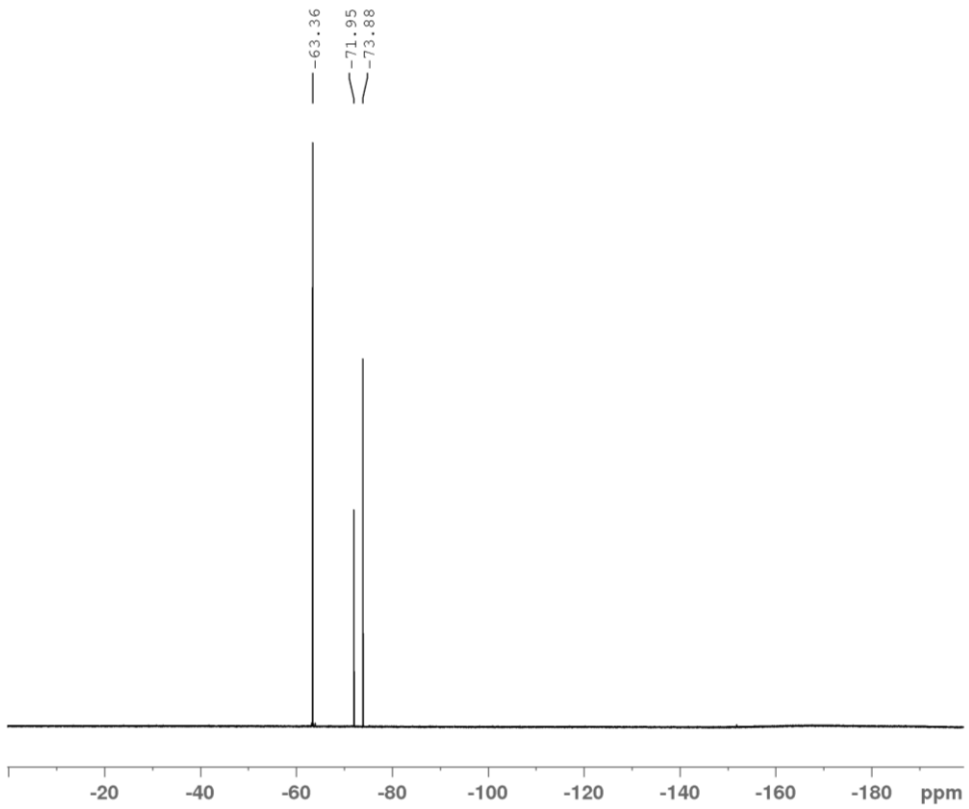

Figure S1.37: ^{19}F NMR spectrum of [(xant)Cu(**L$_A$4**)]PF_6 **C$_A$4** (CD_3CN, 400 MHz).

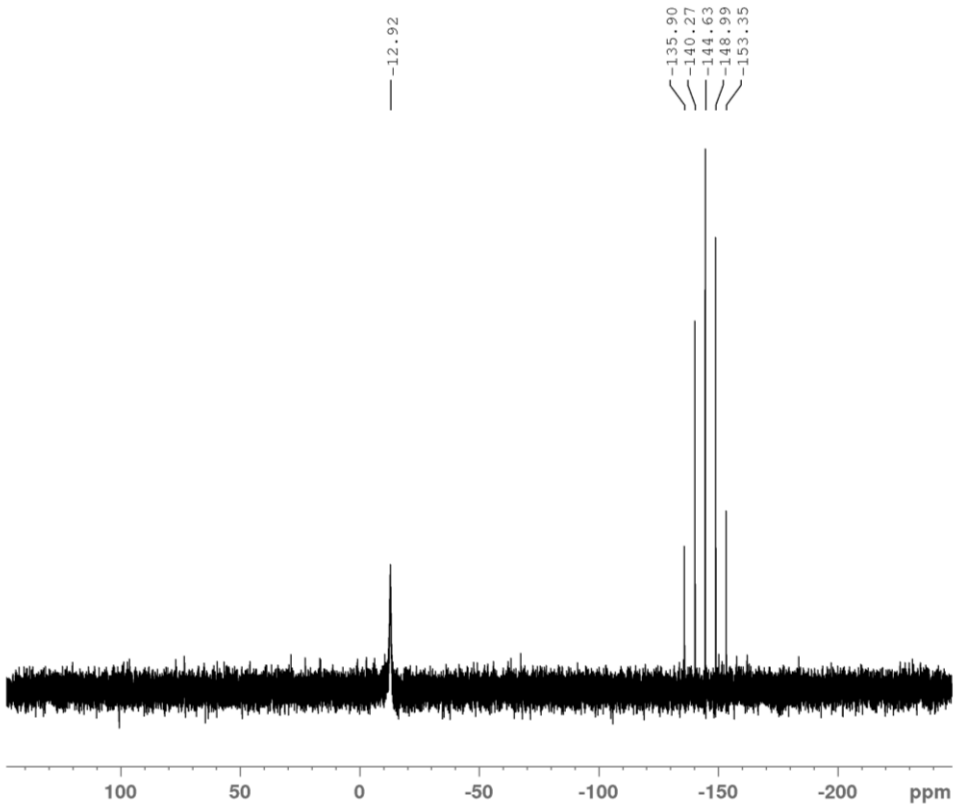

Figure S1.38: ^{31}P NMR spectrum of [(xant)Cu(**L$_A$4**)]PF_6 **C$_A$4** (CD_3CN, 400 MHz).

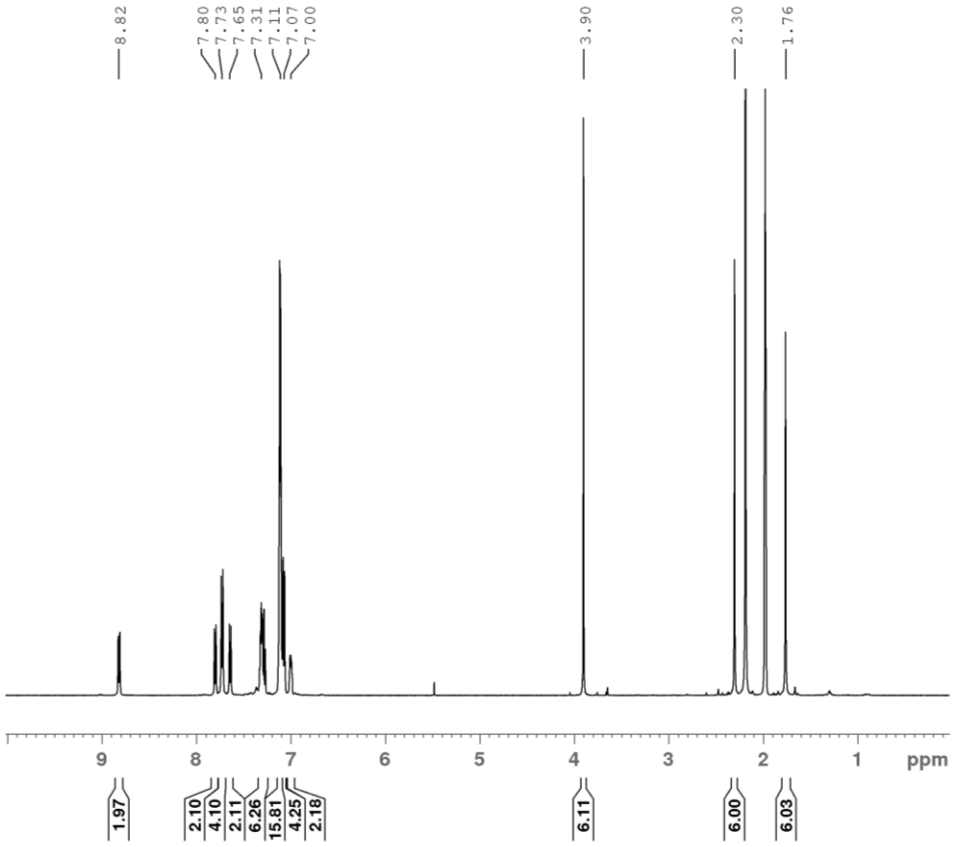

Figure S1.39: ^{1}H NMR spectrum of [(xant)Cu(**L$_A$5**)]PF$_6$ **C$_A$5** (CD_3CN, 500 MHz).

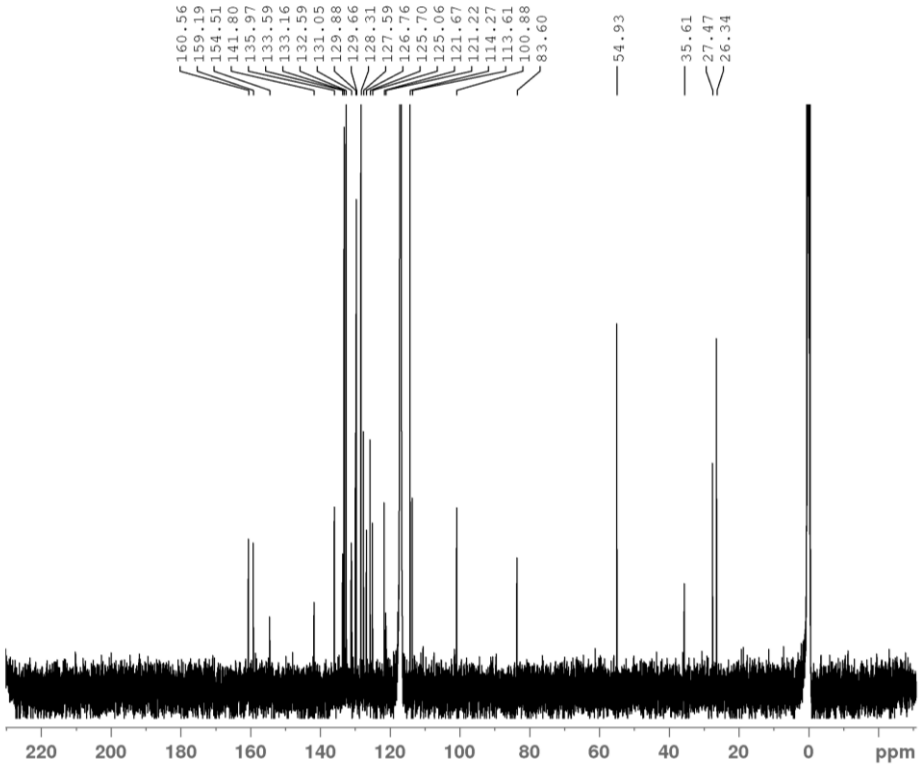

Figure S1.40: ^{13}C NMR spectrum of [(xant)Cu(**L$_A$5**)]PF$_6$ **C$_A$5** (CD_3CN, 500 MHz).

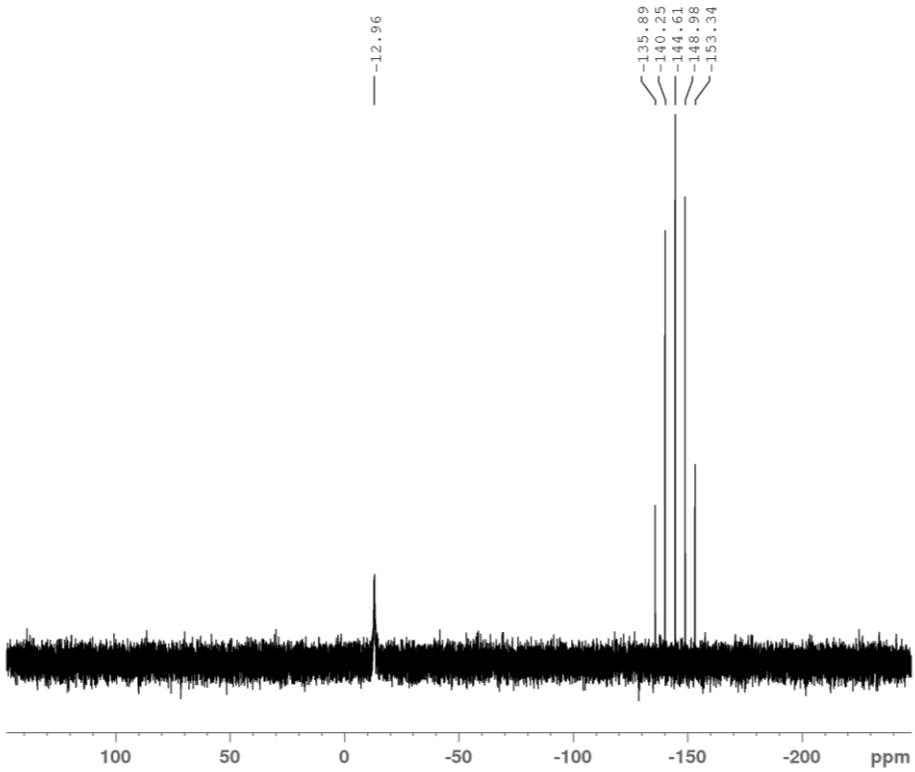

Figure S1.41: ^{31}P NMR spectrum of [(xant)Cu(**L_A5**)]PF_6 **C_A5** (CD_3CN, 400 MHz).

4 MS spectra of the Complexes C1, C_P2-C_P7 and C_A2-C_A5

Acquisition Parameter

Source Type	ESI	Ion Polarity	Positive	Set Nebulizer	0.4 Bar
Focus	Active	Set Capillary	4500 V	Set Dry Heater	200 °C
Scan Begin	250 m/z	Set End Plate Offset	-500 V	Set Dry Gas	4.0 l/min
Scan End	3000 m/z	Set Collision Cell RF	500.0 Vpp	Set Divert Valve	Waste

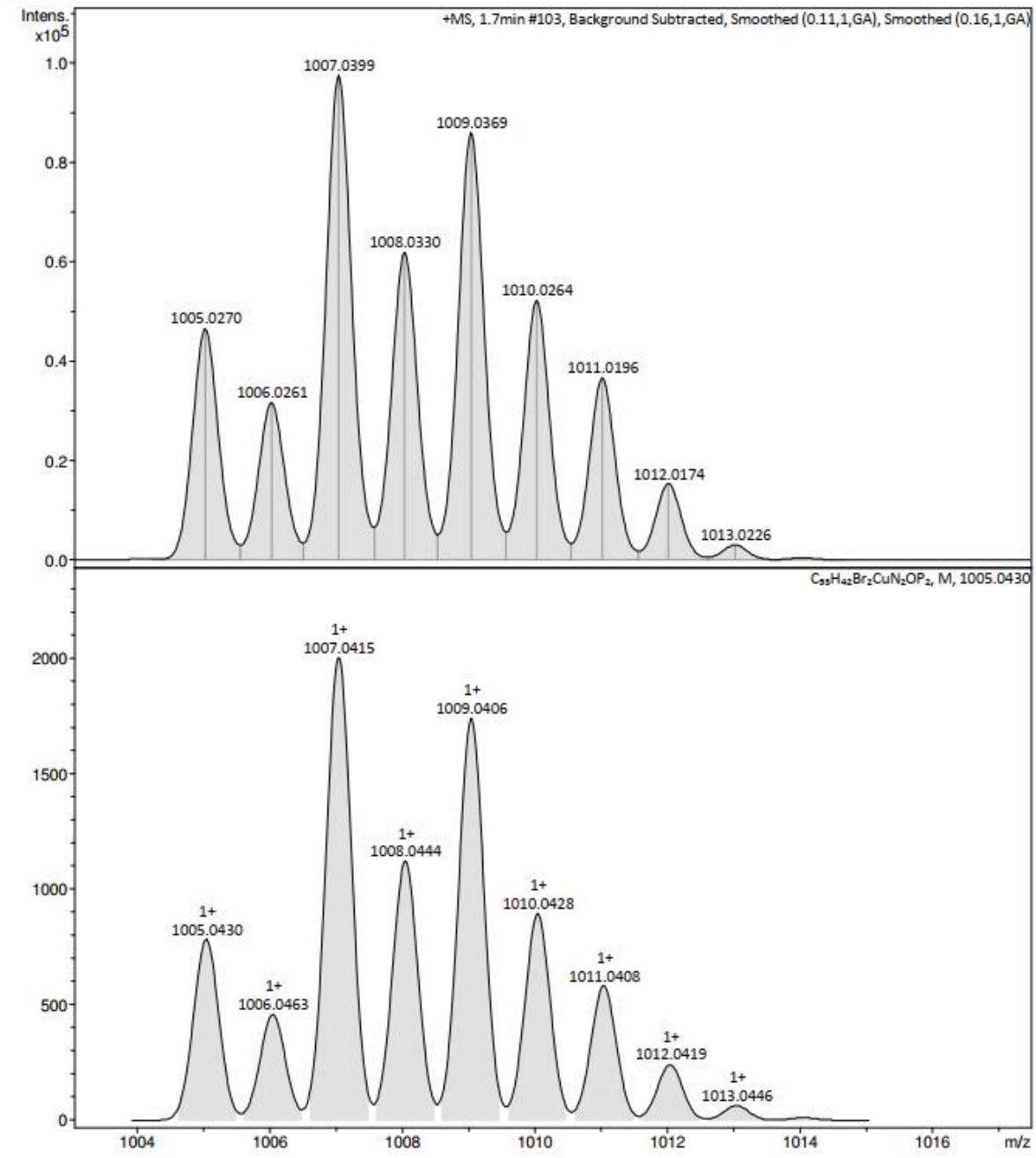

Figure S2.1: Mass spectrum of [(xant)Cu(**L1**)]PF_6 **C1** (experimental (top) *vs*. simulated (bottom)).

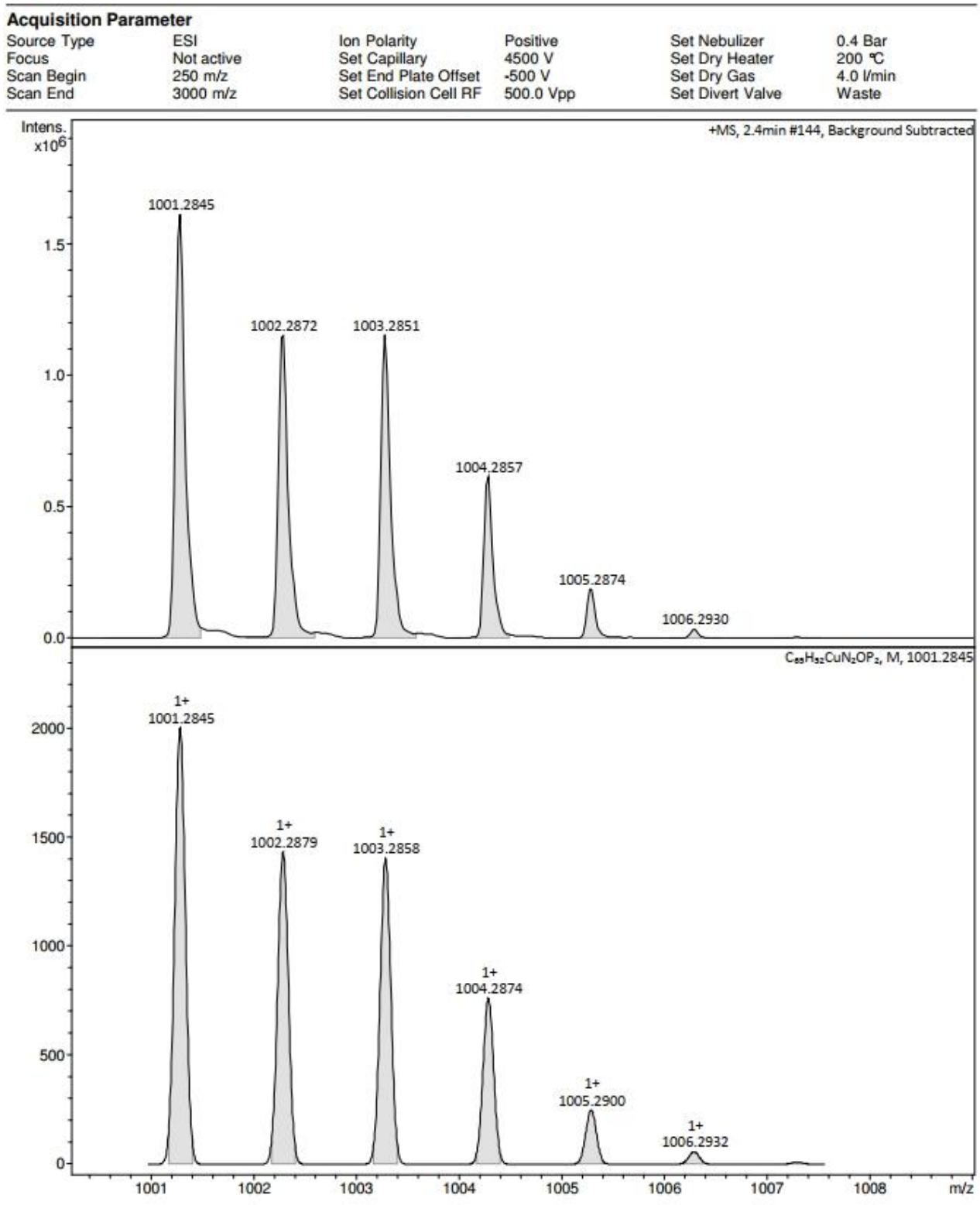

Figure S2.2: Mass spectrum of [(xant)Cu(**L**$_P$**2**)]PF_6 **C**$_P$**2** (experimental (top) *vs*. simulated (bottom)).

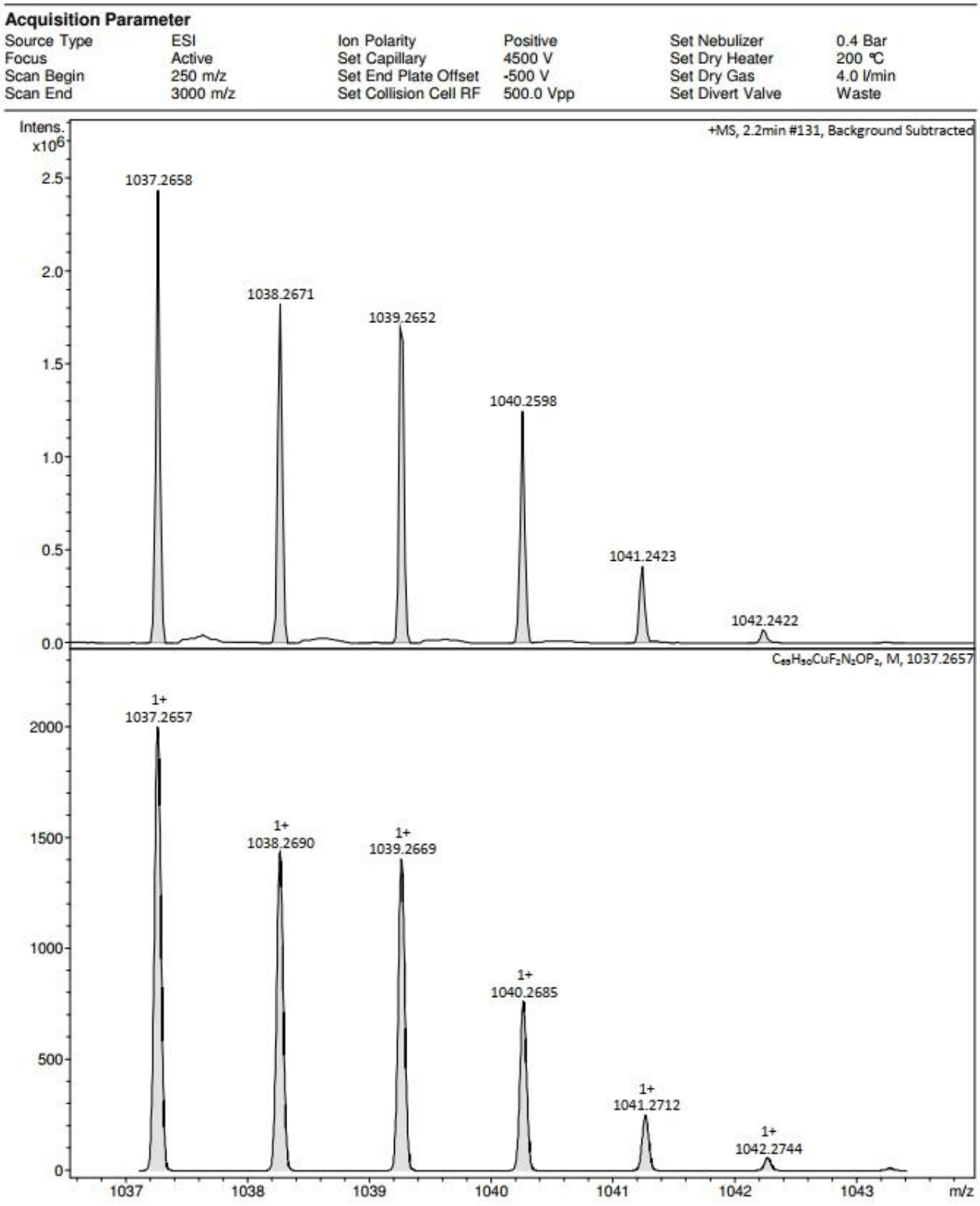

Figure S2.3: Mass spectrum of [(xant)Cu(**L$_P$3**)]PF_6 **C$_P$3** (experimental (top) *vs*. simulated (bottom)).

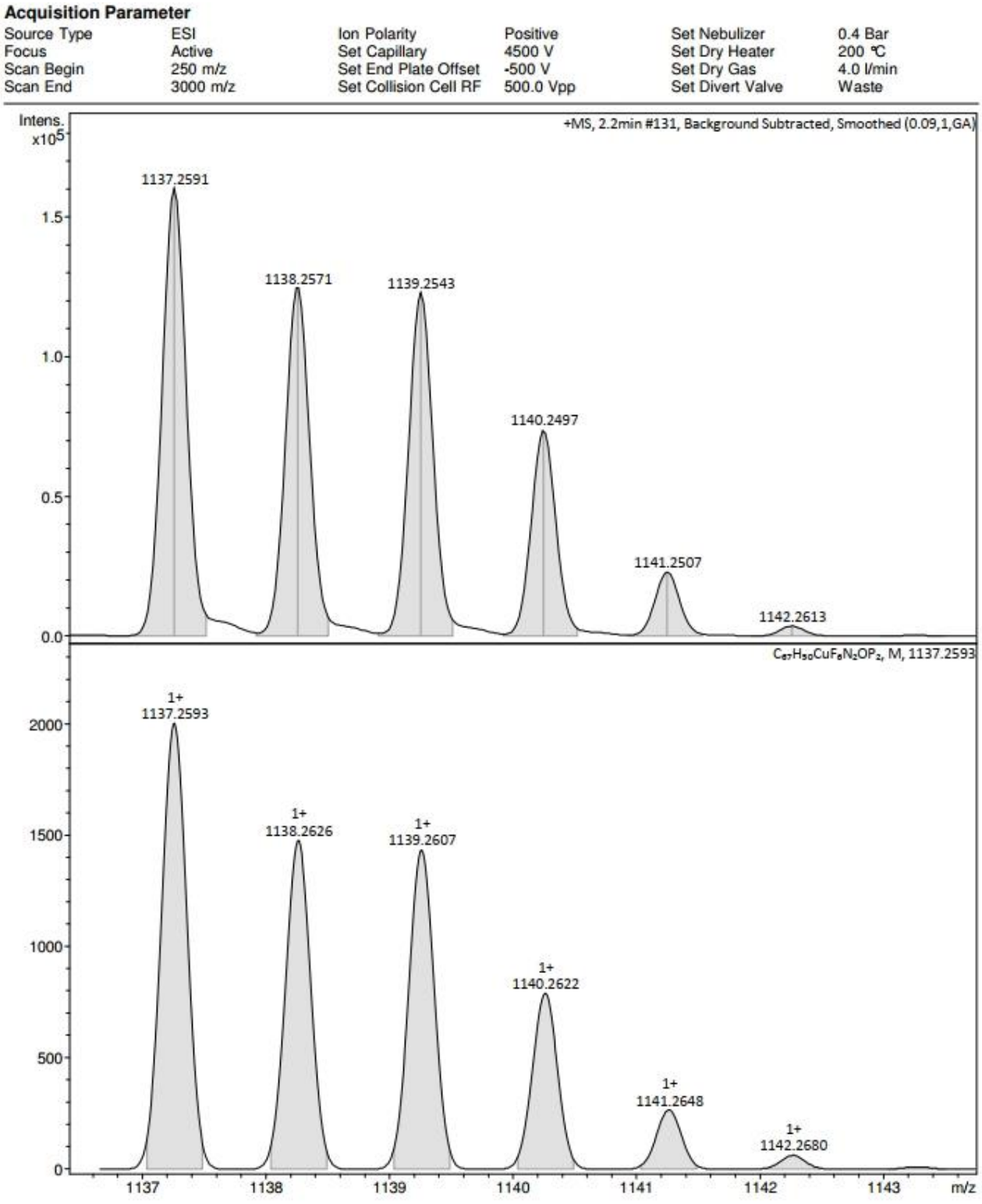

Figure S2.4: Mass spectrum of [(xant)Cu(**L**$_P$**4**)]PF_6 **C**$_P$**4** (experimental (top) *vs*. simulated (bottom)).

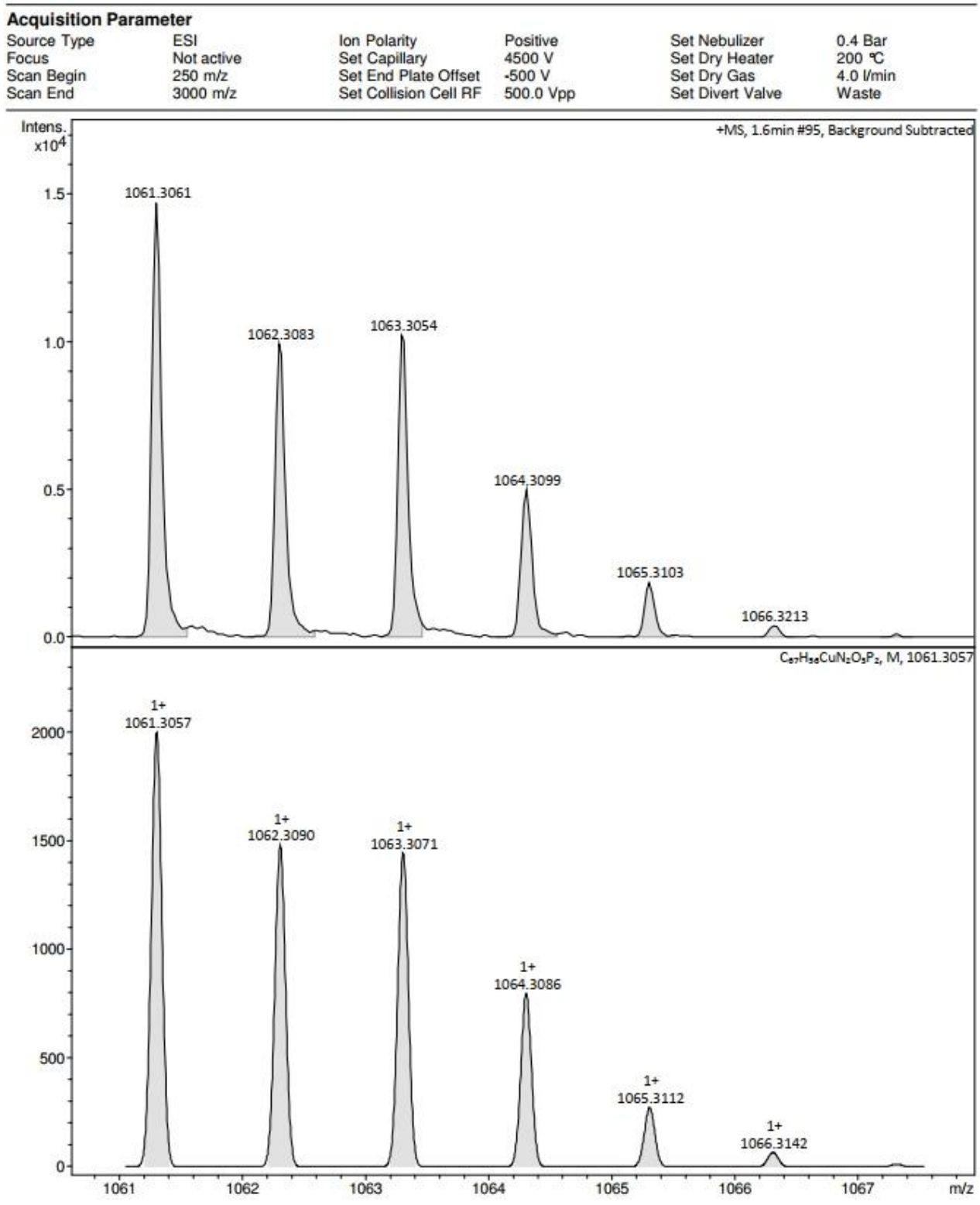

Figure S2.5: Mass spectrum of [(xant)Cu(**L$_P$5**)]PF_6 **C$_P$5** (experimental (top) *vs*. simulated (bottom)).

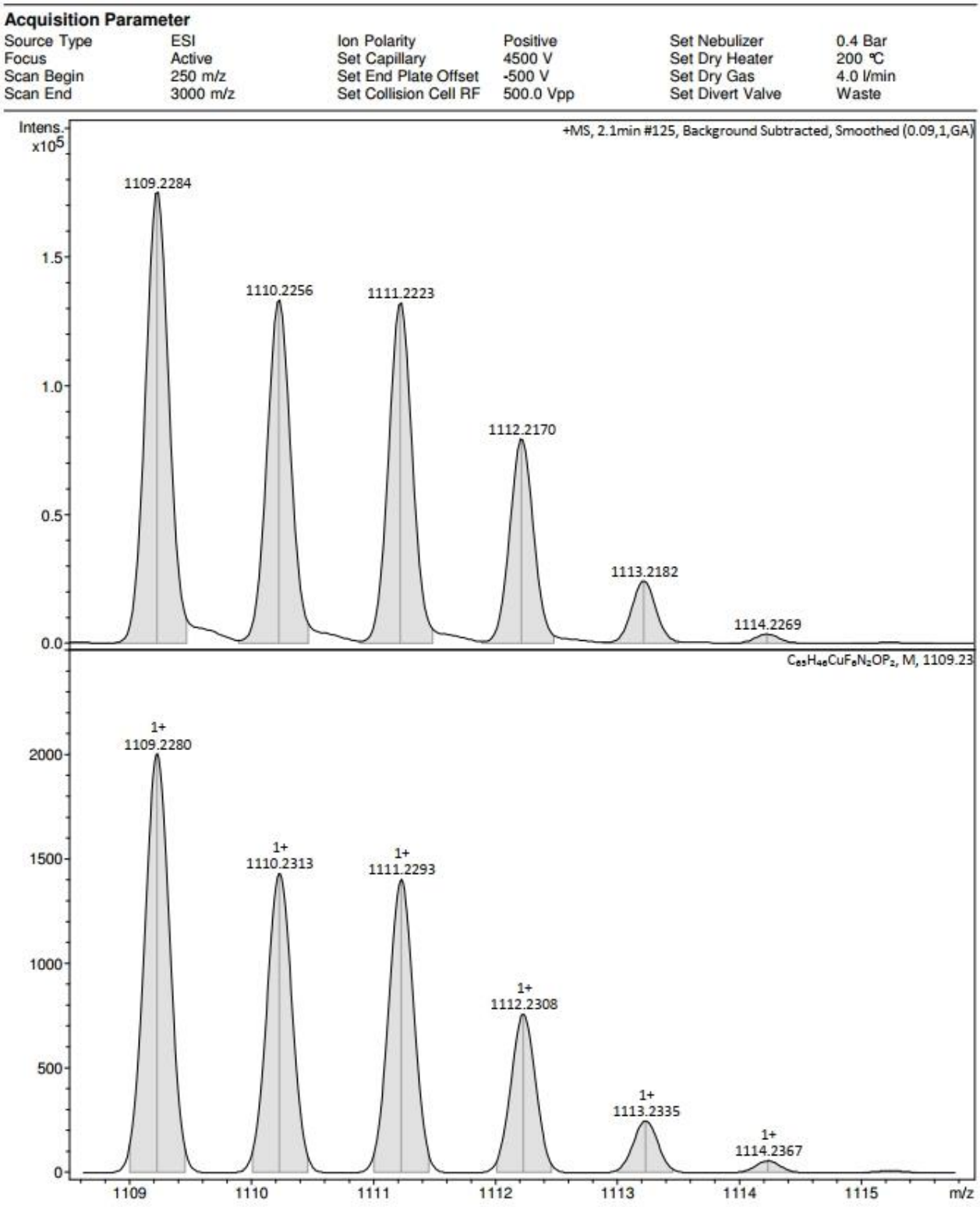

Figure S2.6: Mass spectrum of [(xant)Cu(**L$_P$6**)]PF_6 **C$_P$6** (experimental (top) *vs*. simulated (bottom)).

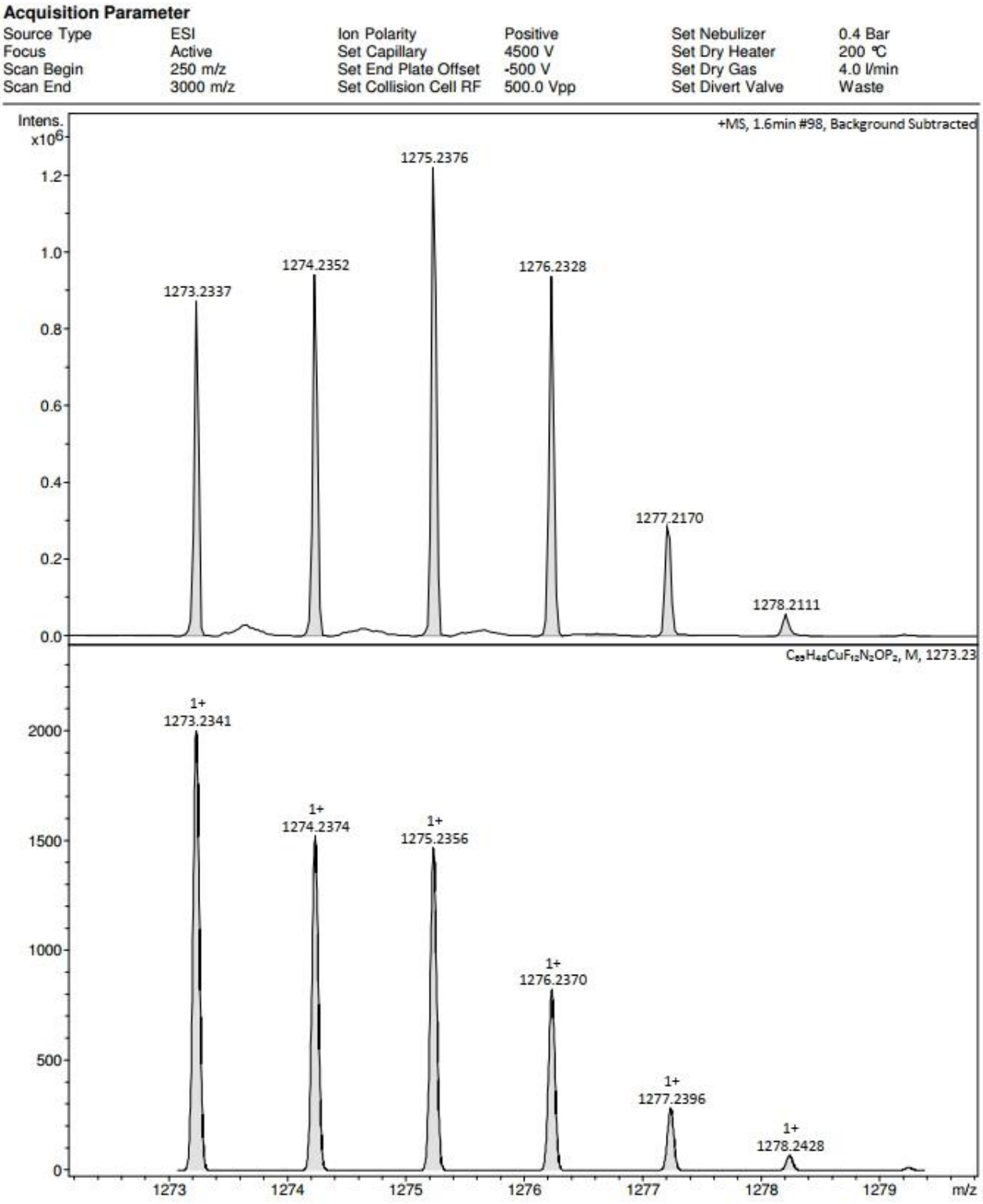

Figure S2.7: Mass spectrum of [(xant)Cu(**L$_P$7**)]PF_6 **C$_P$7** (experimental (top) *vs*. simulated (bottom)).

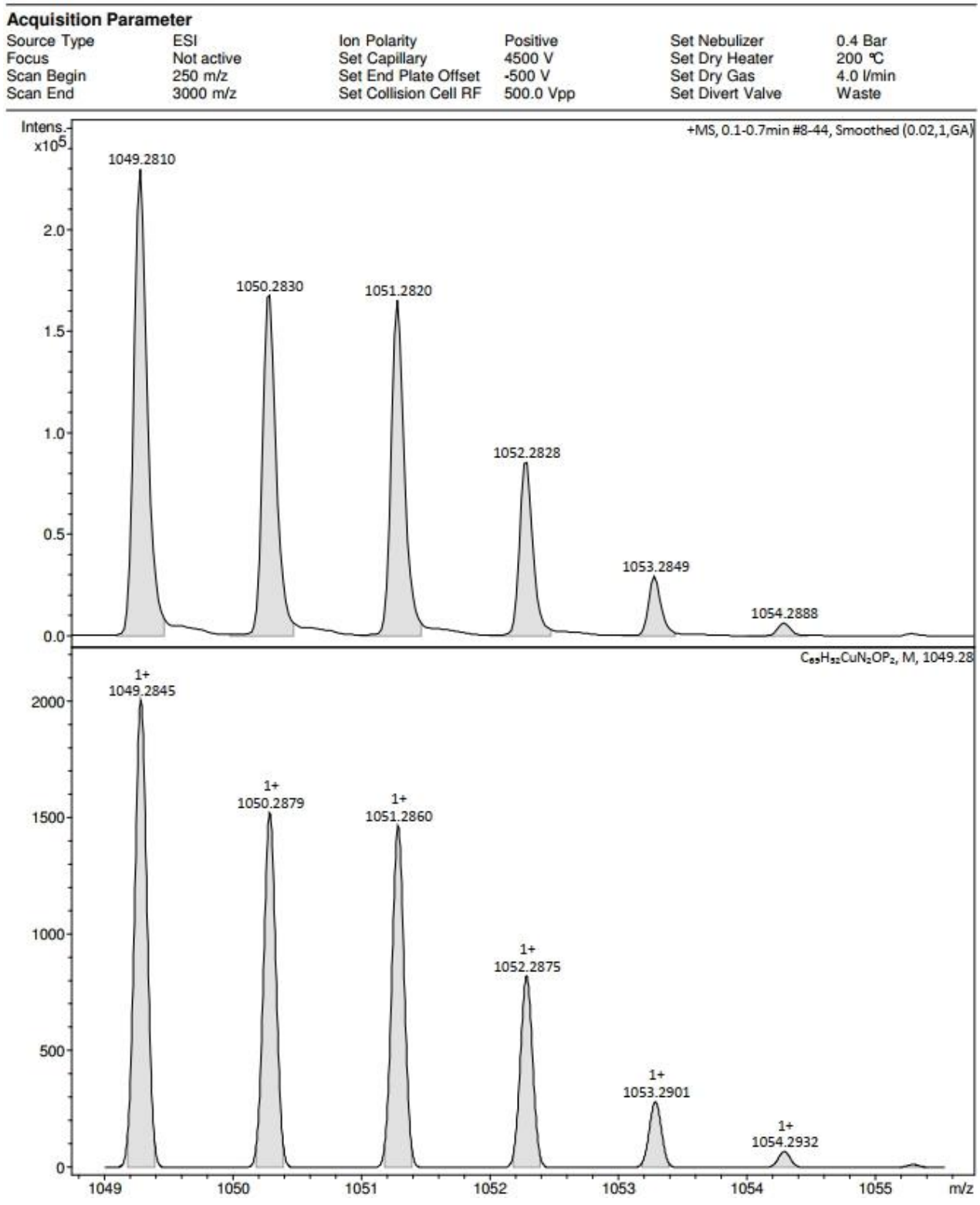

Figure S2.8: Mass spectrum of [(xant)Cu(**L$_A$2**)]PF_6 **C$_A$2** (experimental (top) *vs*. simulated (bottom)).

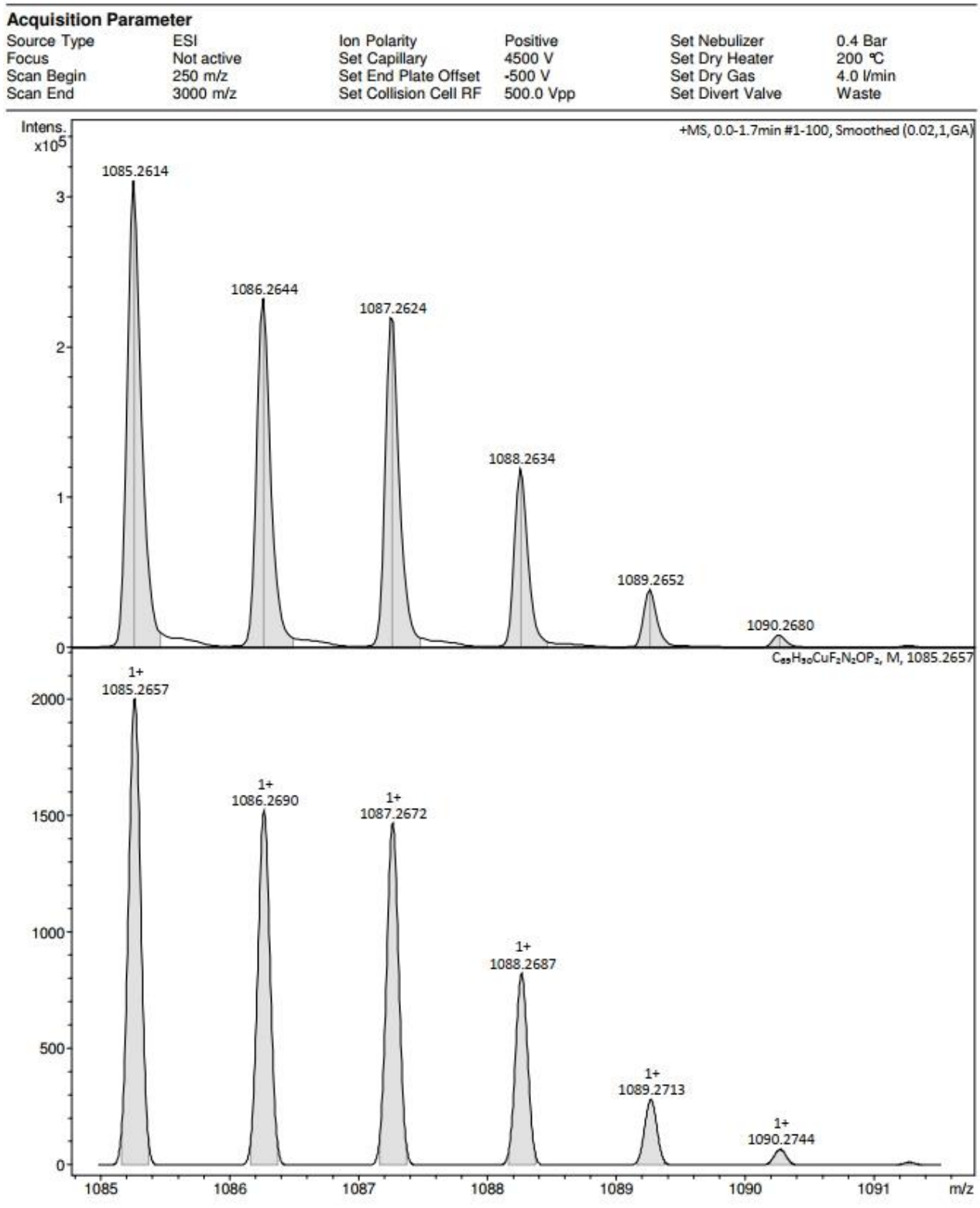

Figure S2.9: Mass spectrum of [(xant)Cu(**L$_A$3**)]PF_6 **C$_A$3** (experimental (top) *vs*. simulated (bottom)).

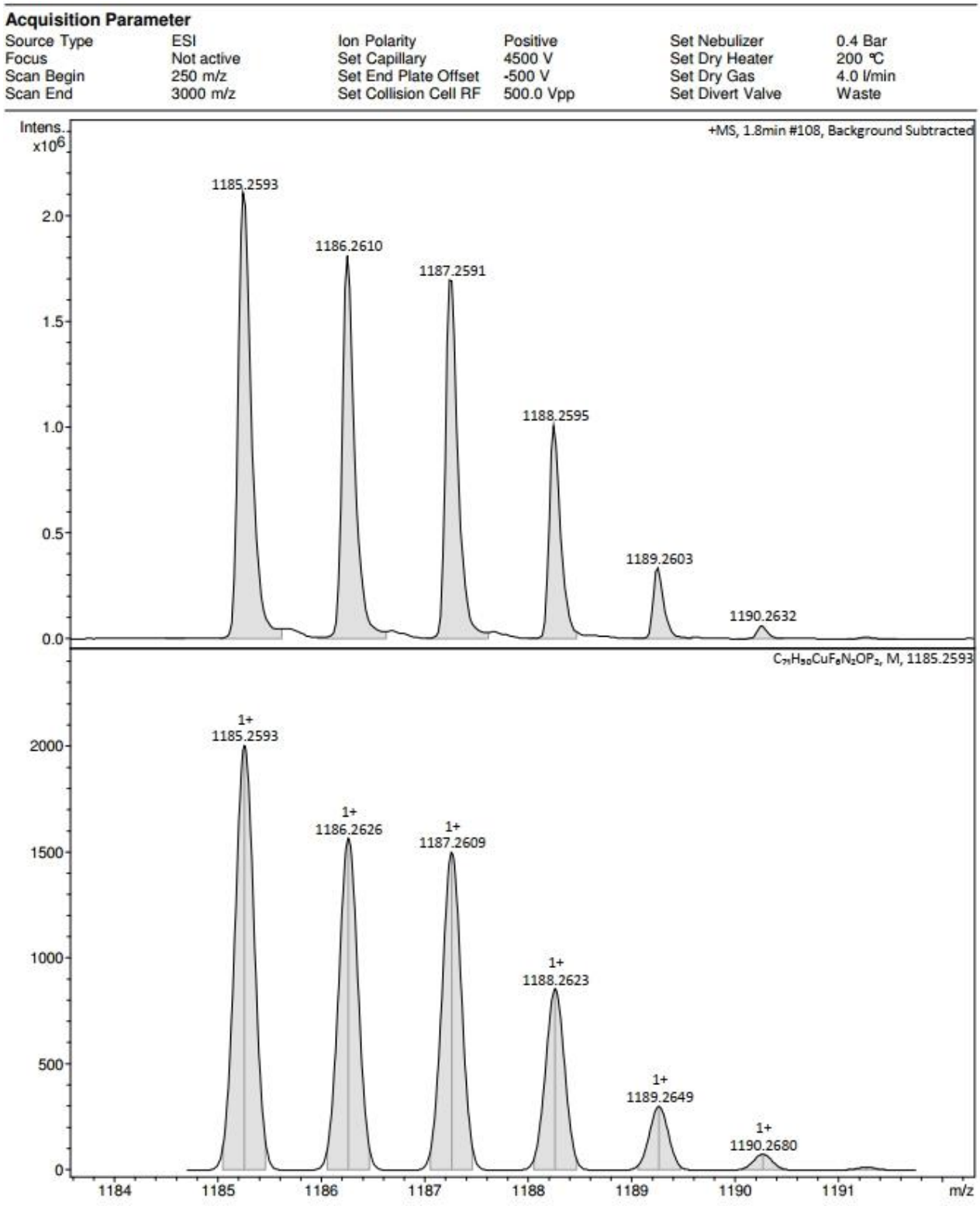

Figure S2.10: Mass spectrum of [(xant)Cu(**L$_A$4**)]PF_6 **C$_A$4** (experimental (top) *vs*. simulated (bottom)).

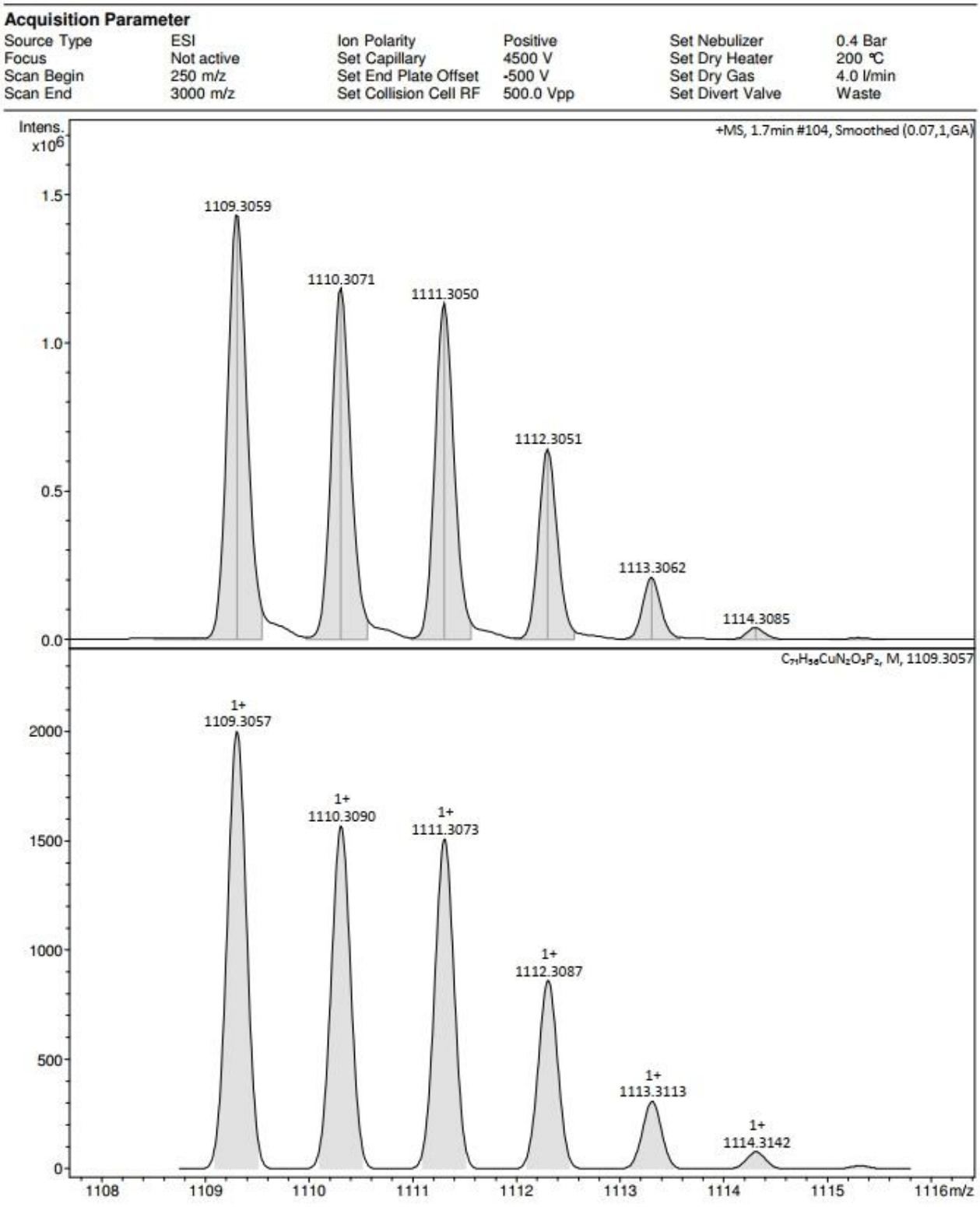

Figure S2.11: Mass spectrum of [(xant)Cu(**L$_A$5**)]PF_6 **C$_A$5** (experimental (top) *vs*. simulated (bottom)).

5 Crystallographic Data and Structures of C1, C_P4, C_P6, C_P7 and C_A4

Single crystals of the complexes **C1**, **C_P4, C_P6, C_P7** and **C_A4** could be obtained by crystallization from a moderately concentrated methylene chloride solution by overlayering firstly with a film of ethanol and secondly with *n*-hexane. Crystal growth was completed after 3-10 days depending on the amount of ethanol and *n*-hexane applied (*e.g.* crystallizing **C_A4** was found to be most challenging demanding to increase the ratio EtOH/*n*-hexane to slow down crystallization).

Table S1: Crystallographic data of the complexes **C1, C_P4, C_P6, C_P7** and **C_A4**

Complex	**C1**	**C_P4**	**C_P6**
CCDC Number [a]	2059397	2059398	2059399
Empirical formula	$C_{53}H_{42}Br_2CuF_6N_2OP_3$	$C_{70}H_{56}Cl_6CuF_{12}N_2O_{1.50}P_3$	$C_{67}H_{50}Cl_4CuF_{12}N_2OP_3$
Formula weight [g/mol]	1153.15	1546.31	1425.34
Temperature [K]	135(2)	135(2)	135(2)
Wavelength [Å]	0.71073	0.71073	0.71073
Crystal system, space group	Triclinic, P-1	Triclinic, P-1	Monoclinic, P2(1)/n
Unit cell dimensions [Å] and [°]	a = 11.4578(4) alpha = 85.881(2) b = 12.5865(5) beta = 71.850(2) c = 17.3085(6) gamma = 82.826(3)	a = 10.8280(8) alpha = 92.634(4) b = 16.9026(11) beta = 102.328(4) c = 20.6531(14) gamma = 103.549(3)	a = 17.2053(9) alpha = 90 b = 14.8342(8) beta = 106.899(3) c = 28.1951(14) gamma = 90
Volume [Å^3]	2351.92(15)	3571.6(4)	6885.4(6)
Z, Calculated density [Mg/m^{-3}]	2, 1.628	2, 1.438	4, 1.375
Absorption coefficient [mm^{-1}]	2.332	0.673	0.617
F(000)	1160	1572	2896
Crystal size [mm]	0.270 x 0.120 x 0.084	0.219 x 0.139 x 0.113	0.353 x 0.175 x 0.090
Theta range for data collection [°]	1.632 to 28.383	1.684 to 24.999	1.510 to 25.499
Limiting indices	-15<=h<=15, -16<=k<=16, -22<=l<=23	-12<=h<=12, -20<=k<=20, -24<=l<=24	-20<=h<=20, -17<=k<=17, -34<=l<=34
Reflections collected / unique	47300 / 11727 [R(int) = 0.0390]	42631 / 12378 [R(int) = 0.0791]	99093 / 12531 [R(int) = 0.1112]
Completeness to theta = X	X=25.242 Completeness: 99.9 %	X=24.999 Completeness: 98.6 %	X=25.242 Completeness: 98.3 %
Absorption correction	Numerical	Semi-empirical from equivalents	Numerical
Max. and min. transmission	0.8932 and 0.6552	0.8620 and 0.7505	0.9689 and 0.7989
Refinement method	Full-matrix least-squares on F^2	Full-matrix least-squares on F^2	Full-matrix least-squares on F^2
Data / restraints / parameters	11727 / 48 / 654	12378 / 180 / 924	12531 / 24 / 815
Goodness-of-fit on F^2	1.013	1.041	1.037
Final R indices [I>2sigma(I)]	1 = 0.0348, wR2 = 0.0695	R1 = 0.1085, wR2 = 0.2571	R1 = 0.0821, wR2 = 0.2032
R indices (all data)	R1 = 0.0635, wR2 = 0.0747	R1 = 0.1785, wR2 = 0.2789	R1 = 0.1385, wR2 = 0.2212
Extinction coefficient	n/a	n/a	n/a
Largest diff. peak and hole [e.A^{-3}]	0.490 and -0.462	1.252 and -0.866	0.888 and -0.986

Complex	**C_P7**	**C_A4**
CCDC Number [a]	2059400	2059401
Empirical formula	$C_{70}H_{50}Cl_2CuF_{18}N_2OP_3$	$C_{72.50}H_{53}Cl_3CuF_{12}N_2OP_3$
Formula weight [g/mol]	1504.47	1458.97
Temperature [K]	135(2)	135(2)
Wavelength [Å]	0.71073	1.54178
Crystal system, space group	Monoclinic, P2(1)/n	Monoclinic, P2(1)/c
Unit cell dimensions [Å] and [°]	a = 18.9277(9) alpha = 90 b = 15.2284(6) beta = 93.399(2) c = 22.3255(11) gamma = 90	a = 10.9736(3) alpha = 90 b = 26.4107(10) beta = 94.986(2) c = 48.6238(16) gamma = 90
Volume [$Å^3$]	6423.8(5)	14038.8(8)
Z, Calculated density [Mg/m^{-3}]	4 , 1.556	8, 1.381
Absorption coefficient [mm^{-1}]	0.598	2.793
F(000)	3048	5944
Crystal size [mm]	0.308 x 0.256 x 0.165	0.281 x 0.111 x 0.030
Theta range for data collection [°]	1.620 to 26.432	1.905 to 65.596
Limiting indices	-23<=h<=23, -19<=k<=11, -27<=l<=26	-12<=h<=12, -30<=k<=30, -43<=l<=57
Reflections collected / unique	55838 / 13176 [R(int) = 0.0598]	85542 / 23471 [R(int) = 0.1162]
Completeness to theta = X	X=25.242 Completeness: 99.9 %	X=65.596 Completeness: 96.9 %
Absorption correction	Semi-empirical from equivalents	Numerical
Max. and min. transmission	0.7454 and 0.7086	0.9840 and 0.5271
Refinement method	Full-matrix least-squares on F^2	Full-matrix least-squares on F^2
Data / restraints / parameters	13176 / 141 / 915	23471 / 176 / 1782
Goodness-of-fit on F^2	1.043	1.036
Final R indices [I>2sigma(I)]	R1 = 0.0513, wR2 = 0.1168	R1 = 0.0931, wR2 = 0.1983
R indices (all data)	R1 = 0.1045, wR2 = 0.1303	R1 = 0.1599, wR2 = 0.2205
Extinction coefficient	n/a	n/a
Largest diff. peak and hole [$e.A^{-3}$]	0.790 and -0.907	1.546 and -0.720

[a] The CCDC reference numbers shown contain the supplementary crystallographic data for this paper. The data can be accessed free of charge at the Cambridge Crystallographic Data Centre via www.ccdc.cam.ac.uk/data_request/cif

Table S2: Selected crystallographic bond lengths (pm), bond angles (°), inter plane angles (P-P-N-N, °), phenyl-to-phenanthroline distances *d* (pm), and torsion angles τ_{Sub} (°) of the complexes **C$_P$4** and **C$_P$7** its corresponding crystal structure (structures not presented in main text).

	C$_P$4
β_{NCuN}	79.7(3)
β_{PCuP}	120.30(9)
P-P-N-N	84.17
Cu-N_1	210.1(6)
Cu-N_2	210.5(6)
Cu-P_1	224.4(3)
Cu-P_2	229.3(3)
$\tau_{Sub,1}$	-59.2(9)
$\tau_{Sub,2}$	-53.0(9)
d_1	367(1)
d_2	371(1)
N_1CuP_1	128.9(2)
N_1CuP_2	103.1(2)
N_2CuP_1	119.3(2)
N_2CuP_2	96.6(2)

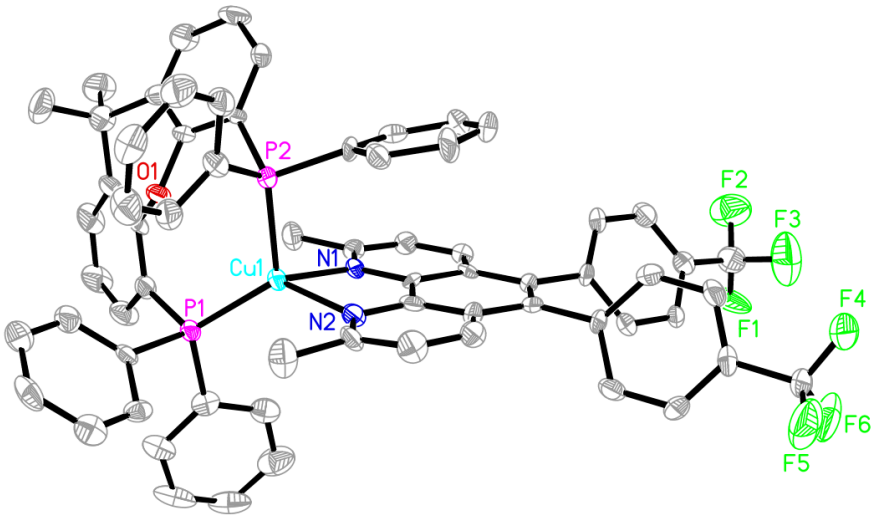

	C$_P$7
β_{NCuN}	79.71(9)
β_{PCuP}	119.43(3)
P-P-N-N	87.19
Cu-N_1	209.9(2)
Cu-N_2	210.0(2)
Cu-P_1	224.40(8)
Cu-P_2	228.78(9)
$\tau_{Sub,1}$	-72.3(4)
$\tau_{Sub,2}$	-69.2(4)
d_1	380.2(4)
d_2	360.5(4)
N_1CuP_1	127.61(7)
N_1CuP_2	102.22(7)
N_2CuP_1	119.00(7)
N_2CuP_2	100.36(7)

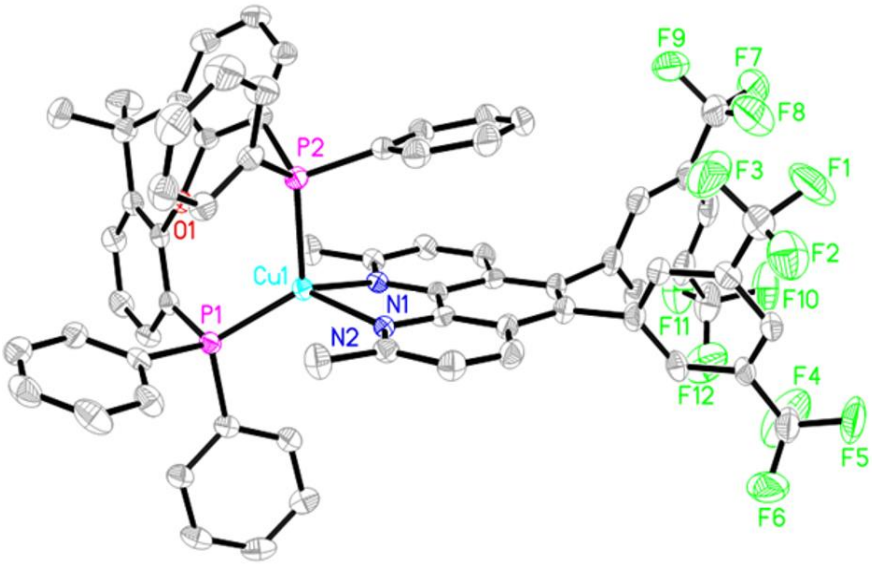

6 Calculated Ground State Structures of the Ligands and Complexes

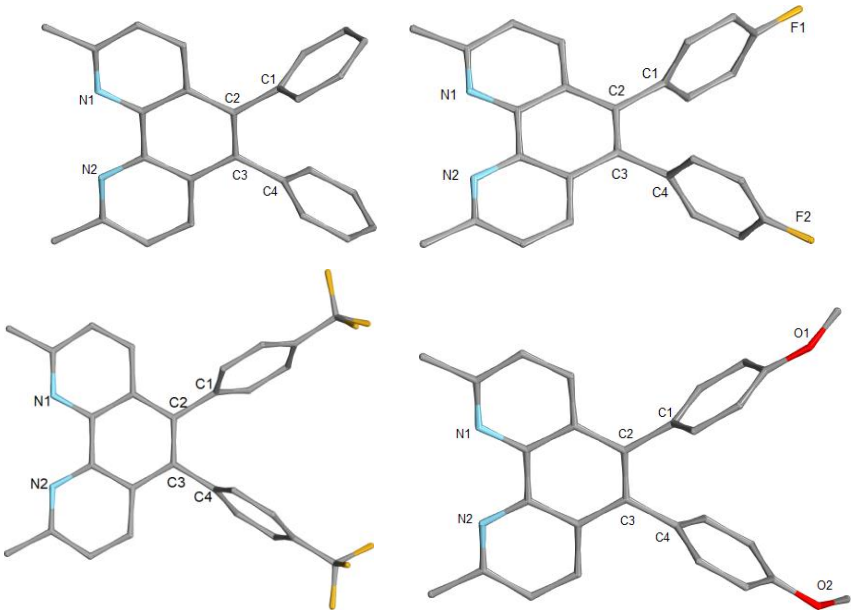

Figure S3.1. Calculated ground state (S_0) structure of **L_P2**, **L_P3**, **L_P4** and **L_P5** optimized at the BP86/def2-TZVP level of theory. Hydrogen atoms are omitted for clarity.

Table S3. Selected bond lengths (pm) and angles (°) of the calculated ground state (S_0) structure BP86/def2-TZVP) of **L_P2**-**L_P5** in acetonitrile. For atom labeling see structures in Figure S3.1.

	S_0 of **L_P2**	S_0 of **L_P3**	S_0 of **L_P4**	S_0 of **L_P5**
N1-N2	275.6	275.6	275.1	275.7
C2-C3	138.1	138.1	138.2	138.2
C1-C4	293.7	293.3	292.5	293.9
C1-C2-C3	121.4	121.3	121.0	121.3
C2-C3-C4	121.2	121.1	121.1	121.1
torsion of phenyl rings	90.1 & 91.0	89.9 & 90.8	107.7 & 73.9	91.1 & 90.3

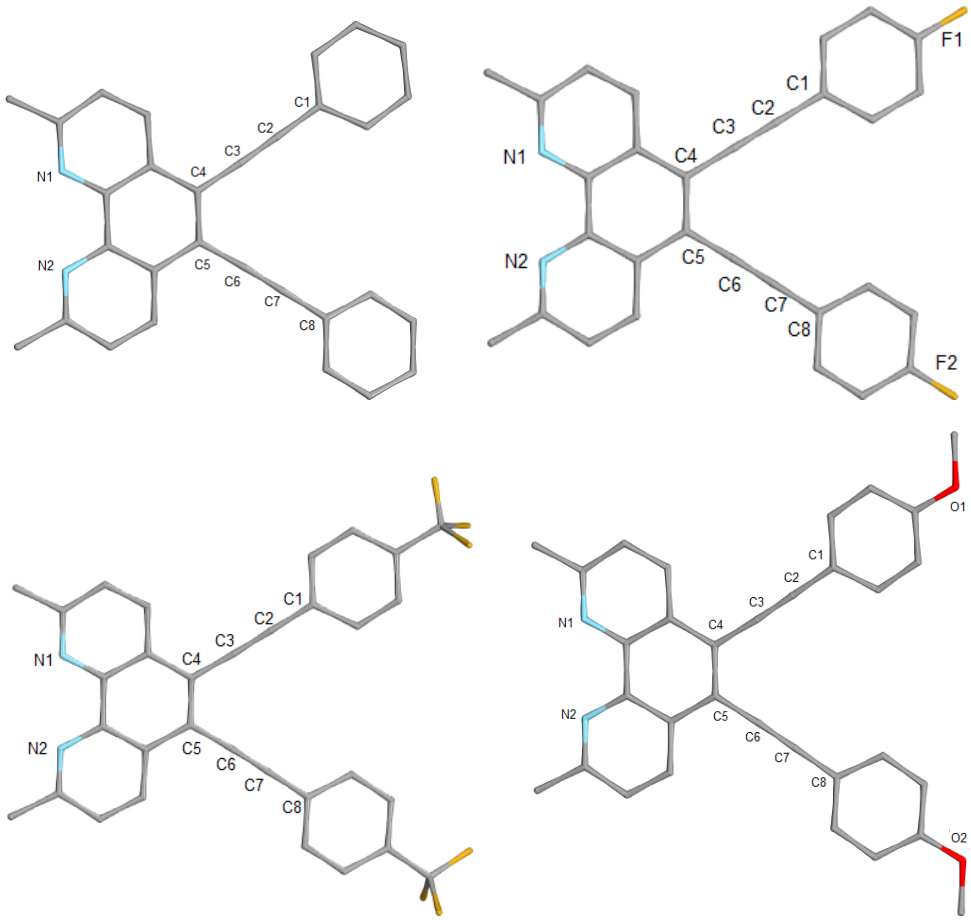

Figure S3.2. Calculated ground state (S_0) structure of L_A**2**, L_A**3**, L_A**4** and L_A**5**. Hydrogen atoms are omitted for clarity.

Table S4. Selected bond lengths (pm) and angles (°) of the calculated ground state (S_0) structure BP86/def2-TZVP) of L_A**2** and L_P**2** in acetonitrile. For atom labeling see structures in Figure S3.2.

	S_0 of L_A**2**	S_0 of L_A**3**	S_0 of L_A**4**	S_0 of L_A**5**
N1-N2	275.0	276.6	274.9	275.1
C3-C6	286.1	283.0	285.6	286.5
C2-C7	421.7	411.1	421.1	422.5
C1-C8	580.0	561.4	579.0	580.9
C3-C4-C5	121.0	120.5	120.9	121.1
C4-C5-C6	121.0	120.9	120.9	121.1
torsion of phenyl rings	-4.4 & -11.2	-5.4 & -18.2	-5.6 & -9.7	-4.1 & -6.1

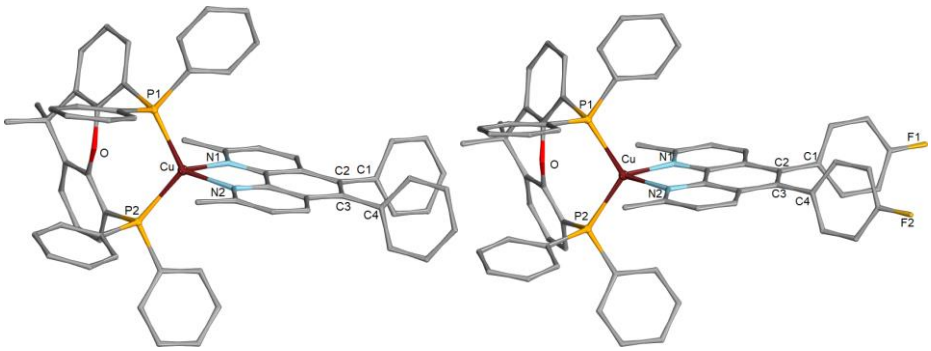

Figure S3.3. Calculated ground state (S_0) structure of **C_P2** and **C_P3** (right). Hydrogen atoms are omitted for clarity.

Table S5. Selected bond lengths (pm) and angles (°) of the calculated ground state (S_0) structure BP86/def2-TZVP) of **C_P2** and **C_P3** in acetonitrile. For atom labeling see structures in Figure S3.3.

	S_0 of **C_P2**	S_0 of **C_P3**
N1-Cu	212.5	212.1
N2-Cu	213.0	213.1
N1-Cu-N2	79.6	79.5
O-Cu	322.8	322.8
P1-P2	395.5	396.1
P1-Cu	233.8	234.0
P2-Cu	234.1	233.8
P1-Cu-P2	115.4	115.7
N1-N2	272.2	272.0
C1-C4	294.3	293.5
C1-C2-C3	121.4	121.3
C2-C3-C4	121.5	120.8

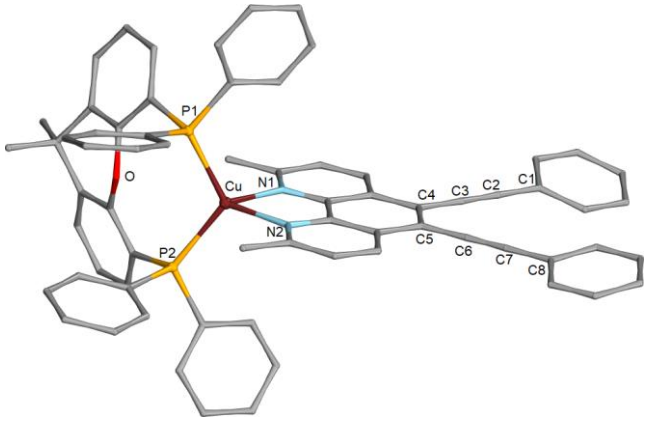

Figure S3.4. Calculated ground state (S_0) structure of $\mathbf{C_A2}$. Hydrogen atoms are omitted for clarity. The structure of $\mathbf{C_A3}$-$\mathbf{C_A5}$ look similar besides the substitution pattern (cf. with ligands in Figure S3.2).

Table S6. Selected bond lengths (pm) and angles (°) of the calculated ground state (S_0) structure BP86/def2-TZVP) of $\mathbf{C_P2}$ and $\mathbf{C_P3}$ in acetonitrile. For atom labeling see structures in Figure S3.4.

	S_0 of $\mathbf{C_A2}$	S_0 of $\mathbf{C_A3}$	S_0 of $\mathbf{C_A4}$	S_0 of $\mathbf{C_A5}$
N1-Cu	212.3	212.5	212.6	212.5
N2-Cu	213.1	213.3	213.3	213.1
N1-Cu-N2	79.6	79.5	79.4	79.5
O-Cu	322.7	323.6	323.4	323.6
P1-P2	396.8	395.9	395.9	395.8
P1-Cu	233.7	234.1	234.3	234.0
P2-Cu	233.9	234.1	234.0	234.1
P1-Cu-P2	116.1	115.5	115.4	115.5
N1-N2	272.3	272.2	272.1	272.2
C3-C6	286.2	286.5	285.8	287.2
C2-C7	420.4	421.4	419.4	423.8
C1-C8	580.0	578.0	575.1	582.2
C3-C4-C5	121.1	121.1	121.0	121.3
C4-C5-C6	121.1	121.2	121.0	121.3
torsion of phenyl rings	9.6 & 14.6	9.6 & 13.6	9.3 & 16.0	0.5 & 0.9

7 Electrochemical Data of C_P2-C_P7 and C_A2-C_A5

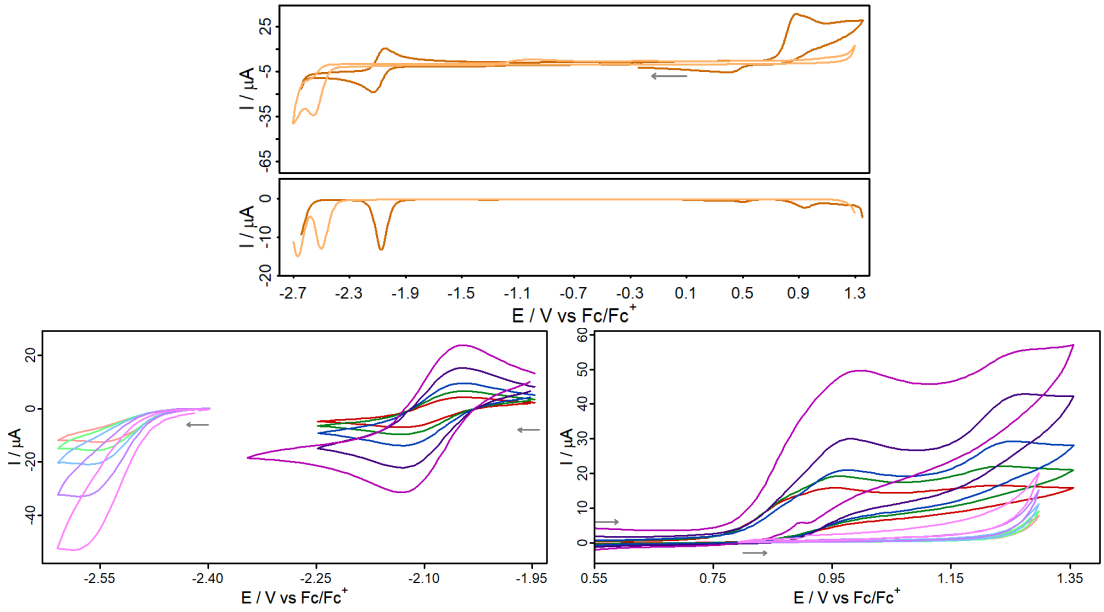

Figure S4.1 Cyclic voltammogram (top) and differential pulse voltammograms (DPV) of of **C_P2** (with dark color, 1 mM) and **L_P2** (with light color, < 1 mM due to low solubility in acetonitrile) in acetonitrile solution referenced vs. the ferrocene/ferricenium (Fc/Fc^+) couple. Conditions: scan rate of 100 mVs^{-1}, $[Bu_4N][PF_6]$ (0.1 M) as supporting electrolyte.
Reductive (bottom left) and oxidative events (bottom right) of the cyclic voltammograms of **C_P2** (with dark color, 1 mM) and **L_P2** (with light color, < 1 mM due to low solubility in acetonitrile) in acetonitrile solution referenced vs. the ferrocene/ferricenium (Fc/Fc^+) couple at different scan rates. Conditions: scan rate of 25 mVs^{-1} (red), 50 mVs^{-1} (green), 100 mVs^{-1} (blue), 250 mVs^{-1} (purple), 500 mVs^{-1} (magenta) and 800 mVs^{-1} (yellow), with Bu_4NPF_6 (0.1 M) as supporting electrolyte. The arrow illustrates the initial scan direction.

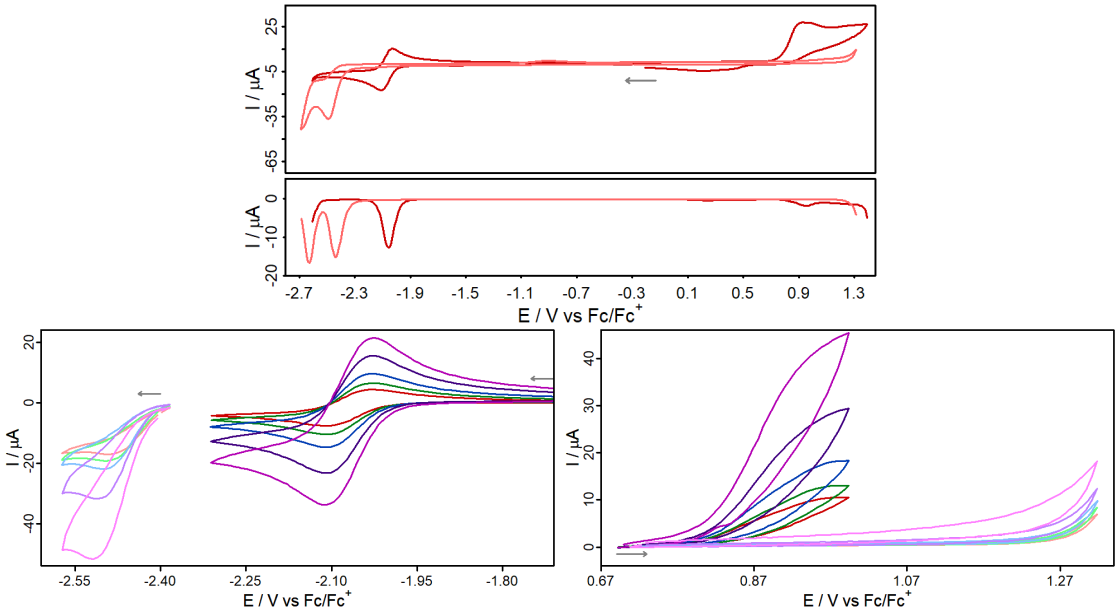

Figure S4.2 Cyclic voltammogram (top) and differential pulse voltammograms (DPV) of of **C_P3** (with dark color, 1 mM) and **L_P3** (with light color, < 1 mM due to low solubility in acetonitrile) in acetonitrile solution referenced vs. the ferrocene/ferricenium (Fc/Fc^+) couple. Conditions: scan rate of 100 mVs^{-1}, $[Bu_4N][PF_6]$ (0.1 M) as supporting electrolyte.
Reductive (bottom left) and oxidative events (bottom right) of the cyclic voltammograms of **C_P3** (with dark color, 1 mM) and **L_P3** (with light color, < 1 mM due to low solubility in acetonitrile) in acetonitrile solution

referenced vs. the ferrocene/ferricenium (Fc/Fc^+) couple at different scan rates. Conditions: scan rate of 25 mVs^{-1} (red), 50 mVs^{-1} (green), 100 mVs^{-1} (blue), 250 mVs^{-1} (purple), 500 mVs^{-1} (magenta) and 800 mVs^{-1} (yellow), with Bu_4NPF_6 (0.1 M) as supporting electrolyte. The arrow illustrates the initial scan direction.

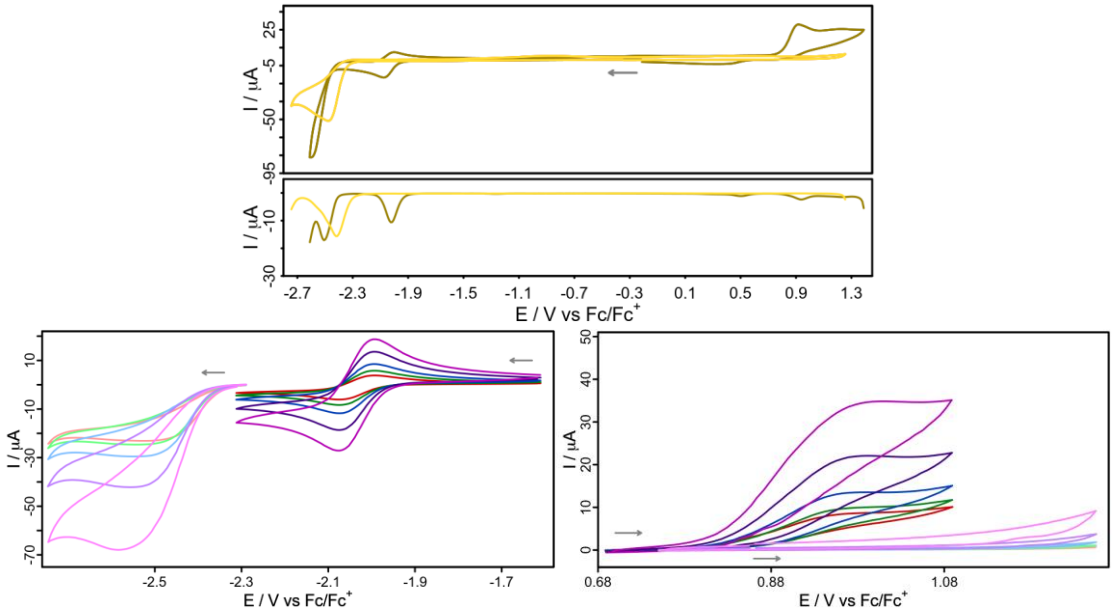

Figure S4.3 Cyclic voltammogram (top) and differential pulse voltammograms (DPV) of of **C_P4** (with dark color, 1 mM) and **L_P4** (with light color, < 1 mM due to low solubility in acetonitrile) in acetonitrile solution referenced vs. the ferrocene/ferricenium (Fc/Fc^+) couple. Conditions: scan rate of 100 mVs^{-1}, $[Bu_4N][PF_6]$ (0.1 M) as supporting electrolyte.
Reductive (bottom left) and oxidative events (bottom right) of the cyclic voltammograms of **C_P4** (with dark color, 1 mM) and **L_P4** (with light color, < 1 mM due to low solubility in acetonitrile) in acetonitrile solution referenced vs. the ferrocene/ferricenium (Fc/Fc^+) couple at different scan rates. Conditions: scan rate of 25 mVs^{-1} (red), 50 mVs^{-1} (green), 100 mVs^{-1} (blue), 250 mVs^{-1} (purple), 500 mVs^{-1} (magenta) and 800 mVs^{-1} (yellow), with Bu_4NPF_6 (0.1 M) as supporting electrolyte. The arrow illustrates the initial scan direction.

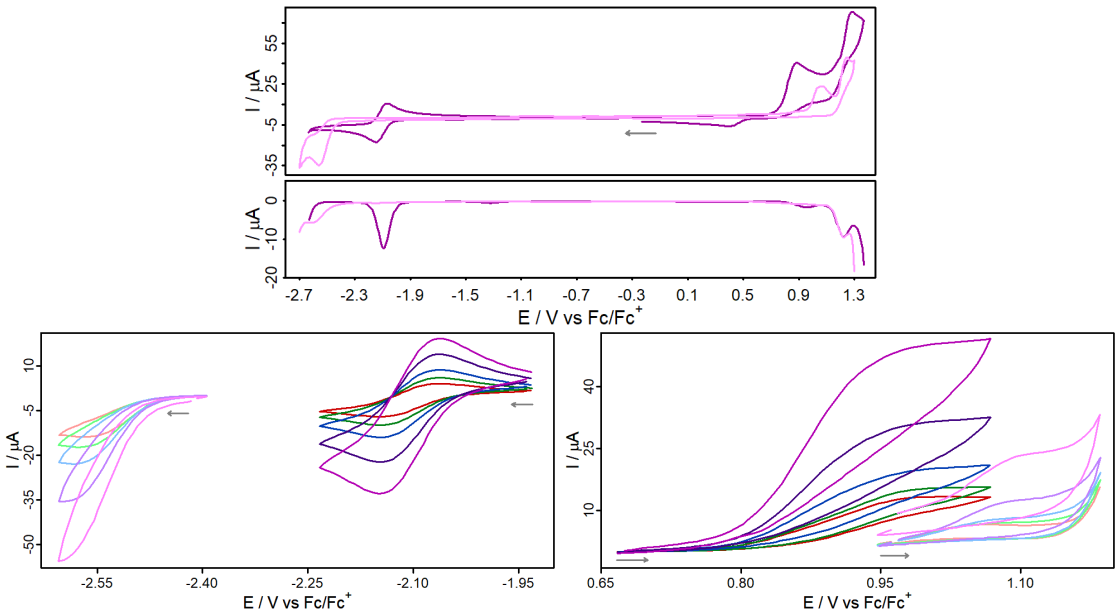

Figure S4.4 Cyclic voltammogram (top) and differential pulse voltammograms (DPV) of of **C_P5** (with dark color, 1 mM) and **L_P5** (with light color, < 1 mM due to low solubility in acetonitrile) in acetonitrile solution

referenced vs. the ferrocene/ferricenium (Fc/Fc^+) couple. Conditions: scan rate of 100 mVs^{-1}, $[Bu_4N][PF_6]$ (0.1 M) as supporting electrolyte.
Reductive (bottom left) and oxidative events (bottom right) of the cyclic voltammograms of **C_P5** (with dark color, 1 mM) and **L_P5** (with light color, < 1 mM due to low solubility in acetonitrile) in acetonitrile solution referenced vs. the ferrocene/ferricenium (Fc/Fc^+) couple at different scan rates. Conditions: scan rate of 25 mVs^{-1} (red), 50 mVs^{-1} (green), 100 mVs^{-1} (blue), 250 mVs^{-1} (purple), 500 mVs^{-1} (magenta) and 800 mVs^{-1} (yellow), with Bu_4NPF_6 (0.1 M) as supporting electrolyte. The arrow illustrates the initial scan direction.

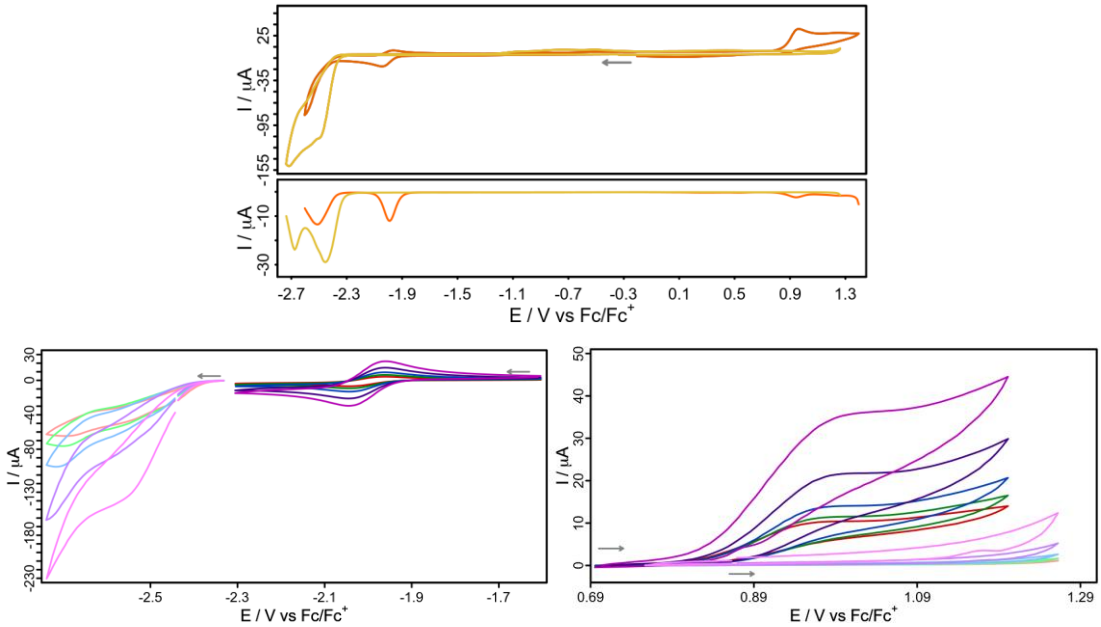

Figure S4.5 Cyclic voltammogram (top) and differential pulse voltammograms (DPV) of of **C_P6** (with dark color, 1 mM) and **L_P6** (with light color, < 1 mM due to low solubility in acetonitrile) in acetonitrile solution referenced vs. the ferrocene/ferricenium (Fc/Fc^+) couple. Conditions: scan rate of 100 mVs^{-1}, $[Bu_4N][PF_6]$ (0.1 M) as supporting electrolyte.
Reductive (bottom left) and oxidative events (bottom right) of the cyclic voltammograms of **C_P6** (with dark color, 1 mM) and **L_P6** (with light color, < 1 mM due to low solubility in acetonitrile) in acetonitrile solution referenced vs. the ferrocene/ferricenium (Fc/Fc^+) couple at different scan rates. Conditions: scan rate of 25 mVs^{-1} (red), 50 mVs^{-1} (green), 100 mVs^{-1} (blue), 250 mVs^{-1} (purple), 500 mVs^{-1} (magenta) and 800 mVs^{-1} (yellow), with Bu_4NPF_6 (0.1 M) as supporting electrolyte. The arrow illustrates the initial scan direction.

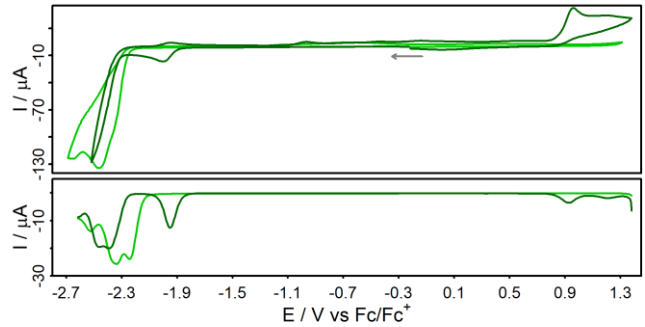

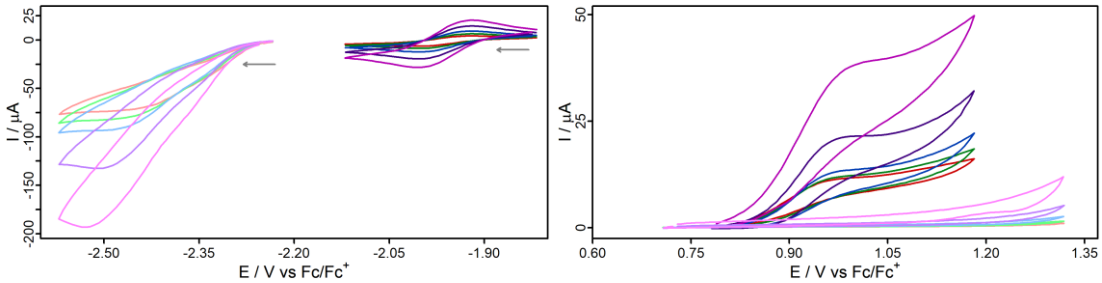

Figure S4.6 Cyclic voltammogram (top) and differential pulse voltammograms (DPV) of $\mathbf{C_P7}$ (with dark color, 1 mM) and $\mathbf{L_P7}$ (with light color, < 1 mM due to low solubility in acetonitrile) in acetonitrile solution referenced vs. the ferrocene/ferricenium (Fc/Fc^+) couple. Conditions: scan rate of 100 mVs^{-1}, $[Bu_4N][PF_6]$ (0.1 M) as supporting electrolyte.

Reductive (bottom left) and oxidative events (bottom right) of the cyclic voltammograms of $\mathbf{C_P7}$ (with dark color, 1 mM) and $\mathbf{L_P7}$ (with light color, < 1 mM due to low solubility in acetonitrile) in acetonitrile solution referenced vs. the ferrocene/ferricenium (Fc/Fc^+) couple at different scan rates. Conditions: scan rate of 25 mVs^{-1} (red), 50 mVs^{-1} (green), 100 mVs^{-1} (blue), 250 mVs^{-1} (purple), 500 mVs^{-1} (magenta) and 800 mVs^{-1} (yellow), with Bu_4NPF_6 (0.1 M) as supporting electrolyte. The arrow illustrates the initial scan direction.

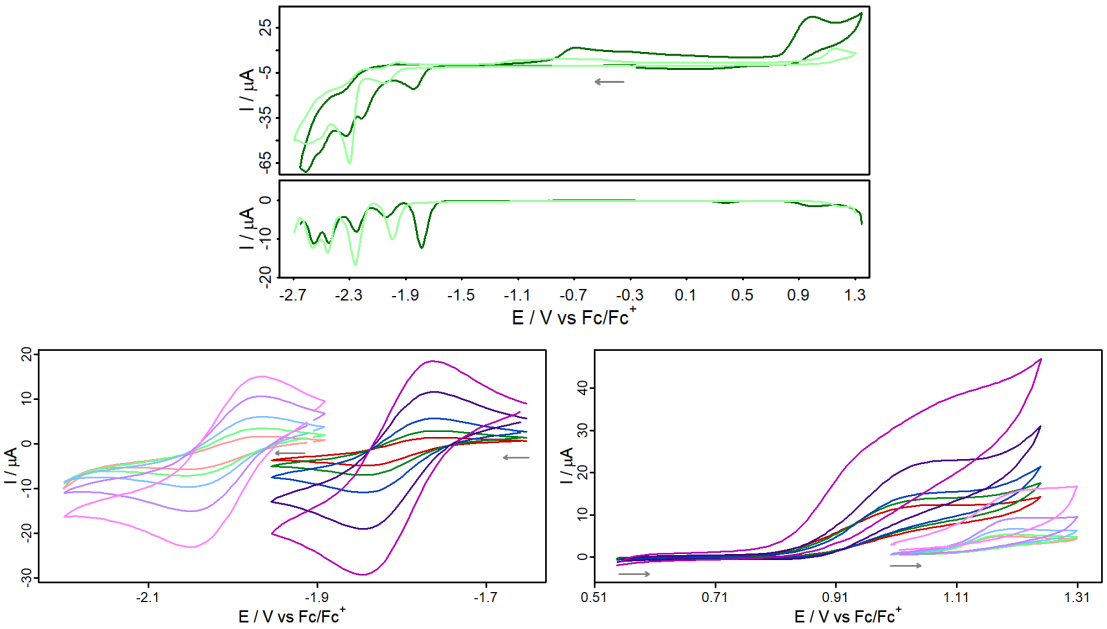

Figure S4.7 Cyclic voltammogram (top) and differential pulse voltammograms (DPV) of of $\mathbf{C_A2}$ (with dark color, 1 mM) and $\mathbf{L_A2}$ (with light color, < 1 mM due to low solubility in acetonitrile) in acetonitrile solution referenced vs. the ferrocene/ferricenium (Fc/Fc^+) couple. Conditions: scan rate of 100 mVs^{-1}, $[Bu_4N][PF_6]$ (0.1 M) as supporting electrolyte.

Reductive (bottom left) and oxidative events (bottom right) of the cyclic voltammograms of $\mathbf{C_A2}$ (with dark color, 1 mM) and $\mathbf{L_A2}$ (with light color, < 1 mM due to low solubility in acetonitrile) in acetonitrile solution referenced vs. the ferrocene/ferricenium (Fc/Fc^+) couple at different scan rates. Conditions: scan rate of 25 mVs^{-1} (red), 50 mVs^{-1} (green), 100 mVs^{-1} (blue), 250 mVs^{-1} (purple), 500 mVs^{-1} (magenta) and 800 mVs^{-1} (yellow), with Bu_4NPF_6 (0.1 M) as supporting electrolyte. The arrow illustrates the initial scan direction.

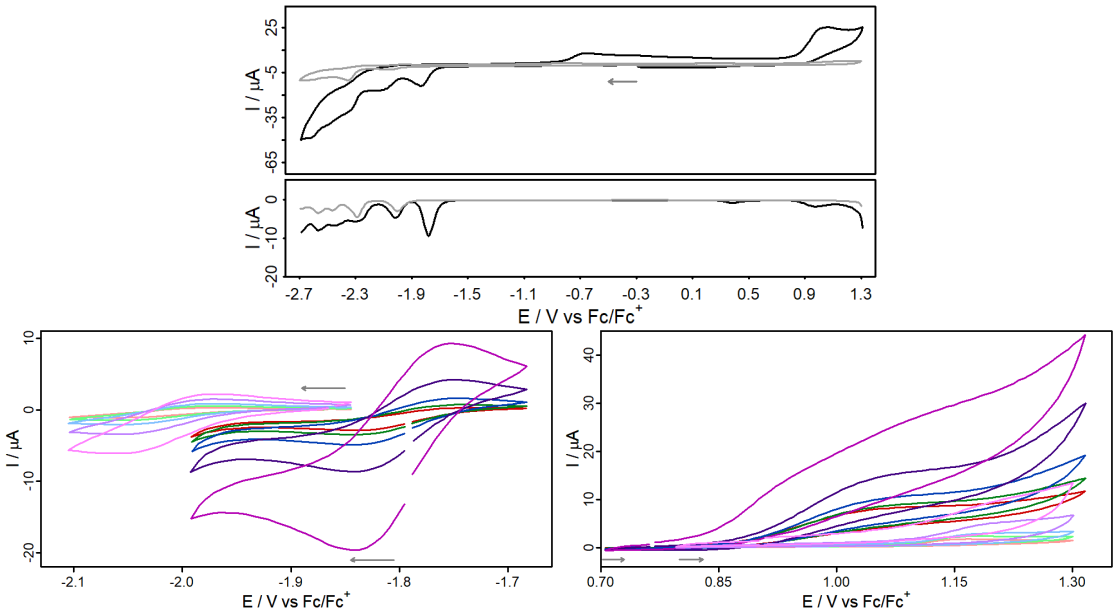

Figure S4.8 Cyclic voltammogram (top) and differential pulse voltammograms (DPV) of of **C_A3** (with dark color, 1 mM) and **L_A3** (with light color, < 1 mM due to low solubility in acetonitrile) in acetonitrile solution referenced vs. the ferrocene/ferricenium (Fc/Fc^+) couple. Conditions: scan rate of 100 mVs^{-1}, $[Bu_4N][PF_6]$ (0.1 M) as supporting electrolyte.
Reductive (bottom left) and oxidative events (bottom right) of the cyclic voltammograms of **C_A3** (with dark color, 1 mM) and **L_A3** (with light color, < 1 mM due to low solubility in acetonitrile) in acetonitrile solution referenced vs. the ferrocene/ferricenium (Fc/Fc^+) couple at different scan rates. Conditions: scan rate of 25 mVs^{-1} (red), 50 mVs^{-1} (green), 100 mVs^{-1} (blue), 250 mVs^{-1} (purple), 500 mVs^{-1} (magenta) and 800 mVs^{-1} (yellow), with Bu_4NPF_6 (0.1 M) as supporting electrolyte. The arrow illustrates the initial scan direction.

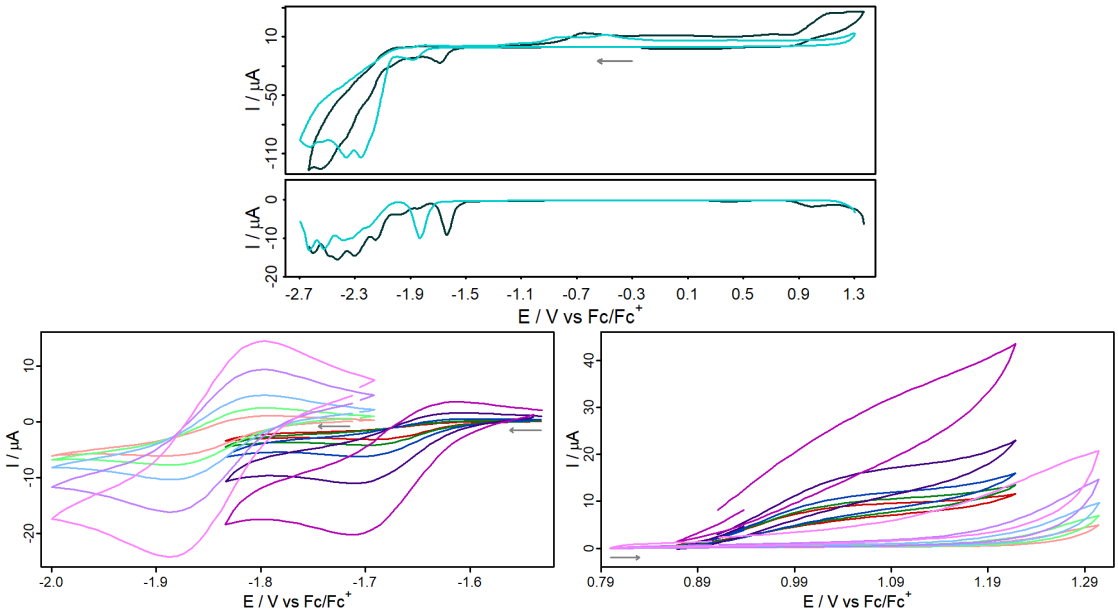

Figure S4.9 Cyclic voltammogram (top) and differential pulse voltammograms (DPV) of of **C_A4** (with dark color, 1 mM) and **L_A4** (with light color, < 1 mM due to low solubility in acetonitrile) in acetonitrile solution referenced vs. the ferrocene/ferricenium (Fc/Fc^+) couple. Conditions: scan rate of 100 mVs^{-1}, $[Bu_4N][PF_6]$ (0.1 M) as supporting electrolyte.

Reductive (bottom left) and oxidative events (bottom right) of the cyclic voltammograms of **C_A4** (with dark color, 1 mM) and **L_A4** (with light color, < 1 mM due to low solubility in acetonitrile) in acetonitrile solution referenced vs. the ferrocene/ferricenium (Fc/Fc^+) couple at different scan rates. Conditions: scan rate of 25 mVs^{-1} (red), 50 mVs^{-1} (green), 100 mVs^{-1} (blue), 250 mVs^{-1} (purple), 500 mVs^{-1} (magenta) and 800 mVs^{-1} (yellow), with Bu_4NPF_6 (0.1 M) as supporting electrolyte. The arrow illustrates the initial scan direction.

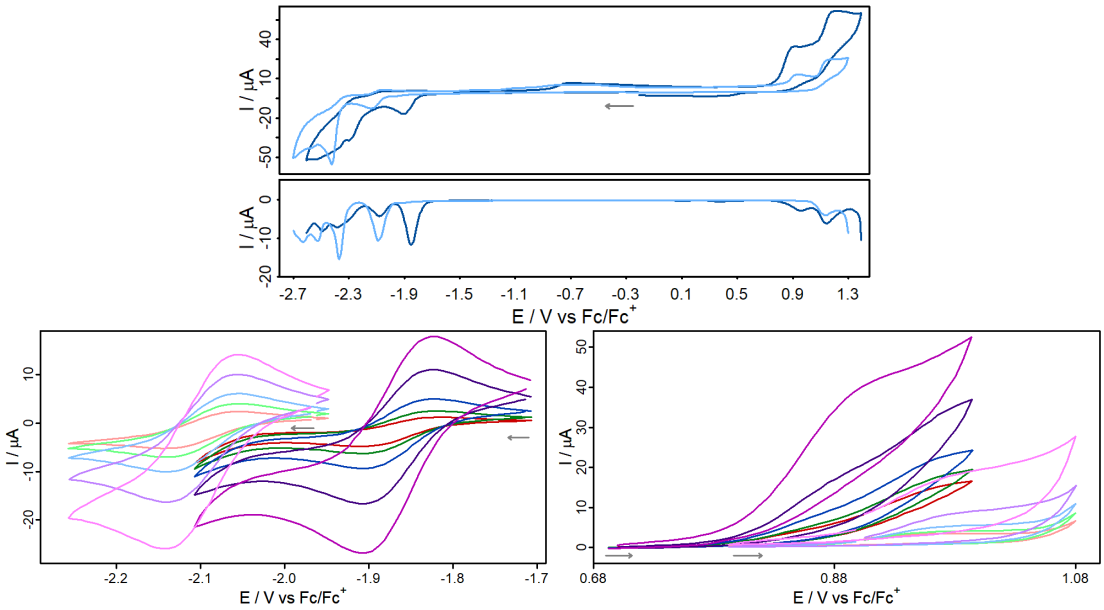

Figure S4.10 Cyclic voltammogram (top) and differential pulse voltammograms (DPV) of of **C_A5** (with dark color, 1 mM) and **L_A5** (with light color, < 1 mM due to low solubility in acetonitrile) in acetonitrile solution referenced vs. the ferrocene/ferricenium (Fc/Fc^+) couple. Conditions: scan rate of 100 mVs^{-1}, $[Bu_4N][PF_6]$ (0.1 M) as supporting electrolyte.

Reductive (bottom left) and oxidative events (bottom right) of the cyclic voltammograms of **C_A5** (with dark color, 1 mM) and **L_A5** (with light color, < 1 mM due to low solubility in acetonitrile) in acetonitrile solution referenced vs. the ferrocene/ferricenium (Fc/Fc^+) couple at different scan rates. Conditions: scan rate of 25 mVs^{-1} (red), 50 mVs^{-1} (green), 100 mVs^{-1} (blue), 250 mVs^{-1} (purple), 500 mVs^{-1} (magenta) and 800 mVs^{-1} (yellow), with Bu_4NPF_6 (0.1 M) as supporting electrolyte. The arrow illustrates the initial scan direction.

8 Absorption and Steady-State Emission

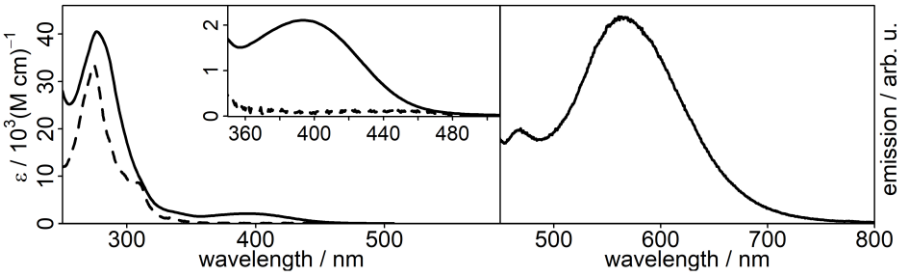

Figure S5.1: UV/vis absorption spectra (left) and emission spectra (right) acetonitrile solution of **C1** (solid) and **L1** (dashed). Emission measured in deaerated solution after excitation at 390 nm.

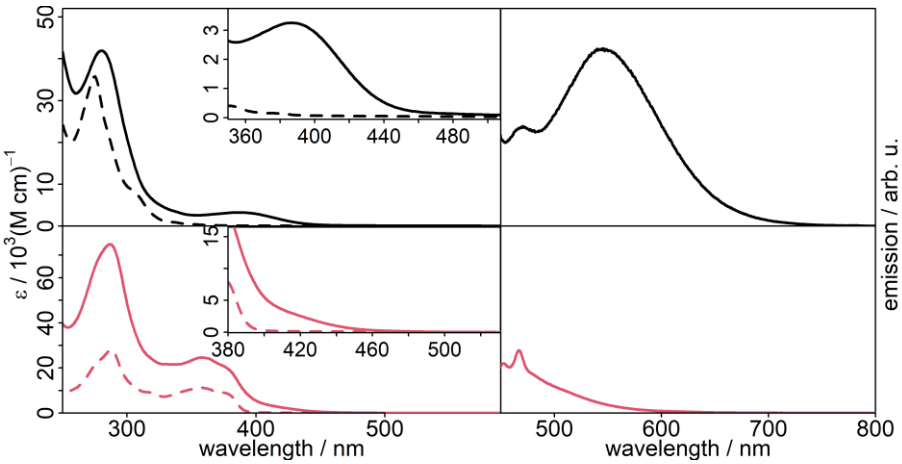

Figure S5.2: UV/vis absorption spectra (left) and emission spectra (right) acetonitrile solution of $\mathbf{C_P2}$ (solid, black), $\mathbf{L_P2}$ (dashed, black), $\mathbf{C_A2}$ (solid, red) and $\mathbf{L_A2}$ (dashed, red). Emission measured in deaerated solution after excitation at 390 nm ($\mathbf{C_P2}$) or 410 nm ($\mathbf{C_A2}$).

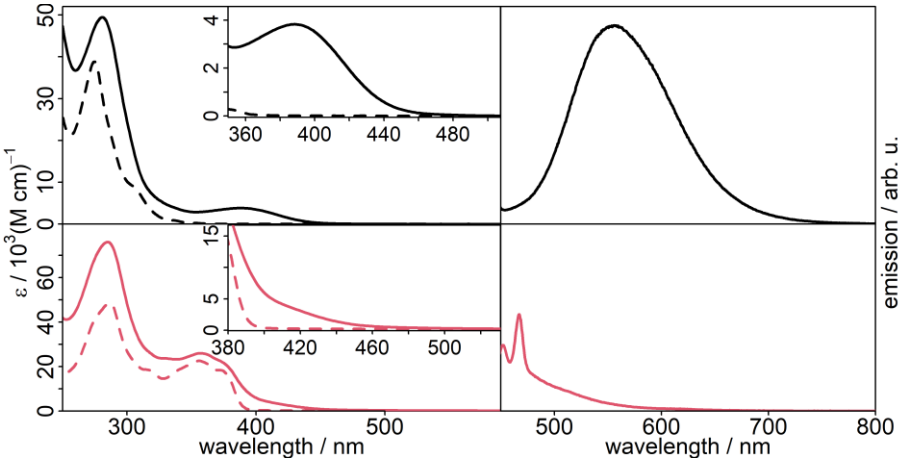

Figure S5.3: UV/vis absorption spectra (left) and emission spectra (right) acetonitrile solution of $\mathbf{C_P3}$ (solid, black), $\mathbf{L_P3}$ (dashed, black), $\mathbf{C_A3}$ (solid, red) and $\mathbf{L_A3}$ (dashed, red). Emission measured in deaerated solution after excitation at 390 nm ($\mathbf{C_P3}$) or 410 nm ($\mathbf{C_A3}$).

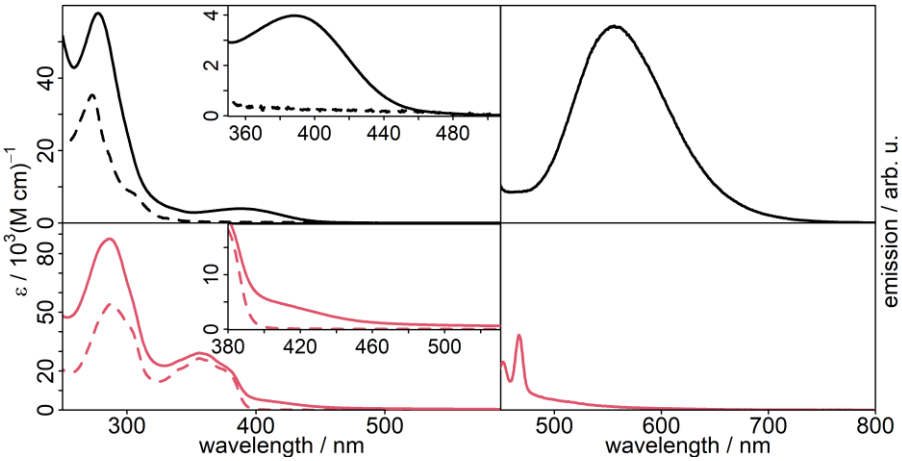

Figure S5.4: UV/vis absorption spectra (left) and emission spectra (right) acetonitrile solution of **C$_P$4** (solid, black), **L$_P$4** (dashed, black), **C$_A$4** (solid, red) and **L$_A$4** (dashed, red). Emission measured in deaerated solution after excitation at 390 nm (**C$_P$4**) or 410 nm (**C$_A$4**).

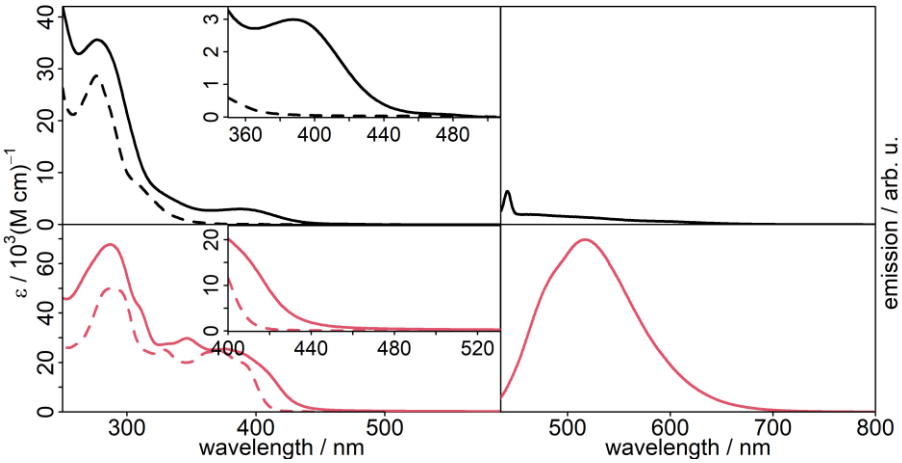

Figure S5.5: UV/vis absorption spectra (left) and emission spectra (right) acetonitrile solution of **C$_P$5** (solid, black), **L$_P$5** (dashed, black), **C$_A$5** (solid, red) and **L$_A$5** (dashed, red). Emission measured in deaerated solution after excitation at 390 nm (**C$_P$5**) or 410 nm (**C$_A$5**).

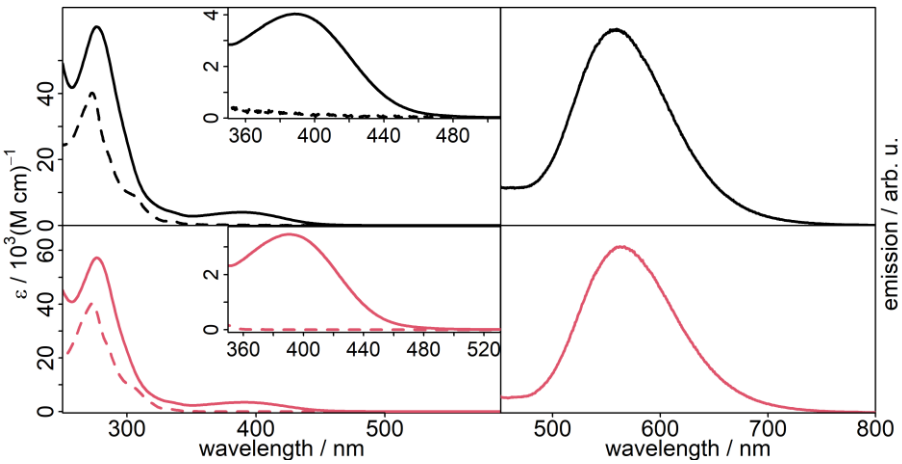

Figure S5.6: UV/vis absorption spectra (left) and emission spectra (right) acetonitrile solution of **C$_P$6** (solid, black), **L$_P$6** (dashed, black), **C$_P$7** (solid, red) and **L$_P$7** (dashed, red). Emission measured in deaerated solution after excitation at 390 nm (**C$_P$6** and **C$_P$7**).

Table S7: Summary of the photophysical properties of all alkynyl-based complexes **C_A2** – **C_A5** in acetonitrile solution at room temperature.

Compound	λ_{abs} [nm] (ε [10^3 M^{-1} cm^{-1}])	λ_{em} [nm] inert	φ_{em} [%] inert	φ_{em} [%] O_2	τ_{em} [ns] inert	τ_{em} [ns] O_2
C_A2	410 [a] (3.6)	[c]	*n.d.*	*n.d.*	*n.d.*	*n.d.*
C_A3	410 [a] (4.2)	[c]	*n.d.*	*n.d.*	*n.d.*	*n.d.*
C_A4	410 [a] (4.7)	[c]	*n.d.*	*n.d.*	*n.d.*	*n.d.*
C_A5	410 [a] (18.6 [b])	517	*n.d.*	*n.d.*	<6ns [d]	<6ns [d]

Emission lifetimes τ_{em} were measured following 355 nm laser pulse excitation. [a] λ_{abs} approximated due to spectral superposition. [b] absorption superimposed by ligandm centered transitions. [c] no detectable emission at λ > 500 nm. [d] below resolution time. *n.d.*: not determined.

9 Emission Lifetime

Table S8: Time resolved emission data of the complexes [(xant)Cu(dmp)]PF_6 (**Ref**), [(xant)Cu(bcp)]PF_6, **C1** and **C_P2**-**C_P7** (dmp=2,9-dimethyl-1,10-phenanthroline; bcp=bathocuproine) in acetonitrile measured under inert and aerobic conditions at the respective emission maxima after pulsed laser excitation at 355 nm. Emission decay observed displayed in orange; calculated fit displayed in black.

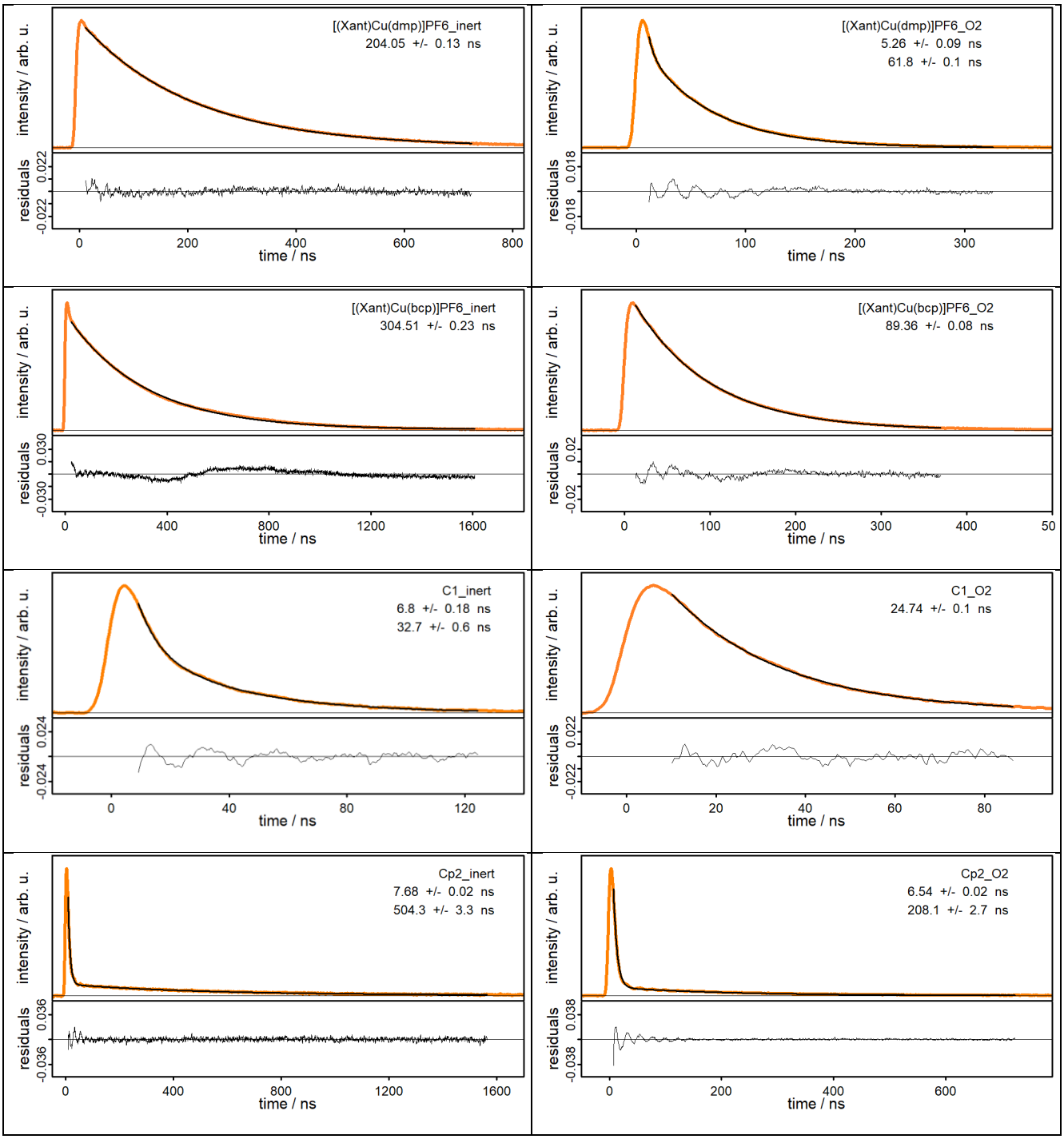

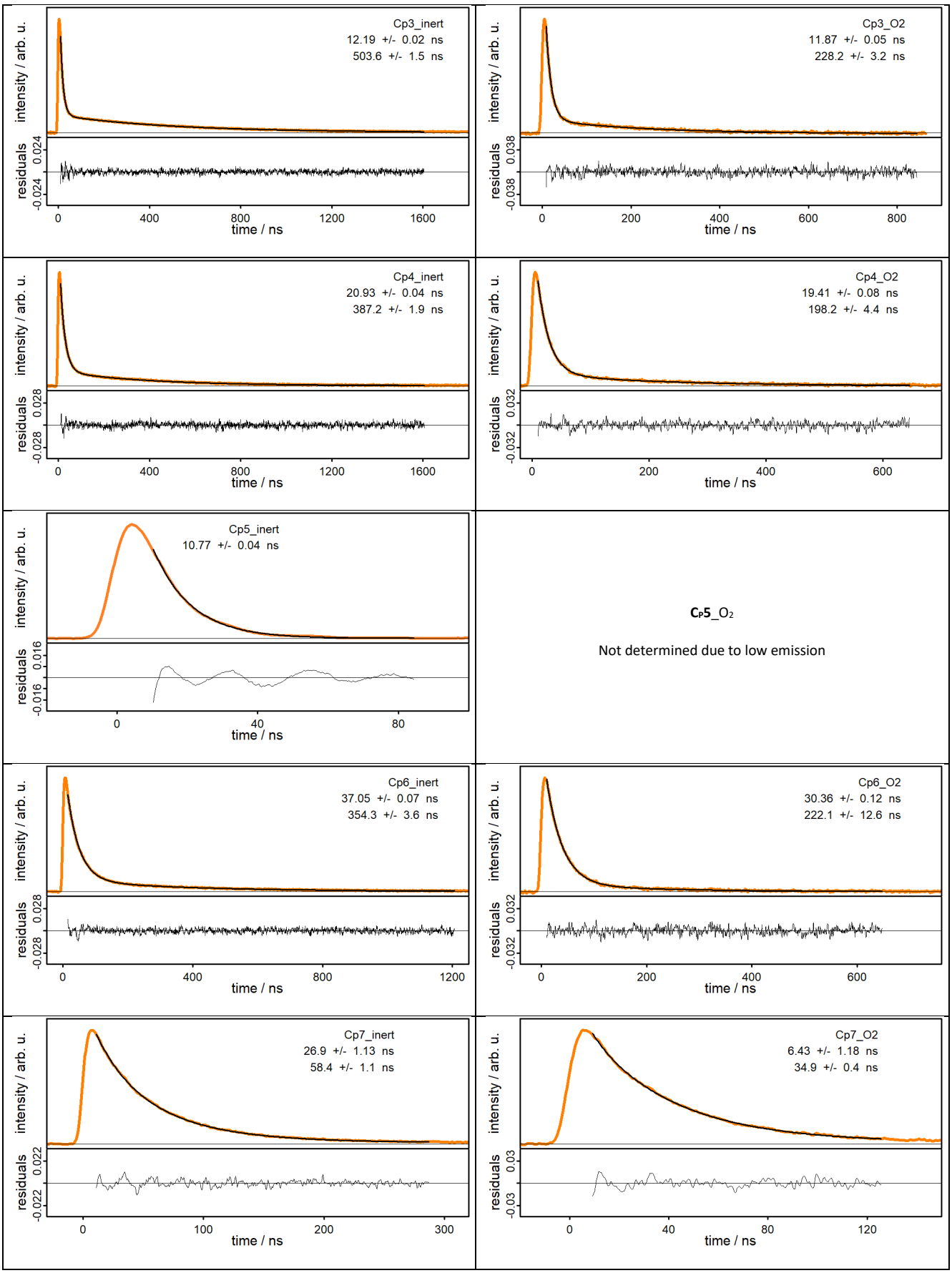
Cp3_inert
12.19 +/- 0.02 ns
503.6 +/- 1.5 ns
Cp3_O2
11.87 +/- 0.05 ns
228.2 +/- 3.2 ns
Cp4_inert
20.93 +/- 0.04 ns
387.2 +/- 1.9 ns
Cp4_O2
19.41 +/- 0.08 ns
198.2 +/- 4.4 ns
Cp5_inert
10.77 +/- 0.04 ns
Cp5_O2
Not determined due to low emission
Cp6_inert
37.05 +/- 0.07 ns
354.3 +/- 3.6 ns
Cp6_O2
30.36 +/- 0.12 ns
222.1 +/- 12.6 ns
Cp7_inert
26.9 +/- 1.13 ns
58.4 +/- 1.1 ns
Cp7_O2
6.43 +/- 1.18 ns
34.9 +/- 0.4 ns
intensity / arb. u.
residuals
time / ns